Institute of Crop Science and Rescource Conservation - Phytomedicine

---

Detection, identification, and quantification of fungal diseases of sugar beet leaves using imaging and non-imaging hyperspectral techniques

Inaugural-Dissertation

zur

Erlangung des Grades

Doktor der Agrarwissenschaften

(Dr. agr.)

der

Hohen Landwirtschaftlichen Fakultät

der

Rheinischen Friedrich-Wilhelms-Universität

zu Bonn

vorgelegt am 04.11.2010

von

Anne-Katrin Mahlein

aus Ansbach

Referent: Prof. Dr. H.-W. Dehne
Koreferent: Prof. Dr. H. Goldbach

Tag der mündlichen Prüfung: 20.01.2011
Erscheinungsjahr: 2011

In liebevoller Erinnerung an meine Großmutter Maria Eff

Abstract

Plant diseases influence the optical properties of plants in different ways. Depending on the host pathogen system and disease specific symptoms, different regions of the reflectance spectrum are affected, resulting in specific spectral signatures of diseased plants. The aim of this study was to examine the potential of hyperspectral imaging and non-imaging sensor systems for the detection, differentiation, and quantification of plant diseases. Reflectance spectra of sugar beet leaves infected with the fungal pathogens *Cercospora beticola*, *Erysiphe betae*, and *Uromyces betae* causing *Cercospora* leaf spot, powdery mildew, and sugar beet rust, respectively, were recorded repeatedly during pathogenesis. Hyperspectral data were analyzed using various methods of data and image analysis and were compared to ground truth data. Several approaches with different sensors on the measuring scales leaf, canopy, and field have been tested and compared. Much attention was paid on the effect of spectral, spatial, and temporal resolution of hyperspectral sensors on disease recording. Another focus of this study was the description of spectral characteristics of disease specific symptoms. Therefore, different data analysis methods have been applied to gain a maximum of information from spectral signatures.

Spectral reflectance of sugar beet was affected by each disease in a characteristic way, resulting in disease specific signatures. Reflectance differences, sensitivity, and best correlating spectral bands differed depending on the disease and the developmental stage of the diseases. Compared to non-imaging sensors, the hyperspectral imaging sensor gave extra information related to spatial resolution. The preciseness in detecting pixel-wise spatial and temporal differences was on a high level. Besides characterization of diseased leaves also the assessment of pure disease endmembers as well as of different regions of typical symptoms was realized. Spectral vegetation indices (SVIs) related to physiological parameters were calculated and correlated to the severity of diseases. The SVIs differed in their sensitivity to the different diseases. Combining the information from multiple SVIs in an automatic classification method with Support Vector Machines, high sensitivity and specificity for the detection and differentiation of diseased leaves was reached in an early stage. In addition to the detection and identification, the quantification of diseases was possible with high accuracy by SVIs and Spectral Angle Mapper classification, calculated from hyperspectral images. Knowledge from measurements under controlled condition was carried over to the field scale. Early detection and monitoring of *Cercospora* leaf spot and powdery mildew was facilitated.

The results of this study contribute to a better understanding of plant optical properties during disease development. Methods will further be applicable in precision crop protection, to realize the detection, differentiation, and quantification of plant diseases in early stages.

Kurzfassung

Pflanzenkrankheiten wirken sich auf die optischen Eigenschaften von Pflanzen in unterschiedlicher Weise aus. Verschiedene Bereiche des Reflektionsspektrums werden in Abhängigkeit von Wirt-Pathogen System und krankheitsspezifischen Symptomen beeinflusst. Hyperspektrale, nicht-invasive Sensoren bieten die Möglichkeit, optische Veränderungen zu einem frühen Zeitpunkt der Krankheitsentwicklung zu detektieren. Ziel dieser Arbeit war es, das Potential hyperspektraler abbildender und nicht abbildender Sensoren für die Erkennung, Identifizierung und Quantifizierung von Pflanzenkrankheiten zu beurteilen. Zuckerrübenblätter wurden mit den pilzlichen Erregern *Cercospora beticola*, *Erysiphe betae* bzw. *Uromyces betae* inokuliert und die Auswirkungen der Entwicklung von *Cercospora* Blattflecken, Echtem Mehltau bzw. Rübenrost auf die Reflektionseigenschaften erfasst und mit optischen Bonituren verglichen. Auf den Skalenebenen Blatt, Bestand und Feld wurden Messansätze mit unterschiedlichen Sensoren verglichen. Besonders berücksichtigt wurden hierbei Anforderungen an die spektrale, räumliche und zeitliche Auflösung der Sensoren. Ein weiterer Schwerpunkt lag auf der Beschreibung der spektralen Eigenschaften von charakteristischen Symptomen. Verschiedene Auswerteverfahren wurden mit dem Ziel angewendet, einen maximalen Informationsgehalt aus spektralen Signaturen zu gewinnen.

Jede Krankheit beeinflusste die spektrale Reflektion von Zuckerrübenblättern auf charakteristische Weise. Differenz der Reflektion, Sensitivität sowie Korrelation der spektralen Bänder zur Befallsstärke variierten in Abhängigkeit von den Krankheiten. Eine höhere Präzision durch die pixelweise Erfassung räumlicher und zeitlicher Unterschiede von befallenem und gesundem Gewebe konnte durch abbildende Sensoren erreicht werden. Spektrale Vegetationsindizes (SVIs), mit Bezug zu pflanzenphysiologischen Parametern wurden aus den Hyperspektraldaten errechnet und mit der Befallsstärke korreliert. Die SVIs unterschieden sich in ihrer Sensitivität gegenüber den drei Krankheiten. Durch den Einsatz von maschinellem Lernen wurde die kombinierte Information der errechneten Vegetationsindizes für eine automatische Klassifizierung genutzt. Eine hohe Sensitivität sowie eine hohe Spezifität bezüglich der Erkennung und Differenzierung von Krankheiten wurden erreicht. Eine Quantifizierung der Krankheiten war neben der Detektion und Identifizierung mittels SVIs bzw. Klassifizierung mit Spektral Angle Mapper an hyperspektralen Bilddaten möglich.

Die Ergebnisse dieser Arbeit tragen zu einem besseren Verständnis der optischen Eigenschaften von Pflanzen unter Pathogeneinfluss bei. Die untersuchten Methoden bieten die Möglichkeit in Anwendungen des Präzisionspflanzenschutzes implementiert zu werden, um eine frühzeitige Erkennung, Differenzierung und Quantifizierung von Pflanzenkrankheiten zu ermöglichen.

List of Abbreviations

ANN	Artificial Neural Networks
ARI	Anthocyanin Reflectance Index
ATCOR4	Atmospheric/Topographic Correction Algorithms for Airborne Sensors 4
BGI2	Blue/Green Index 2
BRDF	Bidirectional Reflectance Distribution Function
Car	Carotenoids
Chl_a	Chlorophyll a
Chl_b	Chlorophyll b
Chl_{total}	total Chlorophyll
CLS	*Cercospora* leaf spot
DMSO	Dimethylsulfoxide
ECa	apparent Electrical Conductivity
FWHM	Full Width at Half Maximum
GIS	Geographic Information System
GPS	Global Positioning System
GS	Growth Stage
HyMap	Hyperspectral Mapper
IDW	Inverse Distance Weighting
LAI	Leaf Area Index
LIBSVM	Library for SVMs
mCAI	Modified Chlorophyll Absorption Integral
MCARI	Modified Chlorophyll Absorption Reflectance Index
mND	Modified Normalized Difference Index
MNF	Minimum Noise Fraction
mSR	Modified Simple Ratio
ND	Normalized Difference Index
NDVI	Normalized Difference Vegetation Index
NIR	Near Infrared Reflectance
OSAVI	Optimized Soil Adjusted Vegetation Index
PA	Precision Agriculture
PM	Powdery mildew
PRI	Photochemical Reflectance Index
PSND	Pigment Specific Normalized Difference
PSRI	Plant Senescence Reflectance Index

PSSR	Pigment Specific Simple Ratio
REP	Red Edge Position
RGB	Red Green Blue
ROI	Region of Interest
ROSIS	Reflective Optics Systems Imaging Spectrometer
$\mathbf{R_{RE}}$	Reflectance at inflection point
SAM	Spectral Angle Mapper
SBR	Sugar beet rust
SG	Sum Green Index
SIPI	Structure Insensitive Pigment Index
SLU	Spectral Linear Unmixing
SR	Simple Ratio
SV	Sum VIS Index
SVI	Spectral Vegetation Indices
SVM	Support Vector Machines
SWIR	Shortwave Infrared Reflectance
VIS	Visible reflection
WI	Water Index

Contents

1. INTRODUCTION

Von Witzke *et al.* (2008) recently demonstrated that the worldwide demand for agricultural products exceeds the supply; hence there is a need to manage the worldwide production of agricultural commodities more efficiently. The potential yield of crops is affected by different stresses (e.g. pest, weed, nutrition deficiencies or water stress), which can reduce the production capacity. Oerke and Dehne (2004) indicated that the impact of diseases, insects, and weeds represents a potential annual loss of 40% of world food production.

Traditional agricultural management practices assume parameters in crop fields to be homogeneous, thus the output of pesticides and managing actions is not in relation to the demands (Steiner *et al.*, 2008). Due to high control costs and the environmental impact of fungicides, a site-specific application according to precision agriculture techniques is of high interest. Precision agriculture – integrating different modern technologies like sensor, information, and management systems – aims to match agricultural input and practices to the spatial and temporal variability within a field. Thus, a better use of resource and an avoidance of great differences in yield quality and quantity due to small-scale site-specific differences can be attained.

Considering that the occurrence of diseases depends on specific environmental factors and that diseases often exhibit a patchy distribution in fields, remote sensing techniques could be useful in identifying primary disease foci and areas differing in disease severity in the field (Franke and Menz, 2007; Franke *et al.*, 2009). Based on the information from remote sensing techniques or non invasive

sensor devices, application maps may be generated to manage agricultural fields in due consideration of spatiotemporal disease heterogeneities. Site-specific applications of pesticides, according to precision agriculture strategies result in a potential reduction in pesticide use, and thus can reduce the economical expenses and ecological impacts in agricultural crop production systems (Gebbers and Adamchuk, 2010). Gerhards and Christensen (2003) have shown that precision agriculture has the potential to reduce the application of herbicides. With online weed detection by image analysis and a map-based GPS-controlled patch spraying, the herbicide output was diminished in winter cereals against dicotyledonous weeds by 60% and for monocotyledonous weeds by 90%. To bring these practices forward to a site-specific application of fungicides, further research has to be implemented. As a basis, automatic disease detection has to be optimized.

Various indicators suggest that a detection, differentiation, and quantification of fungal diseases based on reflectance measurement would be feasible. If a symptom or a disease is detectable by naked eye, it should be measurable with a sensor, recording the reflectance of the symptom different from that of healthy tissue. Crucial points in sensor detection of biotic and abiotic stress factors, in particular of plant diseases, are the sensitivity and the specificity of the devices. Sensitivity denotes the ability of a sensor to detect various changes at a certain time. The specificity is characterized by classifying the change causing agent, or to discriminate between different possible causes. Stress causing agents, and likewise different plant diseases often cause similar symptoms and changes in plant physiology (Nutter *et al.*, 1990; Stafford, 2000). As the primary effects of different diseases to the plant biochemistry and physiology vary, different wavebands should be suitable for detection. However, not only plant pathogens cause chloroses and reduce the chlorophyll content.

A detailed understanding of plant physiological processes depending to a specific disease, as well as knowledge of sensor-object interaction is indispensable.

To implement hyperspectral sensors in threshold-orientated decision making systems, the sensor system has to have the capability for disease quantification. Beside the differentiation of stress factors and plant diseases among each others, hyperspectral sensors have to allow a pre-symptomatic detection of disease infection, to intervene with proper management strategies, like time- and site-specific fungicide application.

This study aims at exploring the potential of non-invasive hyperspectral sensor systems from remote sensing science for the detection of plant diseases. Experiments were carried out on sugar beet plants and their foliar pathogens *Cercospora beticola*, *Erysiphe betae*, and *Uromyces betae* to investigate the use of imaging and non-imaging hyperspectral sensors referring to the following questions: Do plant diseases have specific spectral signatures useful for disease identification? Is an early detection of infection by pathogens possible? What is the potential of sensors to differentiate among leaf diseases? Is a quantification of plant diseases at different stages possible?

Specific spectral signatures of leaves, diseased with *Cercospora* leaf spot, powdery mildew, and sugar beet rust, caused by *Cercospora beticola*, *Erysiphe betae*, and *Uromyces betae*, respectively, have been evaluated and compared during disease development. The three disease causing pathogens differ in their way of life and in their interaction with the host plant sugar beet. Thus, hyperspectral data of three differing host-pathogen systems have been assessed and comparatively analysed.

The sensitivity and specificity of hyperspectral sensing for disease detection is influenced by several factors. Hence, different approaches with different sensor-devices on different measuring scales have been tested and compared (Fig. 1.1). Observing the leaf and canopy level, much attention was paid on requirements on the spectral, spatial, and temporal resolution of hyperspectral sensors for disease detection. Experiments with different sensor systems have been made on the leaf and canopy level under controlled conditions and in the field. One focus

of this study was the comparison of non-imaging and imaging hyperspectral sensors for their suitability of disease detection and for a detailed description of spectral characteristics of disease specific symptoms. Until now disease-specific spectral vegetation indices or the analysis of hyperspectral data for disease detection are not available. Therefore, different data analysis methods have been applied to gain a maximum of information from spectral signatures.

In an interdisciplinary approach with the Institute of Geodesy and Geoinformation, University of Bonn, an optimization of data analysis methods and the development of disease specific spectral indices for an early detection and differentiation of fungal diseases have been realized. This PhD work was embedded in the Research Training Group 722 'Use of Information Techniques for Precision Plant Protection' funded by the German Research Foundation (DFG) from 2007 to 2010.

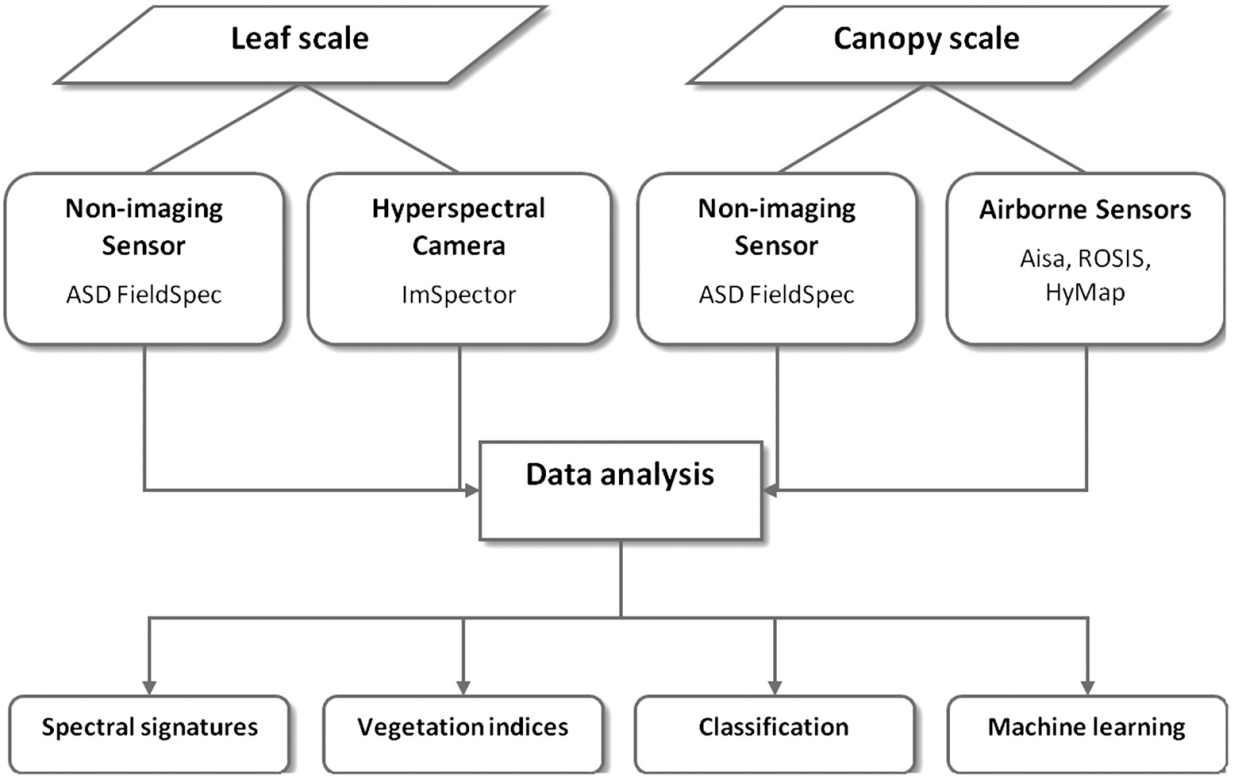

Figure 1.1: Concept of data assessment and data analysis on different scales with specific hyperspectral sensors.

2. LITERATURE REVIEW

2.1 Precision Agriculture

The use of innovative technologies collectively named 'Precision Agriculture' is a promising approach to optimize agricultural production of crops. In field crop production precision agriculture methodologies are applied to site-specific application of fertilizer or pesticides, automatic guidance of agricultural vehicles, product traceability, on-farm research or management of production systems (Gebbers and Adamchuk, 2010). Recently precision agriculture also enhances management decisions in livestock production, pasture management, viticulture, and horticulture (Gebbers and Adamchuk, 2010; Schellberg *et al.*, 2008). Precision crop production aims to match agricultural input and practices to the spatial and temporal variability within a field, instead of managing an entire field based on a hypothetical average. Small-scale site-specific differences can lead to great differences in yield and quality, thus a better use of resources to preserve the quality and quantity of agricultural products with respect on environmental resources is essential (Gebbers and Adamchuk, 2010).

The philosophy behind precision agriculture is not only including a direct economical optimization of agricultural production, it also stands for a reduction of harmful outputs into environment and non-target organisms. In particular a contamination of water, soil, and food resources with pesticides has to be minimized in crop production (Bongiovanni and Lowenberg-Deboer, 2004). With

this aim, site-specific fertilizer application was the first successfully implementation in 1988, soil sampling, yield mapping, and site specific herbicide application succeeded (Adamchuk *et al.*, 2004; Gerhards and Oebel, 2006; Stafford, 2000).

Against the background of food security and sustainable production, adequate technologies are fundamental for this agricultural practice (Zhang *et al.*, 2002). The implementation of information-based management systems into crop production since the mid 1980s implies a huge potential to modernize the agricultural practice. Since then different techniques for the characterization of soils and crops have been engineered and included into decision making systems. To name the most important ones, precision agriculture integrates different technologies like global positioning systems (GPS), geographic information systems (GIS), as well as different kind of sensors and therefore it demands a high level of expertise (Kühbauch and Hawlitschka, 2003; Stafford, 2000).

For the future an information-driven crop production as a combination of geospatial and agricultural data management will encourage the actual utilization of precision agriculture applications (Nash *et al.*, 2009; Reichardt *et al.*, 2009). Current research on precision agriculture for crop production focuses on the development of sensors for remote detection of crops and soil in real time. Relevant field parameters like soil properties, topography, water status, crop micro-climate, nutritional status, weeds, and pests and diseases as well as yield can be monitored and estimated. Integration of different remote sensing techniques and image analysis in combination with a global positioning system will be an essential step towards online application.

Still one limiting factor of a successful use of precision agriculture is the interpretation of properties derived from sensor data, rather than the collection of relevant data (Schellberg *et al.*, 2008). The interpretation of information and its implementation into robust decision support systems will improve the acceptance and implementation of precision agriculture techniques.

2.2 Precision crop protection and monitoring of plant diseases

Precision crop protection is a demanding challenge within precision agriculture and offers high potential to reduce the costs and environmental impact of fungicide use. According to the characteristics of plant diseases, a site-specific crop management requires a high density of spatial and temporal information with regard to the status of any crop growth-relevant parameter. The disease monitoring and decision-making process is the fundamental origin for a site-specific managing of spatially and temporally variable diseased field sites (Steiner *et al.*, 2008).

Currently two different approaches for site specific fungicide application are under examination; indirect decision-making by assessing canopy density or crop growth stage (Dammer *et al.*, 2008; Scotford and Miller, 2005) or direct disease detection (West *et al.*, 2003). These modern methods in plant production and crop protection are closely related to innovative technologies. Near-range and remote sensing, like hyper- and multispectral sensors or thermography in precision pest management possess multiple opportunities to increase the productivity of agricultural production systems and to reduce the environmental burden from pesticides. Real-time decision based on the information of the sensing system- 'spray or don't spray' can control cultural practices (Stafford, 2000). Due to high control costs and the environmental impact of fungicides, a site-specific application according to precision farming techniques – i.e. monitor and manage spatially-variable fields site-specifically (Stafford, 2000) – is of high interest. Therefore, a precise, reproducible, and time-saving disease monitoring method is essential (Bock *et al.*, 2010; Hillnhuetter and Mahlein, 2008; Steddom *et al.*, 2005). Remote sensing technologies are one basic tool of precision agricultural practice which can provide an alternative to visual disease assessment (Nutter *et al.*, 1990). West *et al.* (2003) have provided a detailed overview

of the sensor-based detection of stress. The variety/nature of a to monitored phenomenon and its environmental circumstances thereby defines the required sensor specifications (e.g. spatial and spectral resolution; temporal availability).

Many researchers have shown the potential of remote sensing techniques in the area of agriculture (Combal *et al.*, 2002; Doraiswamy *et al.*, 2003; Galvao *et al.*, 2009; Kruse *et al.*, 2006; Oppelt and Mauser, 2004; Thenkabail *et al.*, 2000) and also in the field of plant disease detection. E.g. Franke and Menz (2007), Huang *et al.* (2007), Moshou *et al.* (2004), Steddom *et al.* (2005), and Zhang *et al.* (2003) have proven the potential of spectral sensor systems for the detection of fungal diseases. To implement these sensors into precision plant protection technologies, they have to be robust, low-cost, and preferably real-time sensing (Zhang *et al.*, 2002).

2.3 Optical sensor systems

Innovative sensor systems can provide detailed and highly resolved information on crop systems and single plants. Different sensor types can assess different characteristics/parameters of the targeted objects, depending on signal-object interactions. Chaerle and van der Straeten (2001) gave a detailed overview on various sensor types used for assessing plant physiological parameters. Encouraging approaches are measurements based on thermal characteristics (Jones and Schofield, 2008; Lenthe *et al.*, 2007; Oerke *et al.*, 2006), chlorophyll fluorescence (Buschmann and Lichtenthaler, 1998; Chaerle *et al.*, 2007a; Rascher *et al.*, 2000), and reflectance of plants (Oppelt and Mauser, 2004; Peñuelas and Filella, 1998; Ustin *et al.*, 2009). As thermal response and modifications in photosynthesis of plants largely lack diagnostic potential for the identification of plant diseases, more sophisticated sensor systems have to be developed. The present work focuses on the use of non-imaging and imaging hyperspectral sensors for the detection, identification, and quantification of plant diseases. Most

of the optical sensor systems originate from geographical or remote sensing science, but there are various approaches in literature to implement these sensors into plant science.

The sensor evolution in remote sensing started from multispectral sensors to hyperspectral sensors and upcoming to ultraspectral sensors (Meigs *et al.*, 2008). These technically complex devices provide a multiplicity of information over the covered spectral range. But depending on the measured object and aim just few regions of the spectral range are of interest. Narrow spectral bands of hyperspectral sensors with a spectral resolution up to 1 nm are highly correlated to each other, redundant information is being measured. Likewise, understanding of spectral characteristics of the object and of signal-object interaction is elementary for optimization of remote sensing sensors for disease detection.

Currently reflectance sensors are classified on their spatial scale, on their spectral resolution, and by their way of data assessed, i.e. imaging or non-imaging sensors (Melesse *et al.*, 2007). Each sensor system covers a different scale, for example airborne or spaceborne far-range systems with a smaller spatial resolution, or near-range sensing systems with maximal spatial resolution. The maximal spatial resolution is defined by the minimum size of one pixel and hence the smallest identifiable symptom or structure. Technological advances in sensor development, in particular progress from multispectral broadband sensors to hyperspectral narrowband sensors have drastically increased the quantity and quality of available information.

The way of data recording is essential for data interpretation and analysis. Non-imaging sensors measure the averaged reflectance over a defined area (depending on the field of view of the sensor), a detailed inference of the reflectance source or pure object reflectance is not feasible (Mahlein *et al.*, 2010; Steiner *et al.*, 2008). Further to non-imaging spectroradiometers, hyperspectral cameras facilitate the detection of both, spectral and spatial information of an object. The information of a hyperspectral image is based on the spatial X- and Y-axes and

a spectral Z-axis, which allows a more detailed and allocated interpretation of the signal object interaction. Each spatially located pixel of an image contains the information of several wavelengths (Fig. 2.1). The use of hyperspectral imaging systems in plant pathology or in disease severity assessment is still in the state of research.

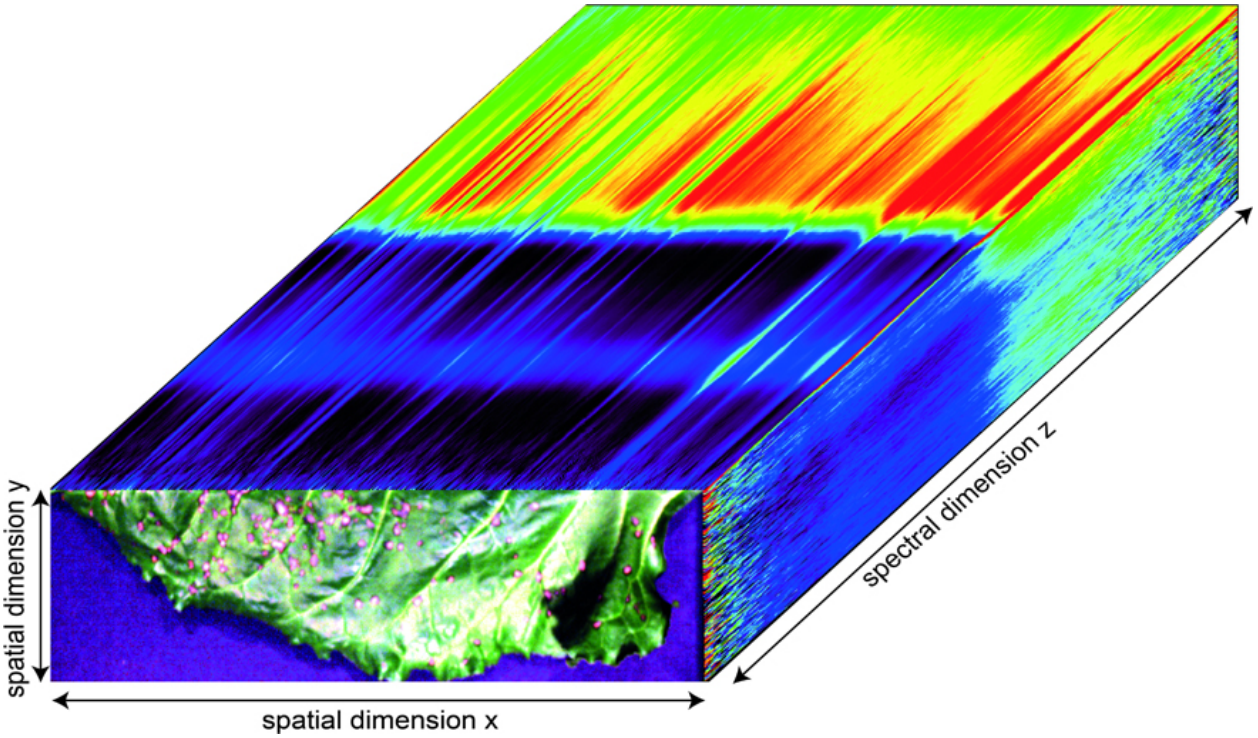

Figure 2.1: Structure of a hyperspectral image data cube of a sugar beet leaf with spatial dimensions X and Y, and the continuous spectrum with 210 reflectance values for an image-pixel from the spectral dimension Z.

2.4 Reflection of vegetation

After various processes of absorption, reflection, and scattering in the atmosphere, approximately 40% of the solar flux impacts to earth surface (Brooks and Miller, 1963; Lacis and Hansen, 1973). This electromagnetic radiation interacts with surfaces in different ways. The main interactions are I) absorption, i.e. the process by which energy of a photon is taken up by matter; II) transmission, the process of light passing through matter; and III) reflectance,

the process by which incident illumination reacts with matter and returns back from its surface, converted to radiant energy (Baranoski and Rokne, 2001). The reflectance is calculated by the ratio of radiant energy reflected from a surface to the radiant energy incident on the surface and is therefore independent of illumination variation (Lillesand and Kiefer, 2000).

Plant - sunlight interaction

In the interaction between sunlight and plant tissue, solar radiation is the engine of photosynthetic processes and therewith the source of life on earth. The attenuation of light insight plant leaves results from complex absorption and scattering processes, influenced by the biochemical composition and morphological characteristics of the leaf tissue (Fig. 2.2; Govaerts *et al.*, 1996). Leaf reflectance of sunlight in the visible (VIS, 400 to 700 nm), near infrared (NIR, 700 to 1100 nm) and short wave infrared (SWIR, 1100 to 2500 nm) are driven by multiple interactions: radiant energy absorption induced by leaf chemistry, scattering of light as a result of leaf surface and internal cellular structures, and radiant energy absorption induced by leaf water content (Fig. 2.3; Carter and Knapp, 2001; Jacquemoud and Ustin, 2001).

The VIS range is characterized by low reflectance, due to absorption by photoactive plant pigments. The chlorophyll amount in the parenchyma and spongy mesophyll controls the level of light absorption (Govaerts *et al.*, 1996). Chlorophyll a and chlorophyll b absorb blue (400 to 495 nm) and red light (620 to 700 nm), and transfer the absorbed energy into the photosynthetic electron chain (Curran, 1989; Gamon and Surfus, 1999; Sims and Gamon, 2002). Carotenoids absorb blue light (400 to 495 nm) and contribute this energy to the photosynthetic system as well (Sims and Gamon, 2002). Furthermore carotenoids have a trapping function to diminish light-induced damages by absorbing light in the UV-region (Merzylak *et al.*, 2008). Anthocyanins which have functions in photoprotection against UV light, osmotic regulation, and warming (Archetti *et al.*, 2009; Gould *et al.*, 1995; Lee *et al.*, 2003) have an absorption maximum at

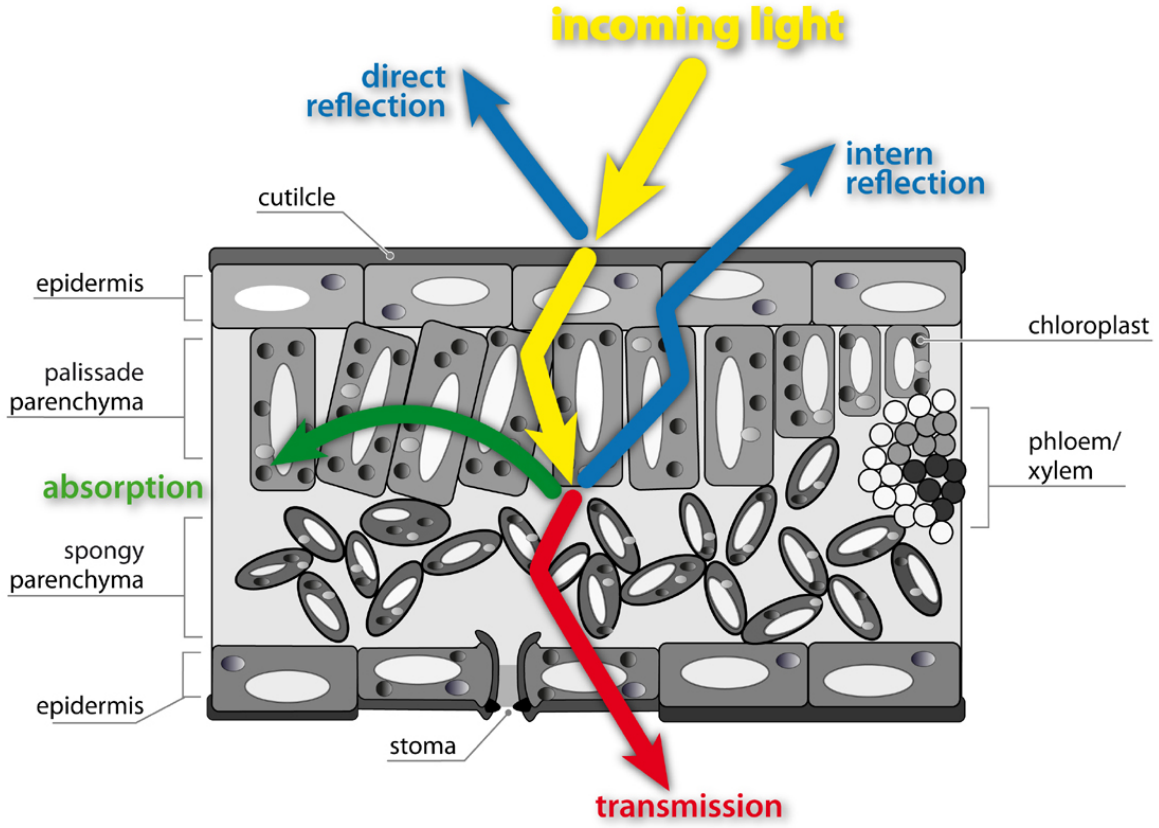

Figure 2.2: Reflection, absorption, and transmission processes in the interaction between sunlight and plant leaves.

550 nm. The transition from VIS to NIR is specified by the so called red-edge, the reflectance slope between 680 and 750 nm (Filella and Peñuelas, 1994).

The reflectance in the NIR is mainly dominated by leaf internal structure, leaf anatomy, and by the characteristics of the epidermal surface (e.g. wax compounds, hairs, etc) (Jensen, 2002). High reflection in this region is influenced by direct reflection on the leaf surface and multiple internal scattering processes within the leaf tissue (Jacquemoud and Ustin, 2001). Govaerts *et al.* (1996) emphasized that the epidermis plays an important role in determining the overall bidirectional reflectance of leaves. Leaf biochemical compounds like cellulose, lignin and carbohydrates causes minor absorption in this region (Fig. 2.3; Asner, 1998; Curran, 1989). Two weak water absorption bands around 970 and 1200 nm are also characteristic for the NIR (Curran, 1989).

Leaf reflectance in the SWIR region is mainly influenced by strong water absorption bands at 1200, 1400, 1940, and 2400 nm. Likewise, absorption of structural compounds like cellulose, lignin, starch, and protein occurs in the SWIR (Fig. 2.3; Asner, 1998; Curran, 1989).

Measurements on the canopy scale are additionally effected by several environmental factors. As a consequence of the complexity of canopy structure, the leaf area, the leaf angle distribution (planophile or erectophile stands), and the fraction of plant organs as green foliage, stems, florescence or reproductive organs impact reflectance patterns (Jackson and Pinter, 1986; Jacquemoud and Baret, 1990). Gitelson *et al.* (2002) emphasized that eminently reflectance in the NIR depends on factors such as canopy architecture, cell structure and leaf inclination and is thus more species-specific than reflectance in VIS, governed mainly by pigment content. Shadow, bidirectional effects, and soil background may interfere with the canopy reflectance as well (Biliouris *et al.*, 2007; Gitelson *et al.*, 2002; Oppelt and Mauser, 2004; Pinty *et al.*, 1998). Phenological stages of plants may also have an impact on spectral reflectance as well, as Delalieux *et al.* (2009) demonstrated in multi-temporal observations of apple plants. The function described by the ratio of the intensity of reflected light to the illuminated light for each wavelength forms the leaf/canopy spectral signature (Carter and Knapp, 2001; Jones *et al.*, 2003; West *et al.*, 2003). Consequently, biophysical and biochemical attributes of vegetation can be concluded from reflectance spectra.

Optical methods like hyperspectral imaging and non-imaging sensors have been proved to be a useful tool to detect changes in plant vitality (Apan *et al.*, 2005; Hatfield *et al.*, 2008; Nilsson, 1995; Pinter *et al.*, 2003; West *et al.*, 2003). Hence, spectral reflectance measurements are applicable for non-destructive assessment of the physiological status of vegetation (e.g. pigment content, leaf area), and in order to discriminate crop species or to detect the impact of stress like plant diseases, drought stress or nutrition deficiencies (Blackburn, 1998b,a,

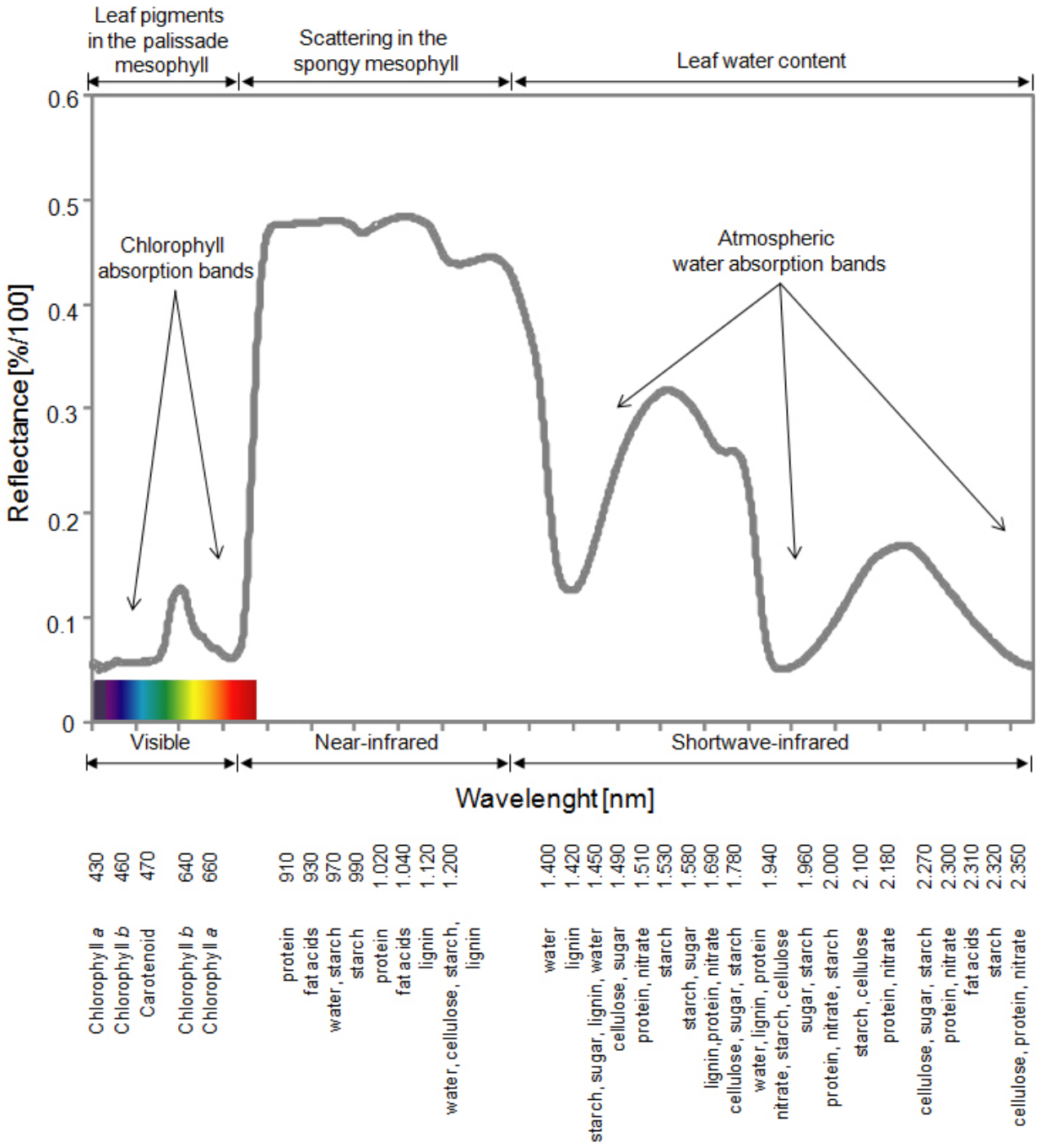

Figure 2.3: Vegetation reflectance spectrum with leaf reflectance influencing factors in the VIS, NIR, and SWIR and absorption characteristics of biochemical plant components (Curran, 1989; Jensen, 2002, both modified).

2007; Gitelson *et al.*, 2002, 2003; Moran *et al.*, 1997; Richardson *et al.*, 2001). Nonetheless, an interpretation of spectral reflectance measurements without knowledge on spectral behaviour of leaves is impossible.

2.5 Hyperspectral sensors for disease detection

Several studies have shown a convincing ability of reflectance measurements in discriminating between healthy and stressed plants. Disease symptoms often result from physiological changes in plant metabolism brought about by the pathogen (Apan *et al.*, 2005; Nilsson, 1995; Oerke *et al.*, 2006). The impact of plant diseases on the physiology and phenology of plants, however, varies with the host-pathogen interaction and may cause modifications in pigments, water content, and tissue functionality of plants or in the appearance of pathogen-specific structures (Gamon and Surfus, 1999; Jing *et al.*, 2007; Pinter *et al.*, 2003). All these individual impacts may alter the spectral pattern of plants. Knowledge on the physiological effects of diseases on the metabolism and tissue structure of plants is therefore essential for the hyperspectral discrimination of healthy and diseased leaf and canopy elements (Moran *et al.*, 1997).

The best results for the detection of diseases were obtained in the VIS and NIR range of the spectrum. Steddom *et al.* (2005) demonstrated that multispectral disease evaluation can be used effectively to measure necrosis caused by *Cercospora* leaf spot in sugar beets. A detection of rhizomania in sugar beet fields was also feasible (Steddom *et al.*, 2003). Using a quadratic discriminating model based on reflectance, Bravo *et al.* (2003) could classify yellow rust infestation on winter wheat with a reliability of 96%. Yellow rust decreases the chlorophyll a concentration, which leads to an increase in canopy reflectance in the VIS range and a decrease in the NIR (Jing *et al.*, 2007). Larsolle and Muhammed (2007) computed disease-specific spectral signatures of *Drechslera tritici-repentis* infected spring wheat. Other researchers successfully used spectral data to detect *Magnaporthe grisea* on rice (Kobayashi *et al.*, 2001), *Phytophthora infestans* on tomato (Zhang *et al.*, 2002), *Venturia inaequalis* on apple trees (Delalieux *et al.*, 2007), yellow rust in wheat (Huang *et al.*, 2007), and *Dothistroma septospora* on pine trees (Coops *et al.*, 2003). Damages to crops caused by virus diseases (Naidu *et al.*, 2009) or insects (Board *et al.*, 2007; Carrol *et al.*, 2008; Xu *et al.*,

2007; Yang *et al.*, 2007) could also be detected using spectral sensors. However, most of these studies used airborne data for the discrimination between mature disease symptoms and healthy leaves at an advanced level of infection.

The detection of a specific plant disease and the discrimination between healthy and diseased plants was the main focus of several research groups. To bring this research forward into field, there are still some difficulties and open questions. First, from the technical side it is still open, which spatial and spectral resolution is required and following which sensor systems harbours the optimal specifications for disease detection (Steiner *et al.*, 2008). Second, an early detection, even before visible symptoms appear, was realized only by few working groups using different technical and analytical approaches (Bravo, 2006; Chaerle *et al.*, 2007b; Rumpf *et al.*, 2010). Third, the assessment of the disease severity or quantification of diseases has to be implemented in further studies. Larsolle and Muhammed (2007) classified disease severity from hyperspectral reflectance in wheat and barley, compared to visual assessments using a nearest neighbour classifier with an accuracy of 86.5%. Fourth, the sensor system should be able to differentiate between different kinds of stresses, especially different diseases. Most stress factors, such as diseases, nutrient deficiency or water stress induce symptoms with little distinguishing spectral characteristics (Stafford, 2000). Recently Moshou *et al.* (2006) discriminated between yellow rust infection and nitrogen deficiency and Qin *et al.* (2009) – using hyperspectral near range imaging – differentiated citrus canker from different kinds of citrus diseases on grapefruit.

Since most of the published studies have used non-imaging hyperspectroscopy, the application of hyperspectral imaging focusing on spectral information of disease symptoms is limited. Bravo *et al.* (2003) used in-field spectral images for an early detection of yellow rust infected wheat, Nansen *et al.* (2009) analyzed hyperspectral data cubes for the detection of insect-induced stress in wheat plants, and Polder *et al.* (2010) have combined different optical sen-

sors for the detection of tulip breaking virus. By now, hyperspectral imaging is more widespread in the field of monitoring fruit/food security and quality. Balasundaram *et al.* (2009) and Qin *et al.* (2009) developed a hyperspectral imaging approach to detect canker lesions on citrus fruits. In other studies hyperspectral imaging has been successfully applied for quality assessment of pickling cucumbers, maize kernels, poultry carcasse or apples (Ariana *et al.*, 2006; Nansen *et al.*, 2008; Park *et al.*, 2007; Xing *et al.*, 2007). Though the use of reflectance measurements in plant pathology research started about 20 years ago, this is still a new technology, not fully tested or adapted to the needs of plant disease detection and severity assessment (Bock *et al.*, 2010).

2.6 Analysis of hyperspectral data

Characteristic for the use of non-imaging hyperspectrometers and especially of hyperspectral imaging systems is the recording of high amounts of information on the object acquired at the same time. Since large amounts of data also implies enormous file sizes and computing times, the analysis of hyperspectral data is a complex domain, and different approaches can be used to obtain the results.

Reflection of contiguous wavebands of electromagnetic radiation by an object results in a spectral signature, the basis of hyperspectral data analyses. Anomalies or differences between spectral signatures can be distinguished by calculating difference spectra, ratios or derivations (Carter and Knapp, 2001; Pietrzykowski *et al.*, 2006; Richardson *et al.*, 2001; Smith *et al.*, 2004; Xu *et al.*, 2007). Different parts of the spectral signatures can be correlated to biochemical or biophysical characteristics (Blackburn, 1998b,a, 2007; Carter and Spiering, 2002; Delalieux *et al.*, 2005; Fourty *et al.*, 1996; Gitelson *et al.*, 2001, 2002; Jacquemoud *et al.*, 1995; Le Maire *et al.*, 2004; Richardson *et al.*, 2001; Ustin *et al.*, 2009). Hosgood (1993) and Jacquemoud *et al.* (1995) established a detailed

database called LOPEX, including spectral reflectance data of over 50 plant species and their corresponding biochemical constituents like lignin, proteins, cellulose, starch, chlorophyll, or water. Jacquemoud and Baret (1990) developed the well established model PROSPECT describing leaf optical properties from 400 nm to 2500 nm. Le Maire *et al.* (2004) tested and established several leaf chlorophyll vegetation indices using this leaf-radiatic transfer model to determine the chlorophyll content.

Spectral vegetation indices

Based on the understanding of these principles and by using further results of analytical investigations, spectral algorithms, based on specific wavelengths of spectral signatures of vegetation, have been developed (Blackburn, 1998b; Carter and Miller, 1994; Gamon and Surfus, 1999; Haboudane *et al.*, 2004; Laudien *et al.*, 2003; Peñuelas *et al.*, 1997). Spectral vegetation indices (SVIs) are widely used for monitoring, analyzing, and mapping temporal and spatial variation in vegetation (Gitelson *et al.*, 2002). By calculating ratios of several bands at different ranges of the spectrum, SVIs result in a reduction of data dimension, which may be also useful in effective data analysis for disease discrimination. They are highly correlated to several biochemical and biophysical plant parameters indicating plant health or vitality and form the basis for many remote sensing applications in crop management. As pigment concentrations provide information on the physiological state of leaves, pigment-specific SVIs may be useful in detecting stresses caused by fungal diseases.

Several approaches have shown that vegetation indices are related to characteristics of crops and in principal they have the potential to detect plant diseases (Hatfield *et al.*, 2008; Thenkabail *et al.*, 2000). E.g., Graeff *et al.* (2006) used hyperspectral reflectance for the detection of powdery mildew (*Blumeria graminis* sp. *tritici*) and take-all disease (*Gaeumannomyces graminis* sp. *tritici*) of wheat, Jing *et al.* (2007) correlated the severity of yellow rust to SVIs, Laudien *et al.* (2003) developed a modified chlorophyll absorption integral for *Rhizocto-*

nia late rot detection in sugar beet, and Delalieux *et al.* (2005) used vegetation indices for the assessment of apple scab due to *Venturia inaequalis*. Steddom *et al.* (2005) calculated SVIs from multispectral data from sugar beet fields and compared these indices to disease severity, visually rated by plant pathologists. Since indices commonly used in remote sensing of vegetations are not disease-specific, the development of disease specific indices could improve the specificity and sensitivity of SVIs for disease detection.

Classification algorithms

In remote sensing applications, many classification and change detection techniques have been developed to obtain maximal information from hyperspectral data and images. Classification is a procedure of assigning a spectral signature to a characteristic group or class, and confines these groups from each other, respectively. The classes can be predefined (supervised classification) or non-predefined (unsupervised classification). Change detection is the process of identifying differences in the state of a spectral signature by observations at different times (Singh, 1989). Since disease epidemiology and symptom development is causing temporal and spatial changes in vegetation reflectance, most classification techniques from remote sensing applications are likely to be useful for the detection of disease-induced spectral changes. Principal component analysis (PCA), spectral mixture analysis (SMA), spectral angle mapper (SAM), and machine learning methods like artificial neural networks (ANN) or support vector machines (SVM) are the most common methods used for data analysis. Although all these algorithms have their own specifications and merits, there is not a single approach which is optimal for all applications (Lu *et al.*, 2004).

The Spectral Angle Mapper is a supervised classification algorithm, comparing the spectral similarity between image spectra to reference spectra (Kruse *et al.*, 1993). This method calculates the spectral angle between image spectra and reference spectra in an n-dimensional space, whereas n is the number of hyper-

spectral bands of the spectral range. Small spectral angles correspond to high similarity, large spectral angles to less similarity. Given spectra from a visually classified pixel can be used as reference spectra from a spectral library. Based on the number of reference spectra, classification of pixels can be processed simultaneously. The accuracy of SAM algorithms is assessed by comparing the classification result with actual disease data (ground truth). The SAM classifier is a common tool in geographical analyses of hyperspectral data for land cover classification (Dennison *et al.*, 2004), to study ecosystem processes (Ustin *et al.*, 2004), and for the classification of urban surface cover (Segl *et al.*, 2003).

2.7 Host-pathogen model

Sugar beet (*Beta vulgaris* L. var. *altissima*) is a member of the *Chenopodiaceae*. The biannual plant forms a fleshy taproot accumulating assimilates like polysaccharides or nitrogen compounds. Sugar beet was first cultivated for sugar production in Europe in the eighteenth century (Van Cleef, 1915). Sugar from sugar beet accounts for 30% of the world's sugar production. Sugar extraction is a highly developed process and high performance varieties from plant breeding may provide high sugar yields. But foliar fungal diseases are serious threats in worldwide sugar beet production. *Cercospora beticola* (Sacc.), *Erysiphe betae* (Vanha) Weltzien and *Uromyces betae* (Persoon) Lev., causing *Cercospora* leaf spot (CLS), powdery mildew (PM), and sugar beet rust (SBR), respectively, are the most relevant fungal leaf pathogens causing losses in yield quantity and quality (Wolf and Verreet, 2002). Disease-specific symptoms of the leaf pathogens cause destruction of the leaf tissue. The sugar beet productivity is highly influenced by solar radiation captured by the crop canopy (Jaggard *et al.*, 2009). Losses are primarily attributed to a reduction in the photosynthetically active leaf area, and secondly to a subsequent reversion of assimilate allocation from the roots to form new foliage. A reduction in root

weight and in the sugar fraction of harvested roots is the consequence (Franc, 2010). Infection process, leaf colonization and spread of each pathogen have specific optima for environmental factors – temperature, relative humidity, leaf wetness – and host-intrinsic factors like nutritional status or ontogenetic status. A heterogenic attribution of the pathogens in the growing area and even a spatial and temporal variability within a field may be monitored (Mahlein *et al.*, 2009; Wolf and Verreet, 2002).

The three foliar diseases are associated with typical symptoms. The perthotrophic pathogen *C. beticola* causes leaf spots with a reddish brown margin of typically 2 to 5 mm diameter (Franc, 2010; Weiland and Koch, 2004; Wolf and Verreet, 2002). Under high temperature conditions and high relative humidity the leaf spots coalesce to form large necrotic areas (Vereijsssen *et al.*, 2006). Pathogenicity of *C. beticola*-isolates is associated with the synthesis of the pathotoxin cercosporin (Daub and Ehrenshaft, 2000). Causing yield losses approaching 40%, *Cercospora* leaf spot is the most important foliar disease in sugar beet production (Lartey *et al.*, 2010).

The biotroph pathogen *E. betae* relies on the functional metabolism of sugar beet tissue as a nutrient source (Francis, 2002). Characteristic symptoms of powdery mildew are white, fluffy mycelia, which covers the upper and lower site of the leaf. At mature infestation, leaf chlorosis and necrosis can be observed. An inhibition of photosynthetic CO^2 assimilation and a decrease of quantum efficiency of light use is also reported (Gordon and Duniway, 1981; Magyarosy *et al.*, 1976). Losses up to 30% can occur under dry and hot conditions during summer. Characteristic for powdery mildew is a fast spread by wind inside the crop stand and across different growing regions (Wolf and Verreet, 2002).

The basidiomycete *U. betae* also is an obligate biotroph plant pathogen. Typical symptoms of sugar beet rust are small pustules (0.5 to 1.5 mm), often encircled by a chlorotic ring, irregularly distributed over the leaves. Reddish-brown uredospores are released after rupturing the epidermal layer. Moderate

climate with temperatures around 20 °C and relative humidity up to 100% are supporting conditions for infection. Thus river and cost regions are imperiled areas (Wolf and Verreet, 2002).

2.8 Disease management of foliar sugar beet diseases

Yield quality and quantity are significantly influenced by crop stand management, in particular by disease control. Foliar diseases of sugar beet are commonly controlled by planting resistant cultivars, crop rotation, or by multiple fungicide applications. Since nonchemical, preventive alternatives like host plant resistance and crop rotation do not provide adequate disease control, fungicides are the most important tool for managing foliar diseases (Ioannidis and Karaoglanidis, 2010). Strategies of chemical control must be based on alternation of fungicides with different modes of action, use of products with mixtures of fungicides differing in the mode of action, and on a threshold-orientated management based on an accurate monitoring of the disease pressure (integrated disease management).

Detailed knowledge on the epidemiology of foliar pathogens and their impact on sugar yield has led to the development of several forecast and decision support systems like the IPM-model Sugar Beet (Wolf, 2001), CERCBET (Racca and Jörg, 2007), ProPlant (Frahm *et al.*, 1996), or BEETCAST (Pitblado and Nichols, 2005). The implementation of these systems has shifted fungicide applications from 'calendar based' spraying to a precise fungicide application considering multiple factors. These factors include disease susceptibility of sugar beet cultivar, planting date, weather data, micro-climate of the canopy, leaf wetness duration, inoculum level of pathogens, disease assessment and monitoring as well as characteristics of the fungicides (Windels, 2010; Wolf and Verreet, 2010). The success of these programs, however, demands a high level of engagement and of awareness of the farmer. Automation of disease assessment using

optical sensor systems can be useful in order to improve existing forecast models. Considerations of temporal and spatial heterogeneities of diseases in field would be just two future trends according to precision agriculture. A precise, reproducible, objective, and time saving monitoring process is a further benefit.

3. MATERIAL AND METHODS

3.1 Organisms

3.1.1 Plants

Sugar beet plants (*Beta vulgaris*, L.), cultivar Pauletta (KWS GmbH, Einbeck, Germany), were used as experimental plants.

3.1.2 Pathogens

Cercospora beticola (Sacc.)
Erysiphe betae (Vanha)
Uromyces betae (Persoon) Lev.
All pathogens originated from the pathogen collection of INRES - Phytomedicine and were collected from the experimental field site Bonn Poppelsdorf, Germany.

3.2 Plant cultivation

3.2.1 Controlled conditions

Sugar beet seeds, cultivar Pauletta were pre-grown in small pots and were piqued when the primary leaves had fully developed. For different experimental

setups, sugar beet plants were cultivated in different pots. Seedlings were transferred into a commercial substrate (Klasmann-Deilmann GmbH, Germany) in plastic pots (⌀13 cm; ⌀17 cm) for experiments on the leaf level. For experiments on canopy level, sugar plants were grown in plant boxes (80 x 120 x 60 cm) in a soil mixture of 50% commercial substrate, 30% C-horizon and 20% sand, or in quadratic big pots (20 x 20 x 30 cm). Plants were cultivated in a controlled environment at 23/20 °C (day/night), 60 ± 10% relative humidity (RH) and a photo-period (> 300 µmol m^{-2} s^{-1}) of 16 h per day. Plants were watered as necessary and fertilized weekly with 100 ml of a 0.2% solution of Poly Crescal (Aglukon GmbH, Düsseldorf, Germany). Plants were used for the experiments after reaching growth stage (GS) 16 (BBCH scale; Meier *et al.*, 1993). Control plants without fungal inoculation were kept healthy by applying the fungicide Vegas®, (Spiess-Urania, Germany; cyflufenamid 51.3 g/l, application rate 650 µl/l) two days before inoculation of the other plants. In order to avoid an unintentional infection of plants inoculated with *C. beticola* and *U. betae*, respectively, with powdery mildew, the selective fungicide Fortress® (Dow AgroScience Ltd., United Kingdom; quinoxyfen 250 g/l, application rate 650 µl/l) was applied two days before inoculation.

3.2.2 Field experiment

A field experiment was conducted at the research station Klein-Altendorf (50° 36′ 55.3″ N, 7° 0′ 0.10″ E) of the University of Bonn in the growing season 2008. Sugar beet plants, cultivar Pauletta were sown on the 24th of April with 1 unit/ha. Three herbicide applications were undertaken to avoid the influences of weeds on sugar beet plant growth and canopy reflectance (10th of May, Betanal Expert®, Bayer CropScience, Mohnheim, Germany, phenmedipham 75 g/l, desmedipham 25 g/l, ethofumesat 151 g/l, application rate 1 l/ha, beetix®, Stähler GmbH & Co.KG, Stade, Germany, metamitron 696 g/l, application rate 1.5 l/ha; 20th of May, Betanal Expert® + beetix®, application

rate 1.25 l/ha + 1.5 l/ha; 28th of May, Betanal Expert® + beetix®, application rate 1.25 l/ha + 2 l/ha). The field was fertilized with 8.5 kg/ha nitro chalk on the 6th of April before sugar beet was sown. At the 20th of June sugar beet plants were fertilized with 8.5 kg/ha epsomite. Insecticide was applied on the 20th of June to avoid leaf damages caused by insects (Karate Zeon®, Syngenta Agro GmbH, Maintal, Germany, lambda-cyhalothrin 100 g/l, application rate 75 l/ha). The field size was about 3 ha with a homogeneous flat topography. The field was divided into two treatments (Fig. 3.1); plot A without fungicide application in order to monitor the occurrence of fungal diseases within the growing season, plot B was treated at GS 39 with the fungicide Spyrale (Syngenta Agro GmbH, Maintal, Germany, difenoconazol 100 g/l; fenpropidin 375 g/l, application rate 1 l/ha) to avoid fungal infections.

Figure 3.1: Field experiment, Klein-Altendorf 2008; plot A without fungicide application, plot B was treated with fungicides to avoid fungal infections of sugar beets.

3.3 Production and inoculation of pathogens

3.3.1 *Cercospora beticola*

Inoculum of *C. beticola*, causal agent of *Cercospora* leaf spot was obtained from heavily infected sugar beet leaves that were stored at room temperature after

slowly drying. For sporulation the leaves were wetted and incubated for 24 h under 100% relative humidity (RH). The spores were washed off with tap water with one droplet of Tween 20 per l. The spore suspension was adjusted to 40000 spores per ml and was sprayed onto the upper and lower side of the leaves. After inoculation, the plants were covered with plastic bags to create 100% RH at 25/20 °C (14/10 hours day/night) for 48 h. For further incubation, plastic bags were removed and the plants were transferred to 23/20 °C (14/10 hours day/night) and 60 ± 10% RH.

3.3.2 *Erysiphe betae*

E. betae, causing powdery mildew of sugar beet was preserved on vital sugar beet plants in the greenhouse. For inoculation, heavily infested plants were used as an inoculum source of *E. betae*. Before these plants were transferred into an inoculation chamber, old conidia-spores were removed from the leaves by agitating. Young, virulent conidia were formed within 24 h and were used for inoculation. Healthy plants were placed under the infested plants in a chamber where a ventilator ran for 5 seconds in order to distribute *E. betae* conidia evenly on the leaf surfaces. Plants were left overnight and were subsequently transferred to a greenhouse at 23/20 °C (14/10 hours day/night) and 60 ± 10% RH, separated from the other plants in order to avoid unintentional infections of healthy plants.

3.3.3 *Uromyces betae*

Spores of *U. betae*, the pathogen causing sugar beet rust, were harvested from sporulating uredia and stored at 8 °C. For inoculation a suspension of *U. betae* urediniospores in tap water (with one droplet of Tween 20 per l), with 40000 spores per ml, was prepared and sprayed onto the upper and lower side of sugar beet leaves. The plants were covered with plastic bags for 48 h (100% RH)

and were incubated in a climate chamber at 19/16 °C (14/10 hours day/night). After removing the plastic bags, the plants were transferred to 23/20 °C and 60 ± 10% RH.

3.4 Assessment of plant physiological and physiochemical parameters

3.4.1 Disease assessment

In greenhouse experiments, disease severity was assessed daily after inoculation according to Wolf and Verreet (2002). For measurements on the leaf scale, the percentage of diseased leaf area of the measured leaf in relation to healthy leaf tissue was estimated visually. For powdery mildew infected plants, the percentage of leaf area covered with white fluffy mycelium in relation to total leaf area was recorded. For canopy scale measurements, the diseased leaf area of plant canopy was classified. Furthermore digital RGB images of the leaves were taken. On the field scale, ground truth data, in particular incidence (= % plants/leaves infected) and severity (= % leaf area affected) of diseases were collected at 50 sample points and geo-referenced.

3.4.2 Microscopic investigations

3.4.2.1 Stereo microscopy

A Leica MZ16 F stereomicroscope (Leica Microsystems, Wetzlar, Germany) was used for monitoring the symptom development of *C.beticola*, *E. betae*, and *U. betae* during pathogenesis. Images were taken daily after inoculation with a fitted digital camera. The images were saved using the programm 'Discus' (Technisches Büro Hilgers, Königswinter, Germany).

3.4.2.2 Scanning electron microscopy

Scanning electron microscopic observations were obtained using a Phenom scanning electron microscope (FEI Europe, Eindhoven, Netherlands) with a 5 kV thermionic source and a backscattered electron detector[1]. Freshly harvested leaves from inoculated sugar beet plants were sputter coated at 30 mA for 100 seconds with platinum.

3.4.3 Pigment assessment

The concentration of sugar beet leaf pigments, which is related to plant vitality and absorption of solar light, was assessed during the progress of diseases.

3.4.3.1 SPAD-meter measurements

A Minolta SPAD-502 meter (Minolta Camera Ltd., Osaka, Japan), was used for non-destructive assessment of leaf chlorophyll content. The instrument determines the relative amount of chlorophyll present, by measuring the transmittance of the leaf at two wave bands (600 to 700 nm and 400 to 500 nm). The dimensionless SPAD-units are proportional to the amount of chlorophyll.

3.4.3.2 Extraction of leaf pigment

Destructive chlorophyll a and b and carotenoid extraction was performed daily after inoculation of pathogens. Five leaf discs with a diameter of 1 cm were collected from the centre of sugar beet leaves, beside the middle leaf vein for each treatment. The content of chlorophyll a, chlorophyll b, total chlorophyll as well as of carotenoids was determined using the method of Hiscox and Israelstam (1979). Leaf disc were weighted and the pigments were extracted in 99% dimethylsulfoxide (DMSO) for 24 h in the dark.

[1] Kindly supported by C. Pape, LOT and Dr. F. Fischer, FZ Jülich

3.4.3.3 Measurement of pigment concentrations

Absorption of the extract was measured at 470 nm, 645 nm and 663 nm with a double beam UV/VIS spectrophotometer, Uvikon 933 (BioTek Instruments, USA). Pigment concentrations were calculated according to Hiscox and Israelstam (1979):

1. $\text{Chl}_\text{a}\ [\mu\text{g Chl/g}] = \frac{\text{solvent [ml]}}{\text{weighted sample [g]} \cdot (12.7 \cdot \text{A}663 - 2.79 \cdot \text{A}645)}$

2. $\text{Chl}_\text{b}\ [\mu\text{g Chl/g}] = \frac{\text{solvent [ml]}}{\text{weighted sample [g]} \cdot (20.7 \cdot \text{A}645 - 4.62 \cdot \text{A}663)}$

3. $\text{Chl}_\text{total}\ [\mu\text{g Chl/g}] = \frac{\text{solvent [ml]}}{\text{weighted sample [g]} \cdot (17.9 \cdot \text{A}645 + 8.08 \cdot \text{A}663)}$

4. $\text{Car}\ [\mu\text{g Car/g}] = \frac{\text{solvent [ml]}}{\text{weighted sample [g]} \cdot (4.37 \cdot \text{A}470 - 0.0143 \cdot \text{Chl}_\text{a} - 0.454 \cdot \text{Chl}_\text{b})}$

3.5 Sensor systems/Hyperspectral measurements

For the acquisition of hyperspectral information from sugar beet leaves various non-imaging and imaging sensor systems were used.

3.5.1 ASD FieldSpecPro FR/ASD FieldSpecPro JR

Spectral reflectance was measured with two different handheld non-imaging spectro-radiometers, the ASD FieldSpecPro FR and the ASD FieldSpecPro JR (Analytic Spectral Devices (ASD), Boulder, USA). The spectral range of the ASD FieldSpecPro is from 350 nm to 1100 nm. Because the reflectance spectra data were noisy at the extremes, only values between 400 to 1050 nm were analyzed. The spectral sampling interval was automatically interpolated from 1.4 nm to 1 nm steps using a linear equation by the RS3 spectral acquisition

software (Analytic Spectral Devices (ASD), Boulder, USA). The spectral range of the ASD FieldSpecPro JR is from 350 to 2500 nm. The sampling interval is 1.4 nm from 350 to 1050 nm and 2 nm for the range 1050 to 2500 nm. Resultant reflectance values were afterwards interpolated by the RS3 software to 1 nm steps. Spectral jumps between the spectrometer's detectors were removed using the ASD ViewSpecPro software (Analytic Spectral Devices (ASD), Boulder, USA). The instruments were warmed up for 90 min previous to measurement to increase the quality and homogeneity of spectral data. Instrument optimization and reflectance calibration were performed prior to sample acquisition. The average of 25 dark-current measurements was calibrated to the average of 25 barium sulphate white reference (Spectralon, Labsphere, North Sutton, NH, USA) measurements. For measurements on the leaf scale, a plant probe foreoptic with a leaf clip holder was used. The contact probe foreoptic has a 10 mm field of view and an integrated 100 W halogen reflector lamp. The internal light source enables constant and reproducible illumination conditions. Thus, the integration time was adjusted to 17 ms per scan constantly. Finally, reflectance spectra were obtained by determining the ratio of recorded sample data to data acquired for the white reflectance standard. Each sample scan represented an average of 25 reflectance spectra. Because reflectance spectra were assessed under constant light and temperature conditions with the plant probe foreoptic, pre-processing to smooth the spectrum and to reduce signal noise was not necessary.

In each treatment (inoculated and non-inoculated sugar beet leaves), spectra from 15 plants and 2 leaves per plant from the adaxial leaf surface were taken. To realize a multi-temporal measurement, the sugar beet leaves were signed and the leaf clip was placed in the middle of the leaf beside the middle leave vein. Reflectance of leaves was measured with the ASD FieldSpecPro FR daily after inoculation, with the ASD FieldSpecPro JR 0, 7, 14, and 21 days after inoculation (dai). Measurements on the canopy level were conducted in a dark room. A pistol grip foreoptic was used and mounted on a tripod, 50 cm above the

target canopy. To realize constant and homogeneous illumination conditions, three ASD-Pro-Lamps (Analytic Spectral Devices (ASD), Boulder, USA) surrounded the target area. Sugar beet plants, grown in boxes were placed under the optic and, using a field of view of 25°, two areas of each plant box could be measured. For reflectance normalisation a barium sulphate white reference was centred under the pistol grip optic on the same level with the sugar beet canopy. Reflectance spectra were obtained with an integration time of 134 ms per scan, 25 averaged reflectance spectra resulted in one sample scan. Each sample scan was repeated five times, the plant boxes were measured daily from day 0 to day 21 after inoculation. The Savitzky-Golay filter (Savitzky and Golay, 1964), a simplified least square procedure was applied afterwards, in order to smooth the spectrum and to reduce the signal noise. A filtersize of 32 and polynomial degree of 4 were used as parameters for the Savitzky-Golay filter.

3.5.2 Hyperspectral camera system ImSpector V10E

Hyperspectral images were taken in a dark chamber using the hyperspectral imaging system ImSpector V10E (Spectral Imaging Ltd., Oulu, Finland), with a spectral range from 400 to 1000 nm (Fig. 3.2). The ImSpector V10E system is a line scanner with a spectral resolution up to 2.8 nm. The maximal image size of the sensor slot results in 1600 pixels per line with a sensor pixel size of 0.0074 mm. Limited by the distance between target and sensor system (0.60 m), a spatial resolution of 0.019 mm per pixel could be achieved. To obtain images from the target, a mirror scanner was mounted in front of the objective lens. The maximal field of view of the mirror scanner is 80°. Using the software SpectralCube (Spectral Imaging Ltd., Oulu, Finland) the angle of the mirror scanner as well as the spectral and spatial resolution could be adapted manually to the target. Images on leaf level were taken with spectral binning 4 and spatial binning 1, on canopy level with spectral binning 4 and spatial binning 2. Frame rate and exposure time was adjusted to the chosen

binning and to the target. The camera system was focused manually to a calibration bar (Spectral Imaging Ltd., Oulu, Finland) with black rhombi on a white background, placed in the same distance to the camera as the target. During measurements constant illumination intensity was provided by ASD-Pro-Lamps (Analytic Spectral Devices (ASD), Boulder, USA) radiating a near-solar light spectrum. The distance between lamps and the leaf target was 50 cm with a vertical orientation of 45°, between lamps and canopy target 80 cm. For subsequent calculation of reflectance, three images were grabbed. To examine the sensor sensitivity, a dark current image by closing an internal shutter of the camera and an image of a white reference bar (Spectral Imaging Ltd., Oulu, Finland), with the same horizontal size and on the same level like the target area were recorded, both with the same exposure time. Subsequently an image of the target area was recorded with improved exposure time.

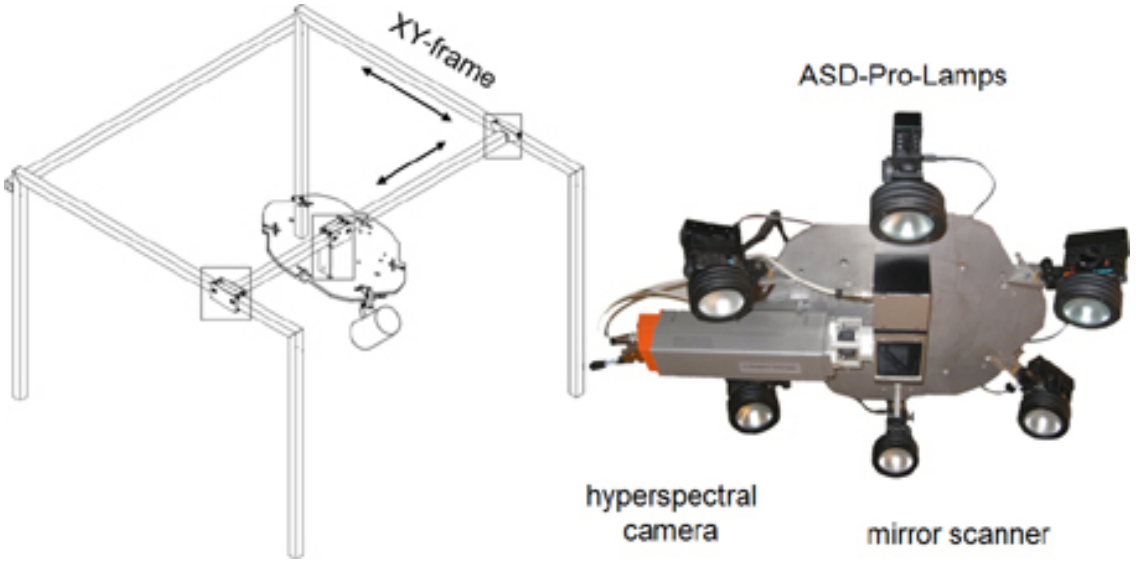

Figure 3.2: Manual positioning XY-frame and hyperspectral sensor system ImSpector V10 with the mirror-scanner, surrounded by six ASD-Pro-Lamps. The XY-frame was developed by the technical service of the Institute of Agricultural Engineering, University of Bonn.

3.5.2.1 Technical setup

The hyperspectral sensor system ImSpector V10 was mounted on a manual positioning XY-frame, developed by the technical service of the Institute of Agri-

cultural Engineering, University of Bonn surrounded by six ASD-Pro-Lamps (Analytical Spectral Devices Inc., Boulder, USA), placed in a dark chamber (Fig. 3.2)[2]. In order to realize optimal and reproducible illumination and constant measurement conditions the plants were moved into the dark chamber. Starting two days after inoculation, hyperspectral images were taken daily until 21 dai. All measurements were recorded between 8:00 and 12:00 AM in order to reduce the effect of diurnal physiological changes in plant processes. For image acquisition on the leaf level, the pots with sugar beet plants were placed on mobile tables (0.8 m x 0.8 m, four plants per table) 2 dai. According to Chaerle *et al.* (2007a), the fifth fully developed leaf pair of each sugar beet plant was fixed horizontally on a frame between a grid patterns made of two layers of rubber laminated mesh wire (Fig. 3.3). The frame and the grid pattern were coated with a black, matte colour to reduce the reflectance of the material. The mesh wire largely avoided movements of leaves which were subdivided into equally-sized squares (2 x 2 cm) on the images.

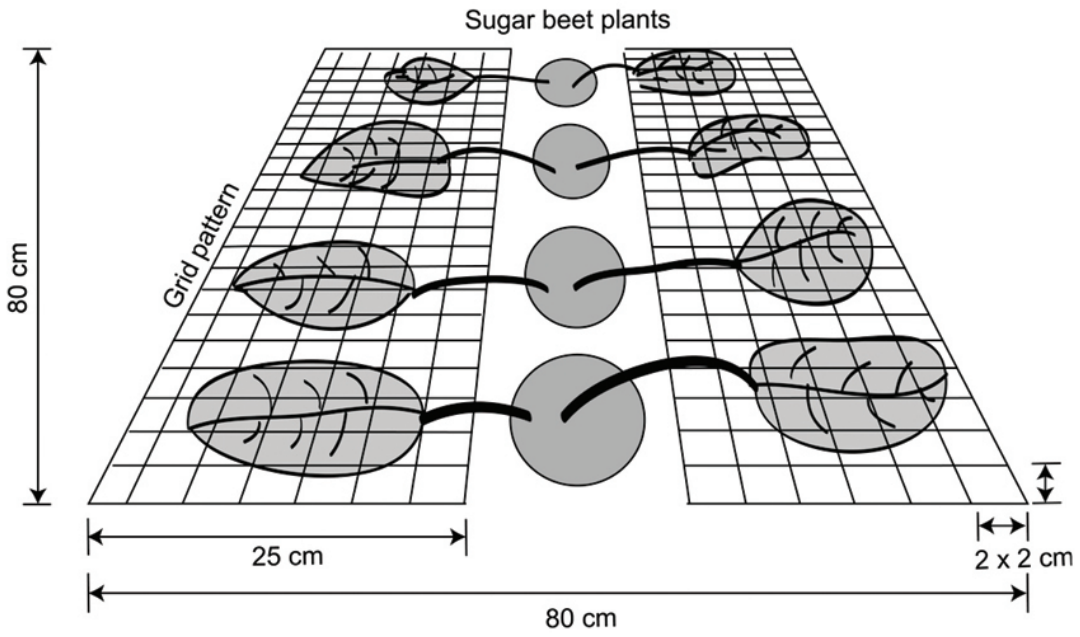

Figure 3.3: Schematic diagram of sugar beet leaves fixed under a grid pattern. Two leaves per plant were chosen for multi-temporal hyperspectral imaging and were measured consecutively.

[2] Kindly supported by Dr. L. Damerow and A. Berg, Institute of Agricultural Engineering, University of Bonn

3.5.2.2 Normalization and preprocessing of hyperspectral data

Calculations of reflectance relative to a white reference bar and the dark current measurement were performed using the ENVI 4.6 + IDL 7.0 software (ITT Visual Information Solutions, Boulder, USA). After this normalization process the Savitzky-Golay filter (Savitzky and Golay, 1964) was applied to smooth the signals from hyperspectral images. The parameters for the smoothing process were 5 supporting points to the left and right, respectively, and a polynomial degree of 5. The pre-processed images were used for further analysis using the ENVI 4.6 + IDL 7.0 software.

3.5.3 Airborne sensors

On 1th July 2008 hyperspectral data from the high resolution airborne imaging sensor system ROSIS were acquired at GS 39 of sugar beets. The Reflective Optics Systems Imaging Spectrometer (ROSIS) was developed by the German Aerospace Center (DLR), Cologne, Germany. The sensor provides 103 spectral bands in the range from 430 to 850 nm with a spectral resolution of 4 nm. The flight height of about 2880 meters resulted in a ground resolution of 2 m for the ROSIS sensor. A HyMap flight campaign was conducted on 6th August 2008 at GS 45. HyMap is an aircraft-mounted hyperspectral sensor (Integrated Spectronics, Sydney, Australia) which uses a whisk-broom scanner with 512-pixel per line. It provides 126 spectral bands between 450 and 2500 nm. The bandwidths depend on the full width at half maximum (FWHM) of the spectral bands, which is 15 nm in the VIS and NIR, 13nm in SWIR1, and 17nm in SWIR2. A nominal spatial resolution of 4 m was achieved. Both flight campaigns were realized by the DLR. The datasets were radiometric calibrated and an atmospheric correction was carried out using ATCOR4 to derive nadir-normalized ground reflectance by the DLR, Oberpfaffenhofen, Germany.

3.6 EM 38 soil sensor

The apparent electrical conductivity (ECa) of the soil in Klein-Altendorf was measured using an EM 38 (Geonics Ltd., Mississauga, Ontario, Canada) on 15^{th} of April 2008[3].

3.7 Data analysis

3.7.1 Development of spectral signatures

Characteristic spectral signatures were evaluated for each disease and diseased leaves, respectively, depending on the day after inoculation and the disease stage. Changes in spectral signature during pathogenesis as well as between the diseases have been analyzed. In order to extract the wavelength(s) suitable for the differentiation among diseases and disease severities, difference spectra were calculated by subtracting the mean reflectance μ of diseased sugar leaves from that of healthy sugar beets at each wavelength λ, where $\lambda = 400 - 1050$ nm.

$$\text{Diff}_\lambda = \mu_{\text{diseased}} - \mu_{\text{healthy}}$$

Reflectance sensitivity for each wavelength was calculated as the reflectance of diseased leaves divided by the mean reflectance of healthy leaves.

$$\text{Sensitivity}_\lambda = \mu_{\text{diseased}} / \mu_{\text{healthy}}$$

Changes in the spectral signature for each disease were evaluated by simple linear correlation analyses. Correlations between disease severity and reflectance data were tested by computing Pearson's coefficient of correlation (r) using the Superior Performing System SPSS 17.0 (SPSS Inc., Chicago, USA). With correlation curves, the intensity and direction of the relationship of each narrow band of the spectrum was visualized and specific wavebands of the spectral signature, closely related to disease infestation were selected.

[3] Kindly conducted by C. Hbirkou, INRES-soilscience, University Bonn

3.7.2 Spectral vegetation indices

Spectral vegetation indices (SVIs) are algorithms, calculated from hyperspectral data, which are closely correlated to specific plant parameters, e.g. plant vitality, biomass, pigment, or water content. An advantage of calculating SVIs is a reduction of data dimensionality from hyperspectral sensors. To evaluate the suitability of SVIs widely applied in remote sensing sciences for the identification and discrimination between foliar diseases of sugar beet, SVIs related to various plant parameters were calculated. Tab. 3.1 lists the SVIs calculated and summarizes information related to disease relevant biophysical and biochemical parameters of plants from literature. Simple ratio (SR), modified simple ratio (mSR), normalized difference vegetation index (NDVI), red edge inflection point (REP), and plant senescence reflectance index (PSRI) have been used as indicators for plant vitality and for the estimation of plant biomass. Normalized difference index (ND), modified normalized difference index (mND), photochemical reflectance index (PRI), structure insensitive pigment index (SIPI), pigment-specific simple ratios for chlorophyll a and b (PSSRa /PSSRb) and for carotinoids (PSSRc), pigment-specific normalized differences for chlorophyll a and b (PSNDa /PSNDb) and for carotinoids (PSNDc), the modified chlorophyll absorbtion reflectance index (MCARI), and the modified chlorophyll absorption integral (mCAI) are indices related to leaf pigments involved in photosynthesis. The anthocyanin reflectance index (ARI) is specific for the anthocyanins. The blue/green index (BIG2) analyses the relation between blue and green reflectance, the SumGREEN and SumVIS indices analyse absolute reflectance in the green region and in the VIS, respectively. Correlation and regression analyses between vegetation indices and disease severities for each disease were conducted. In a next step, index combinations were tested to classify different disease situations more specifically. 2D-scatter matrixes for all index combinations were mapped, and the best differentiating combinations were examined. Eight SVIs were used as features for supervised classification and early detection of plant diseases using support vector machines (see 3.7.4).

Table 3.1: Spectral vegetation indices and ratios correlated to various plant parameters used in this study.

Index	Equation	Indicator	Reference
Simple ratio	**SR** $= R800/R670$	Green biomass	Birth and McVey (1968)
Modified simple ratio	**mSR** $= (R750 - R445) / (R705 - R445)$	Green biomass	Sims and Gamon (2002)
Normalized difference index	**ND** $= (R750 - R705) / (R750 + R705)$	Chlorophyll content	Gitelson and Merzlyak (1994)
Modified normalized difference index	**mND** $= \frac{R750-R705}{R750+R705-2 \cdot R445}$	Chlorophyll content	Sims and Gamon (2002)
Normalized difference vegetation index	**NDVI** $= (R800 - R670) / (R800 + R670)$	Biomass, leaf area	Rouse *et al.* (1974)
Photochemical reflection index	**PRI** $= (R531 - 570) / (R531 + R570)$	Epoxidation state yanthophylls cycle; pigments and photo-synthetic radiation use efficiency	Gamon *et al.* (1992)
Structure insensitive pigment index	**SIPI** $= (R800 - R445) / (R800 + R680)$	Carotinoid: chlorophyll a ratio	Peñuelas *et al.* (1995)
Pigment specific simple ratio	**PSSRa** $= R800/R680$ **PSSRb** $= R800/R635$ **PSSRc** $= R800/R470$	Chlorophyll a Chlorophyll b Carotinoid	Blackburn (1998a)
Pigment specific normalized difference	**PSNDa** $= (R800 - R680) / (R800 + R680)$ **PSNDb** $= (R800 - R635) / (R800 + R635)$ **PSNDc** $= (R800 - R470) / (R800 + R470)$	Chlorophyll a Chlorophyll b Carotinoid	Blackburn (1998a)
Anthocyanin reflectance index	**ARI** $= 1/R550 - 1/R700$	Anthocyanin	Gitelson *et al.* (2001)

Tab. 3.1 continued

Index	Equation	Indicator	Reference
Modified chlorophyll absorption integral	$\mathbf{mCAI} = \frac{(R_{545}+R_{752})}{2} \cdot (752-545) - \left(\sum_{R_{545}}^{R_{752}} R \cdot 1.423\right)$	Chlorophyll content	Laudien *et al.* (2003)
Red edge position	$\mathbf{REP} = 700 + \frac{40 \cdot (R_{RE}-R_{700})}{(R_{740}-R_{700})}$	Inflection point red edge	Guyot and Baret (1988)
Plant sensecence index	$\mathbf{PSRI} = (R680 - R500)/R750$	Plant sensecence	Merzlyak *et al.* (1999)
Water index	$\mathbf{WI} = R900/R970$	Water content	Peñuelas *et al.* (1997)
Optimized soil adjusted vegetation index	$\mathbf{OSAVI} = \frac{(1+0.169)\cdot(R800-R670)}{R800+R670+0.16}$	Biomass with constant soil adjustment factor	Rondeux *et al.* (1996)
Modified chlorophyll absorption reflectance index	$\mathbf{MCARI} = ((R701 - R670) - 0.2 \cdot (R701 - R550)) \cdot \frac{R701}{R670}$	Chlorophyll content	Daughtry *et al.* (2000)
SumGREEN index	$\mathbf{SG} = \text{Average of} \quad R500 : R600$	Green reflectance	Gamon and Surfus (1999)
SumVIS index	$\mathbf{SV} = \text{Average of} \quad R400 : R600$	VIS reflectance	unpublished
Blue/Green index	$\mathbf{BIG2} = R450/R550$	Chlorophyll content	Zarco-Tejada *et al.* (2005)

3.7.3 Spectral Angle Mapping classification

Automatic classification known from remote sensing image analysis was applied to hyperspectral images of diseased sugar beet leaves for the differentiation of diseases. The Spectral Angle Mapping method (SAM, Yuhas *et al.*, 1992) was performed using the ENVI 4.6 + IDL 7.0 software. Spectral classification approaches assign each image pixel to one out of several known categories or classes (endmembers) through a statistical approach. Spectrally unique signatures of pure image components, i.e. endmembers, have to be defined, and specific classification algorithms can be calculated to classify the image pixel. The data set was divided into a set of training data and a set of test data, to train the classifiers. The classification decomposes the hyperspectral image into a false colour image, containing thematic information of the previously selected classes.

SAM calculates the spectral similarity of spectra and reference spectra using the spectral angle between the two spectra in an n-dimensional space dependent on the number of spectral bands (Fig. 3.4). The output of SAM is an angular difference for each pixel which can be illustrated in a false colour image; small spectral angles correspond to high similarity, large spectral angles to low similarity (Kruse *et al.*, 1993; Van der Meer *et al.*, 2001). Because the analysed spectra are transferred as vectors, variable illuminations due to the surface structure and veins of sugar beet leaves were attenuated (darker pixel will plot along the same vector, but closer to the origin). The method proceeds in various steps. Since SAM is a supervised classification method, the first step was the identification of reference spectra which were transferred from the spectral library (see paragraph: 'disease specific spectra'). Subsequently the spectral similarity of image spectra and reference spectra is calculated by the spectral angle between the two spectra in an n-dimensional space. For the validation 15-20 polygons per endmember-class with 15-200 pixel per polygon were selected as ground reference. The polygons were defined with the ROI function using

ENVI 4.6. The areas did not overlap with the training polygons. A confusion matrix was generated from the validation pixels for each classification. As measures of classification accuracy the overall accuracy, quantifying the percentage of cases correctly classified, and the kappa coefficient which accommodates for the effects of change agreement were calculated.

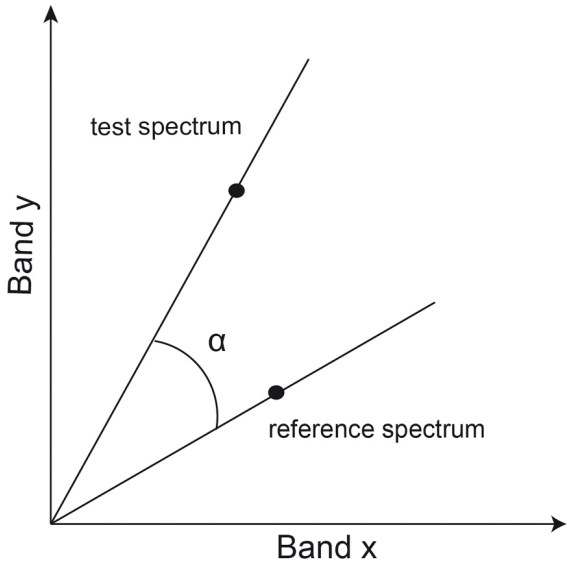

Figure 3.4: Concept plot of the Spectral Angle Mapper with a test spectrum and a reference spectrum. The angle α between the vectors, starting in the origin and projected trough the points representing the actual spectra, represents the spectral similarity (Kruse *et al.*, 1993, modified).

3.7.4 Machine learning

In cooperation with Till Rumpf, Institute of Geodesy and Geoinformation, Department of Geoinformation, University Bonn, machine learning techniques have been proven in their suitability for analyzing hyperspectral data. Support vector machines (SVMs) are a supervised, dichotomous classification algorithm, based on the theory of Vapnik (1982). SVMs determine an optimal separating hyperplane by quadratic optimisation aiming at maximising the margin between two classes. Different labels define different classes, e.g. healthy sugar beet leaves and leaves inoculated with different pathogens, respectively. Spectral vegetation indices (NDVI, SR, SIPI, PSSRa, PSSRb, ARI, REP, and

mCAI) and the SPAD-value were used as features for automatic classification. A linear function which has a fixed number of parameters given by the number of features is a simple case of separation between the two classes. In order to decide to which class a sample belongs, a measure of similarity to the function is necessary. In SVMs, the dot product in the input space is used as similarity parameter which describes the distance. The basic idea behind SVMs is to separate the two different classes through a hyperplane which is constructed by its normal vector and the bias. Using also a linear separation function for a non-linear separation between the classes, a transformation into a higher dimensional space has been done. A linear separation is possible through the mapping into a high-dimensional feature space, however, is computationally expensive. Furthermore, the description of the separating hyperplane in the low-dimensional input space is rather complex. For this reason a kernel function is introduced to increase the efficiency of computation (Boser, 1992). In order to extend the dichotomous SVMs classifiers for a multi-class classification of healthy leaves and leaves diseased by *Cercospora* leaf spot, powdery mildew, and sugar beet rust effectively, a library for SVMs (LIBSVM) has been used for classification (Chang and Lin, 2001). Here the 'one against one' approach (Knerr *et al.*, 1990) was applied. The suitability of the model established by using the training data set was evaluated by cross-validation. Specificity gives the proportion of the correctly classified healthy leaves of all classified healthy leaves. Sensitivity gives the proportion of correctly classified inoculated sugar beet leaves in relation to all classified inoculated leaves. Accuracy is given by the average of sensitivity and specificity. For more details on computation, see Rumpf *et al.* (2010).

3.7.5 Geo-referenced maps

Values of SVIs, ECa as well as disease ratings from the field experiment were displayed as geo-referenced maps using the Inverse Distance Weighting (IDW)

function of ArcMap 9.2 (ArcGIS, ESRI Inc., Redlands, USA). NDVI values from airborne sensor images were displayed as geo referenced maps in ENVI 4.6.1 (Research Systems Inc., Boulder, CO, USA).

3.8 Statistical analysis

Statistical analyses were performed using the Superior Performing System SPSS 17.0 (SPSS Inc., Chicago, USA). Data from repeated measures was analysed using a general linear model and the Bonferroni test to determine statistically significant differences ($p = 0.01$; $p = 0.05$). Data were analysed by standard analysis of variance (ANOVA) and homogeneous subgroups were built using the Tukey-test, with a significance level of $p = 0.05$. For pair wise comparison, Students *t*-test with a level of significance of $p = 0.05$, was undertaken. Correlations between disease severity and reflectance data and spectral vegetation index values, respectively, were tested by computing Pearson's coefficient of correlation (r), and coefficients of determination $\left(R^2\right)$ were estimated by a linear model. The experiments were repeated at least twice, except for the field experiment.

4. RESULTS

The present work focuses on the potential of hyperspectral non-imaging and imaging sensors for the detection, differentiation and quantification of foliar diseases of sugar beet. The hypothesis was that the three diseases *Cercospora* leaf spot, powdery mildew, and sugar beet rust influence the optical properties of a plant in different ways. Experiments under both, controlled and field conditions with different sensor systems on different scales have been undertaken and compared, since the measuring method is the groundwork of disease detection. Thereby, different developing stages and different severities of the diseases have been taken into account. To gain a maximum on information from hyperspectral data, different data analysis methods have been applied. The pathogenesis of the three diseases *Cercospora* leaf spot, powdery mildew, and sugar beet rust have been observed. In a first approach, disease specific spectral signatures have been assessed with a non-imaging spectroradiometer. Multiple spectral vegetation indices from literature, related to biophysical and biochemical plant parameters have been applied on hyperspectral data, and their ability for a detection and discrimination has been proven. Building on that, a more detailed observation of the temporal and spatial symptom development has been undertaken with a hyperspectral camera system. Additionally, image based automatic classification methods have been applied on hyperspectral images. In a last step the potential and negotiability of hyperspectral disease detection in the field has been analysed.

4.1 Etiology of sugar beet diseases

4.1.1 Disease progress on leaf scale

The temporal development of the diseases on the leaf scale varied for the three pathogens (Fig. 4.1).

Cercospora leaf spot
First symptoms of *Cercospora* leaf spot appeared 6 days after inoculation (Fig. 4.1 A). Disease severity increased slowly up to 10% diseased leaf area until 10 dai; 21 dai disease severity increased constantly up to 85%. Fifteen days after inoculation the mean disease severity reached 25%. Variation in disease severity among the leaves inoculated with *C. beticola* decreased with time and increasing mean disease severity. Minimum disease severity was 25% and maximal assessed disease severity was 80%, whereas mean disease severity was about 55% 18 dai.

Powdery mildew
Infestation of sugar beet leaves with powdery mildew exhibited faster development (Fig. 4.1 B). Symptoms could be monitored already 5 dai. Further spread of the powdery mildew- characteristic mycelium on the leaf surfaces proceeded faster than symptoms of the other diseases. An average disease severity of 17.5% was assessed 10 dai. Disease severities beyond 80% have been monitored 15 dai with a mean disease severity of 70%. The whole leaf area was covered with white fluffy mycelia 17 dai. The density of mycelia coverage increased within the next few days. The colonization progress of powdery mildew was more consistent compared to infestation progress by *Cercospora* leaf spot or sugar beet rust.

Sugar beet rust
With 8 days the latent period of *U. betae* was the longest among the pathogens (Fig. 4.1 C). Single chlorotic pustules could be detected on the leaf surface.

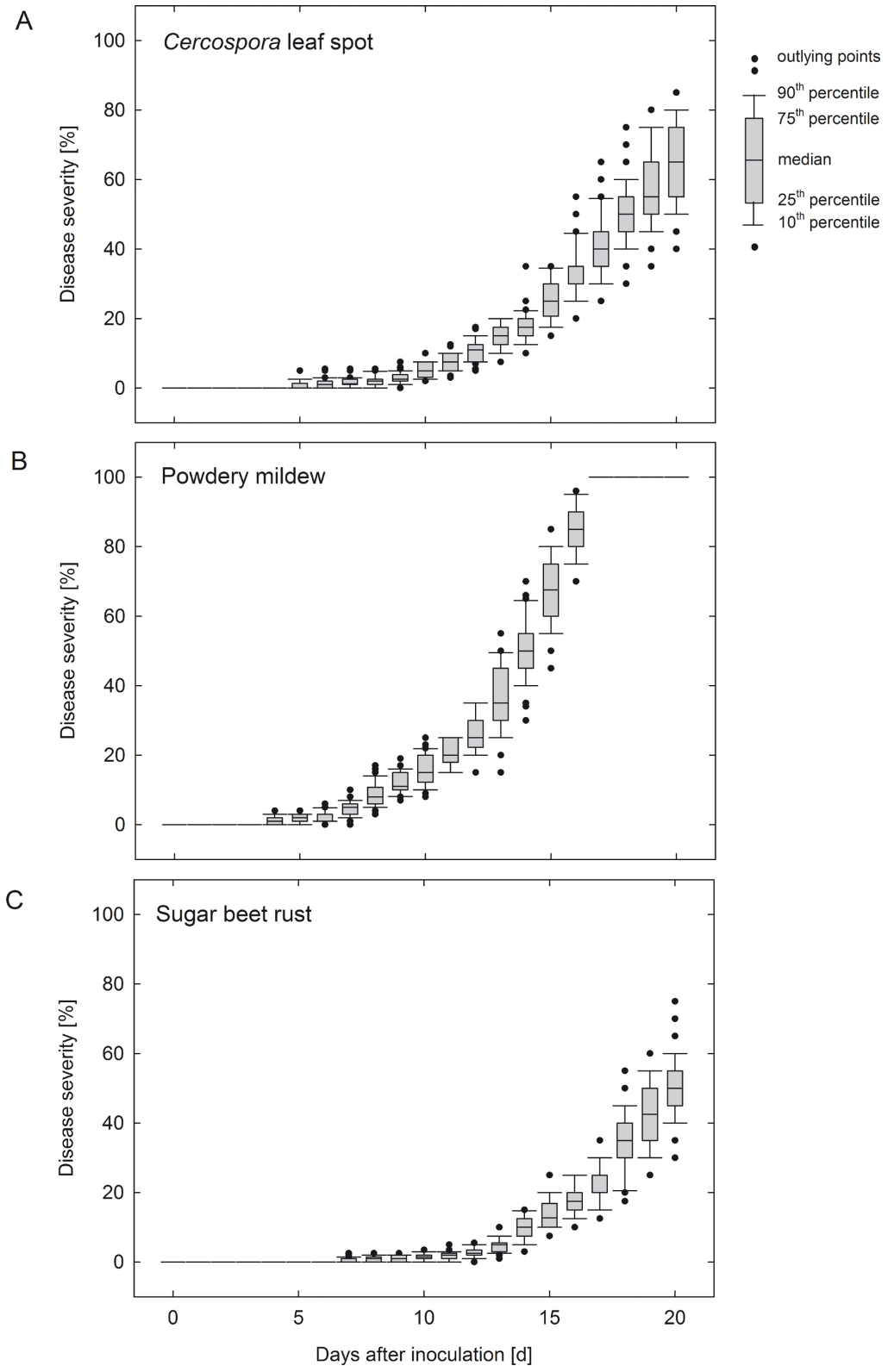

Figure 4.1: Progression of disease severity of (A) *Cercospora* leaf spot, (B) powdery mildew, and (C) sugar beet rust on sugar beet leaves.

They increased slowly in number and size by 14 dai. A mean disease severity of 35% was monitored 18 dai. At this time some leaves had a disease severity below 17.5%, whereas other leaves showed disease severities above 55%. The maximal mean disease severity reached 50% 20 dai. Single leaves with a disease severity up to 75% could be monitored in the end of the measuring period, while several leaves showed disease severities still below 30%.

4.1.2 Disease progress on canopy scale

Disease severity assessed on the canopy scale differed marginal from disease severity assessed on the leaf scale (Fig. 4.2). First symptoms of *Cercospora* leaf spot appeared 7 dai. 5% of the leaf area showed characteristic symptoms 10 dai. Disease severity increased up to 17.5% leaf area 15 dai and to 60% 20 dai. First symptoms of powdery mildew occurred 5 dai and spread rapidly over the sugar beet canopy. Nearly 20% of the leaf area was covered by white mycelium 10 dai; disease severity reached 80% 15 dai, and 17 dai the whole canopy was covered by powdery mildew. The disease progress of sugar beet rust on the canopy scale was comparative to the progress of *Cercospora* leaf spot. First rust pustules occurred 8 dai. Disease severity increased slowly, 17.5% of the canopy was diseased 15 dai. The maximal disease severity of sugar beet rust monitored on the canopy scale was 55% 20 dai.

4.1.3 Temporal and spatial symptom development

Depending on the biology of the pathogens, each foliar diseases of sugar beet were characterized by disease-specific symptoms (Fig. 4.3). Inoculated plants were first colonized without symptoms, after a latent period typical symptoms appeared.

Cercospora leaf spot
Small, nearly circular necroses appeared as the first symptoms of *Cercospora* leaf

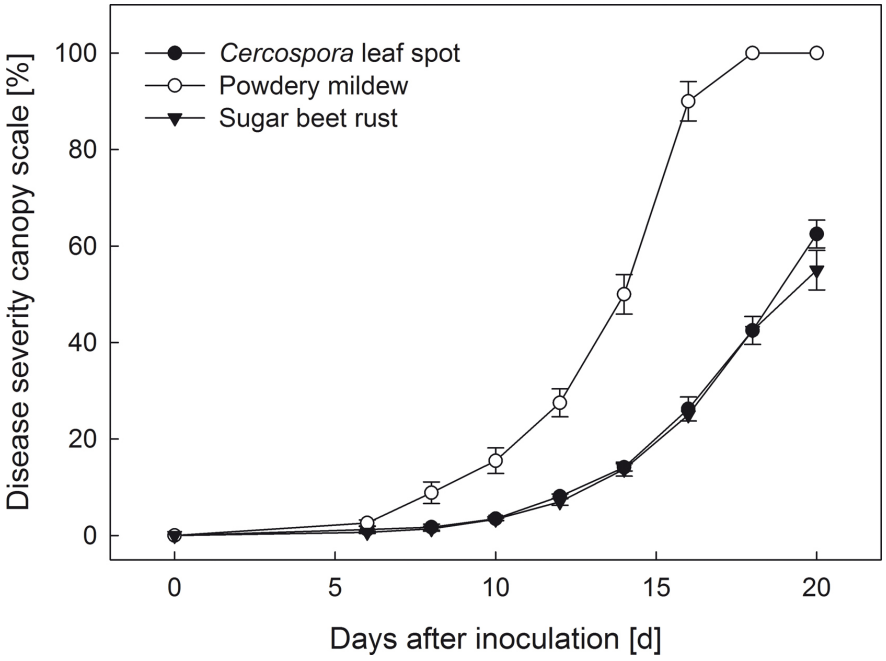

Figure 4.2: Progression of disease severity of *Cercospora* leaf spot, powdery mildew, and sugar beet rust on the canopy scale of sugar beet (bars denote standard derivation).

spot 6 to 8 dai (Fig. 4.3 A). Slight depressions in the leaf tissue with a diameter of 0.5 mm and a greyish to dark greenish colouration were detectable. Adjacent leaf tissue appeared green and healthy. From day 8 to 10 after inoculation, the sunken lesions enlarged to 1.0 mm diameter, and the centre of the lesions became dry and necrotic, while a margin circumvented the spot to healthy leaf tissue. With further pathogenesis the margin became more evident. Lesion centres appeared in light grey or beige hue. The colour shade of the lesion border varied from grey over brown to deep red. Mature lesions developed black pseudostroma, distributed within the centre. The spots coalesced and formed large necrotic areas 14 dai. Heavily infested leaves became chlorotic and often collapsed. As a consequence of leaf collapse, sugar beet plants responds with increasing formation of new leaves. Symptoms of *Cercospora* leaf spot typically appeared first on older sugar beet leaves, followed by younger leaves. Appearances of characteristic leaf spots were the same on both, upper and lower leaf surface. Elongated necrotic spots could be also reported on petioles and leaf veins.

Powdery mildew

First symptoms caused by *E. betae* appeared 5 dai (Fig. 4.3 B). Slight, nearly circular mycelium colonies with about 0.5 cm diameter appeared on the upper side of leaves. With further pathogenesis these colonies expanded rapidly and also the lower leaf surface was colonized. The white mycelium covered both, the total upper and lower leaf surface and became more and more dense until 14 dai. The colour of mycelial structures changed from white to grey. At high disease severity stages accelerated senescence and earlier degradation into yellowing and necrotic parts of powdery mildew diseased leaves was noticed. Leaves became chlorotic 18 dai and finally necrotic 21 dai. Conidia production could be observed from the second day after symptom appearance. Conidia were continuously released in dusty clouds, when sugar beet leaves were moved, resulting in new infections of non-diseased and younger leaves. Initial growth and accumulation of colonies around leaf veins could be observed. Symptoms were also observed on leaf petioles.

Sugar beet rust

First symptoms due to *U. betae* became visible 9 dai (Fig. 4.3 C). Small chlorotic spots, about 0.2 mm in size, appeared on the upper and lower side of the leaf surface. These circular lesions grew up to 0.5 - 1 mm in diameter, and the epidermis became scabby. The centre of the early rust symptoms appeared in light brown 12 dai. With proceeding disease development, rust spores ruptured the epidermis and amber uredinia became visible 14 dai. The rust pustules were encircled by a chlorotic halo. In some cases a second circle of rust spores ruptured the epidermis in a distance of 1 mm around the primary symptom 16 to 21 dai. At high disease severity, the chlorotic ring around the rust pustules expanded and contiguous leaf tissue was affected. Pustules of sugar beet rust were also observed on leaf petioles. In addition, an accumulation of rust spores along the leaf veins and the axilla of the rosulate ordered leaves near the beet root was detectable. Symptoms of sugar beet rust appeared on young and older leaves simultaneously.

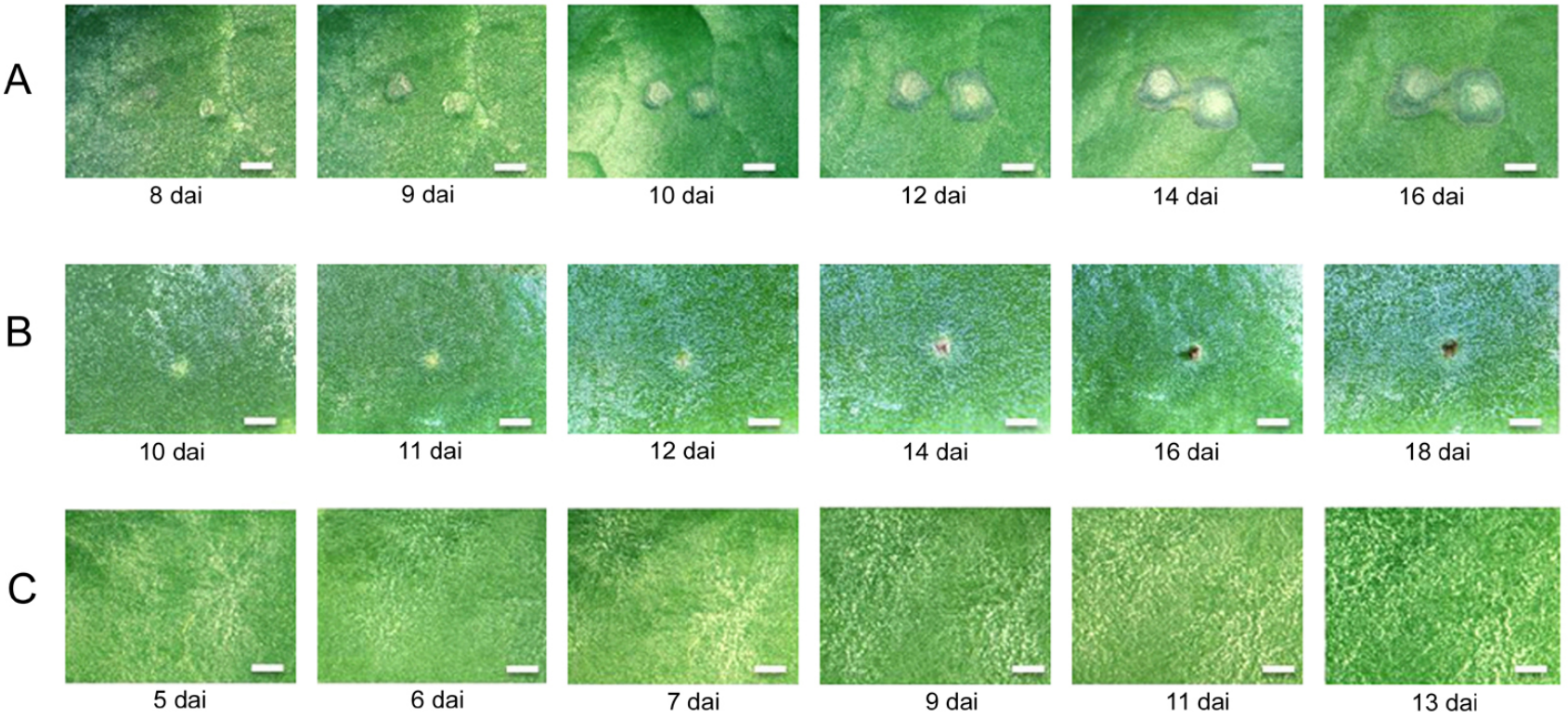

Figure 4.3: Development of disease specific symptoms of *Cercospora* leaf spot (A), sugar beet rust (B), and powdery mildew (C) on sugar beet leaves (bar = 1000 µm).

4.1.4 Modifications of leaf structure during pathogenesis

Scanning electron microscopic images visualize the typical infection structures of the fungal pathogens *Cercospora beticola*, *Erysiphe betae*, and *Uromyces betae* on the host plant (Fig. 4.4). Each pathogen influenced the sugar beet leaf tissue in a specific way.

Cercospora leaf spot
C. beticola entered the leaf through closed or open stomata with a germ tube. Intercellular mycelia were formed and pseudostroma was developed in the substomatal area. On the surface of one day old lesions, conidiophores emerged from pseudostroma through stoma aperture, with protruding conidia (Fig. 4.4 A). Ample hyphal growth, visible as thin, filamentous strands, occurred within sporulating, older lesions (Fig. 4.4 B). On the border between *Cercospora* leaf spot lesions and healthy tissue, deep splits and sulcate leaf tissue occurred. The area of the lesions was obviously sunken.

Powdery mildew
The electron microscopic view of characteristic symptoms of powdery mildew showed dense and multiple-branched mycelia structures covering the leaf surface (Fig. 4.4 C). Conidia chains protruded from the mycelia. *E. betae* penetrated the host tissue directly, no mycelial growth through stomata could be observed.

Sugar beet rust
A highly magnified pustule caused by *U. betae* is shown in Fig. 4.4 D. Swelling of leaf tissue, caused by spore accumulation under the epidermis, was observed. At advanced disease stages, accumulated uredina ruptured the epidermal layer. The roundish uredinia were released and spreaded onto the neighbouring leaf area.

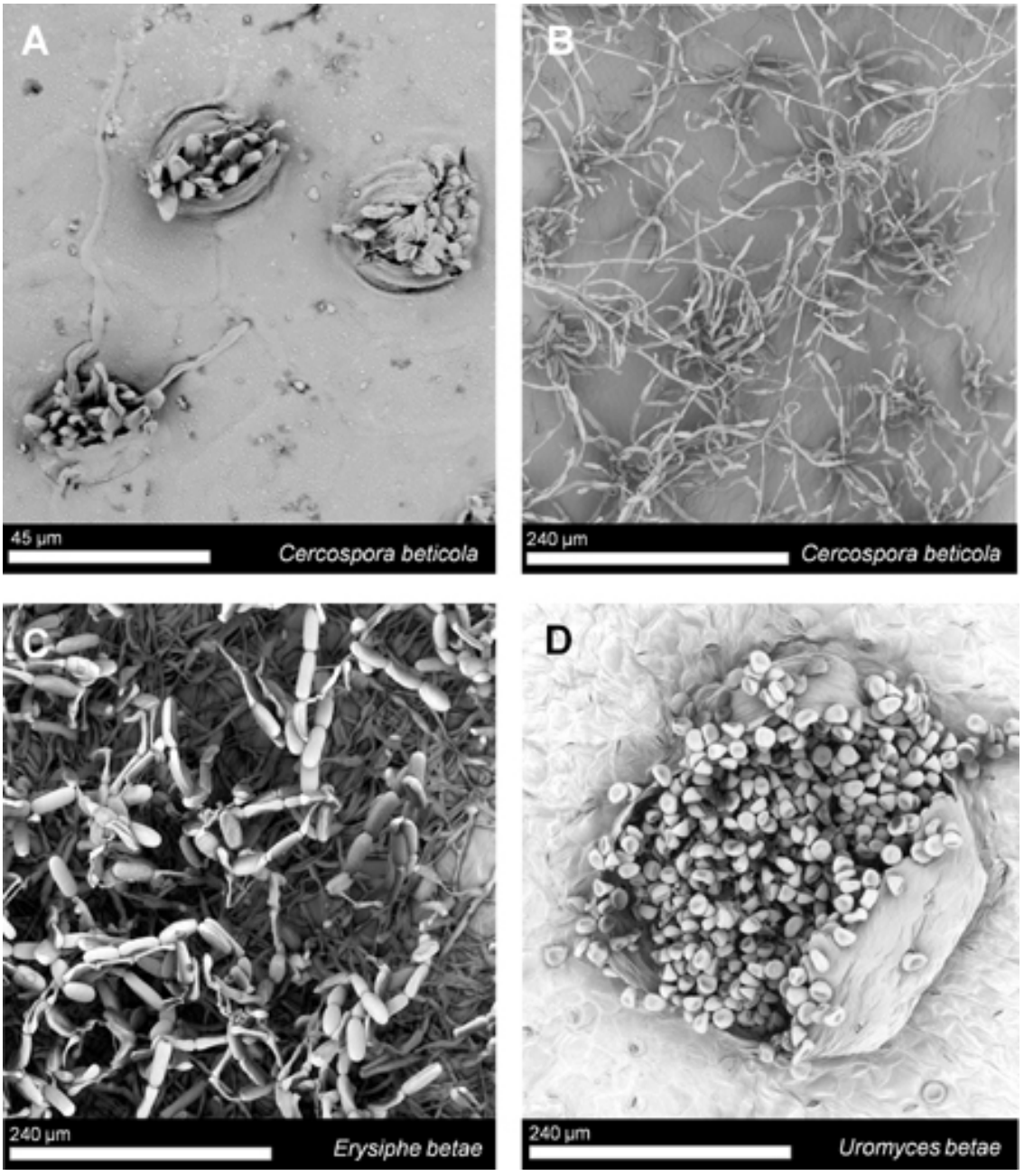

Figure 4.4: Fungal structures on the leaf surface of sugar beet leaves 21 dai. (A, B) Emerging hyphal structures and conidia of *Cercospora beticola* from stomatal openings of sugar beet lesions. (C) Dense mycelia of *Erysiphe betae* with conidia growing on the leaf surface of sugar beet. (D) Ruptured epidermis of sugar beet by *Uromyces betae* uredinio-spores.

4.1.5 Effect of foliar diseases on leaf pigment content

The impact of the three foliar sugar beet diseases on biochemical parameters, particularly on the leaf pigment content, was assessed by non-destructive

(SPAD-meter) and destructive (chlorophyll extraction) analysis methods during disease development (Tab. 4.1).

The chlorophyll index of healthy sugar beet leaves over a period of 20 days varied between SPAD values of 43.6 to 47.0. No significant differences could be detected. Leaves infected by *Cercospora* leaf spot showed a slight increase in SPAD-meter values 5 to 9 dai. SPAD values decrease from 39.8, 10 dai to 28.8, 20 dai. First significant differences occurred 12 dai with a SPAD-meter value of 36.2. SPAD values for powdery mildew diseased leaves decreased from 42.4, 6 dai to 38.1, 20 dai. Significant differences could be observed 16 dai and later. SPAD values for sugar beet rust ranged from 39.1 to 34.4. A slight significant difference was measured 16 dai, a significant difference only 20 dai.

The destructive assessment of total chlorophyll, chlorophyll a, chlorophyll b, and carotenoid contents for healthy sugar beet leaves revealed no significant differences during the measuring period (Tab. 4.1). After an increase in pigment content, a general decrease without significant differences has been assessed for all pigments because of senescence 5 to 8 dai. The mean pigment content of leaf tissue with *Cercospora* leaf spot, powdery mildew, and sugar beet rust declined with disease progress, but only slight differences could be detected (Tab. 4.1). As the standard derivation of the individual groups was high and the number of samples per treatment was low (n = 5) significant differences were rare.

Total chlorophyll content of tissue diseased with *Cercospora* leaf spot decreased from a maximum of 2219 µg/ml 7 dai to 780 µg/ml 20 dai. The difference to non-diseased was significant 16 dai with 1248 µg/ml. The chlorophyll a content of *Cercospora* leaf spot diseased leaves decreased from 1814 µg/ml 5 dai to 614 µg/ml 20 dai. Significant differences were detected first 16 dai.

The mean amount of chlorophyll b decreased from 218 µg/ml 5 dai to 165 µg/ml 20 dai with significant differences 16 dai and later. Values of carotenoids receded from 519 µg/ml 7 dai to 256 µg/ml 20 dai. The first significant differences were detected 12 dai.

Table 4.1: Effect of *Cercospora* leaf spot, powdery mildew, and sugar beet rust, respectively, on pigment concentration of sugar beet leaves 5 to 20 days after inoculation[1].

	Treatment[3]	**Days after inoculation**											
		5	6	7	8	9	10	11	12	14	16	18	20
SPAD[2]	Healthy	43.6	44.3	44.2	46.1	46.0	47.0	46.1	46.5	46.5	45.8	46.1	45.8
	CLS	39.2	39.4	39.8	40.5	40.1	39.8	37.5	**36.2***	**36.6**	**34.5**	**31.7**	**28.8**
	PM	42.0	42.4	41.9	41.2	40.8	40.4	41.3	42.2	41.2	**39.9***	**38.5**	**38.1**
	SBR	38.8	38.6	38.5	38.7	38.9	39.1	38.9	38.6	38.8	37.7	**36.6***	**34.4**
Chl$_{total}$[2]	Healthy	2016	2017	2181	2387	2057	2180	1977	2264	2272	1889	1957	1661
(µg/ml)	CLS	2030	2021	2219	2179	1913	1957	1732	1535	1452	**1248***	**1232**	**780**
	PM	2063	2315	2206	2619	1960	1778	1649	1652	1630	1535	1458	**1156***
	SBR	2118	2233	2021	2428	2059	1951	1829	1835	1727	1519	**1472***	**1289**
Chl$_{a}$[2]	Healthy	1804	1783	1908	2159	1821	1915	1760	2038	2021	1687	1751	1468
(µg/ml)	CLS	1814	1794	1986	1915	1524	1750	1544	1337	1278	**1120***	**1084**	**615**
	PM	1841	2020	1965	2330	1734	1573	1446	1469	1415	1337	1278	**993***
	SBR	1875	1985	1783	2172	1818	1721	1622	1640	1518	1356	**1288***	**1117**
Chl$_{b}$[2]	Healthy	212	231	274	229	237	266	217	227	252	203	208	193
(µg/ml)	CLS	218	235	234	266	216	208	189	198	174	**129***	**149**	**165**
	PM	223	296	242	290	226	205	203	184	215	198	181	163
	SBR	243	249	239	257	242	231	208	196	209	163	184	173
Car[2]	Healthy	494	506	562	589	503	514	454	547	512	431	476	470
(µg/ml)	CLS	467	524	519	514	426	475	440	**343***	**362**	**315**	**304**	**256**
	PM	446	512	475	569	421	399	362	363	359	343	330	236
	SBR	500	516	489	557	476	439	422	438	397	**357***	**359**	**334**

[1] for each parameter, bold letters with asterisk marks within a row denote first occurrence of significant differences during the measuring period, according to a general linear model GLM and Bonferroni-test (p = 0.05; SPAD-meter measurements: n= 30; destructive pigment analysis: n = 5)

[2] **SPAD** = SPAD-Meter values; **Chl**$_{total}$ = total Chlorophyll content; **Chl**$_{a}$ = Chlorophyll a content; **Chl**$_{b}$ = Chlorophyll b content; **Car** = Carotenoids content

[3] CLS = *Cercospora* leaf spot, PM = powdery mildew, SBR = sugar beet rust

Note: highlighted date indicates first appearance of visible disease symptom

The total chlorophyll content of powdery mildew diseased leaf tissue decreased from 2233 µg/ml 6 dai to 1156 µg/ml 20 dai (Tab. 4.1). Significant differences could be found for total chlorophyll and chlorophylla only 20 dai. Concentrations of chlorophyll b and carotenoids showed similar tendencies, however, without statistically significant differences.

The total chlorophyll content of leaves diseased with sugar beet rust decreased from 2428 µg/ml 8 dai to 1289 µg/ml 20 dai (Tab. 4.1). Significant differences were measured 18 dai. Decreasing pigment contents were also observed for chlorophyll a, chlorophyll b and carotenoids. Significant differences were detected for chlorophyll a content 18 dai and for carotenoids content 16 dai; changes in chlorophyll b content were not significant.

4.2 Differentiation of foliar diseases based on spectral signatures of infected leaves

During pathogenesis spectral reflectance of diseased sugar beet leaves was measured with hyperspectral non-imaging sensors in the VIS, NIR, and SWIR (ASD FieldSpec FR and ASD FieldSpecPro JR). Measurements were undertaken at controlled conditions. Reflectance spectra on the leaf scale were assessed with a plant probe foreoptic with an integrated light source, on the canopy scale with a pistol grip foreoptic and ASD-Pro-Lamps as light source.

4.2.1 Impact of foliar diseases on the spectral reflectance of sugar beet

Reflectance of non-inoculated leaves and leaves inoculated with the foliar pathogens was recorded for 21 days after inoculation. In this period, reflectance spectra of non-inoculated sugar beet leaves were characteristic for

healthy leaves and remained largely constant (Fig. 4.5 A): strong absorption of light by photosynthetic pigments in the VIS, high reflectance plateau in the NIR. For the differentiation of leaf diseases based on reflectance measurement, specific spectral signatures at different disease severities have been measured and compared. Standard derivations were assessed to validate the disease-specific changes in spectral signature compared to the reflectance of healthy sugar beet leaves. Fig. 4.5 summarizes the averaged spectral signatures of sugar beet leaves with *Cercospora* leaf spot, powdery mildew, and sugar beet rust at 0%, 10%, 20%, 50%, and 80% disease severity, respectively. Compared to the spectra of healthy leaves, each disease had a divergent, characteristic reflectance curve. The changes in reflectance were strongly correlated to the occurrence of disease-specific symptoms.

Cercospora leaf spot

Spectral signatures of leaves, inoculated with *C. beticola*, changed evidently in reflectance values with first disease symptoms. Reflectance between 550 to 700 nm and between 700 to 900 nm increased 12 dai and later according to increasing disease severity (Fig. 4.5 B). Reflectance of *C. beticola*-infected leaves (Fig. 4.6 A) increased in the VIS mostly in the green and red ranges of the spectrum between 500 to 700 nm and decreased from 700 to 900 nm. With disease severity $>$ 10%, reflectance values in the VIS increased. This increment was less pronounced between 450 to 530 nm and most pronounced between 550 to 700 nm. In the NIR, decreasing reflectance between 700 to 900 nm, and slightly increasing reflectance from 900 to 1050 nm could be noticed. With disease severities of 20% to 50% this effect on leaf reflectance intensity in these regions became more pronounced. In addition, the slope at the red edge position between VIS and NIR became less steeply. A blue shift of the red edge position depending on *Cercospora* leaf spot disease severity was obvious. At a disease severity of 80%, reflectance increased over the whole spectrum and a typical spectral signature of vegetation was no longer detectable.

Depending on disease severity, standard derivation of specific bands of the spectra changed (Fig. 4.7). Standard derivation of reflectance of healthy sugar beet leaves ranged between 0.008 to 0.02 and was most pronounced next to the green peak at 550 nm and in the NIR between 700 to 900 nm. For *Cercospora* leaf spot diseased leaves, standard derivation varied depending on disease severity (Fig. 4.7 A). At 10%, 20%, and 50% disease severity of highest derivations were noticed between 550 to 700 nm and 700 to 900 nm. These high values were in the spectral bands, affected by *Cercospora* leaf spot, and ranged from 0.01 to 0.04. At 80% disease severity standard derivation was high between 600 to 850 nm, with a peak at 670 nm. Maximal derivation was comparatively lower than at 20% to 50% disease severities. The results suggested that bands with high reflectance differences among the *Cercospora* leaf spot disease severities featured highest standard derivation due to variability among the leaves.

Powdery mildew

Reflectance of leaves colonized by the ectoparasite *E. betae* rose consecutively within the measuring period and with increase in disease severity, starting 9 dai (Fig. 4.5 C, Fig. 4.6 B). This steady increment was most distinctive in the VIS and less pronounced in the NIR. Powdery mildew rather affected the overall level of reflectance than the profile of spectra. The overall standard derivation ranged from 0.005 to 0.025. At 10% and 20% disease severity standard derivation in the VIS was similar to healthy plants, and lower in the NIR compared to healthy plants (Fig. 4.7 B). At higher disease severities standard derivation in the VIS raised to 0.015 to 0.025. A higher standard derivation compared to healthy leaves was also noticed in the NIR.

Sugar beet rust

Due to the small symptoms of the biotroph *U. betae* scattered on the leaf area, changes in reflectance spectra were comparatively low for leaf rust (Fig. 4.6 C). First changes in reflectance were measurable 15 dai (Fig. 4.5 D). At 10% disease severity, changes were not significant compared to healthy leaves. In

contrast, standard derivation at 10% disease severity was high from 500 to 700 nm, with a peak at 710 nm (Fig. 4.7 C). Reflectance of leaves with 20% disease severity was higher than at healthy leaves from 550 nm to 700 nm. Explicit changes were measured at 50% disease severity; i.e. high reflectance between 550 to 700 nm and low reflectance from 700 to 900 nm. The presence and growth of uredinia increased the reflectance between 550 and 700 nm. With increasing disease severity, standard derivation rose between 550 to 700 nm and at a peak around 710 nm.

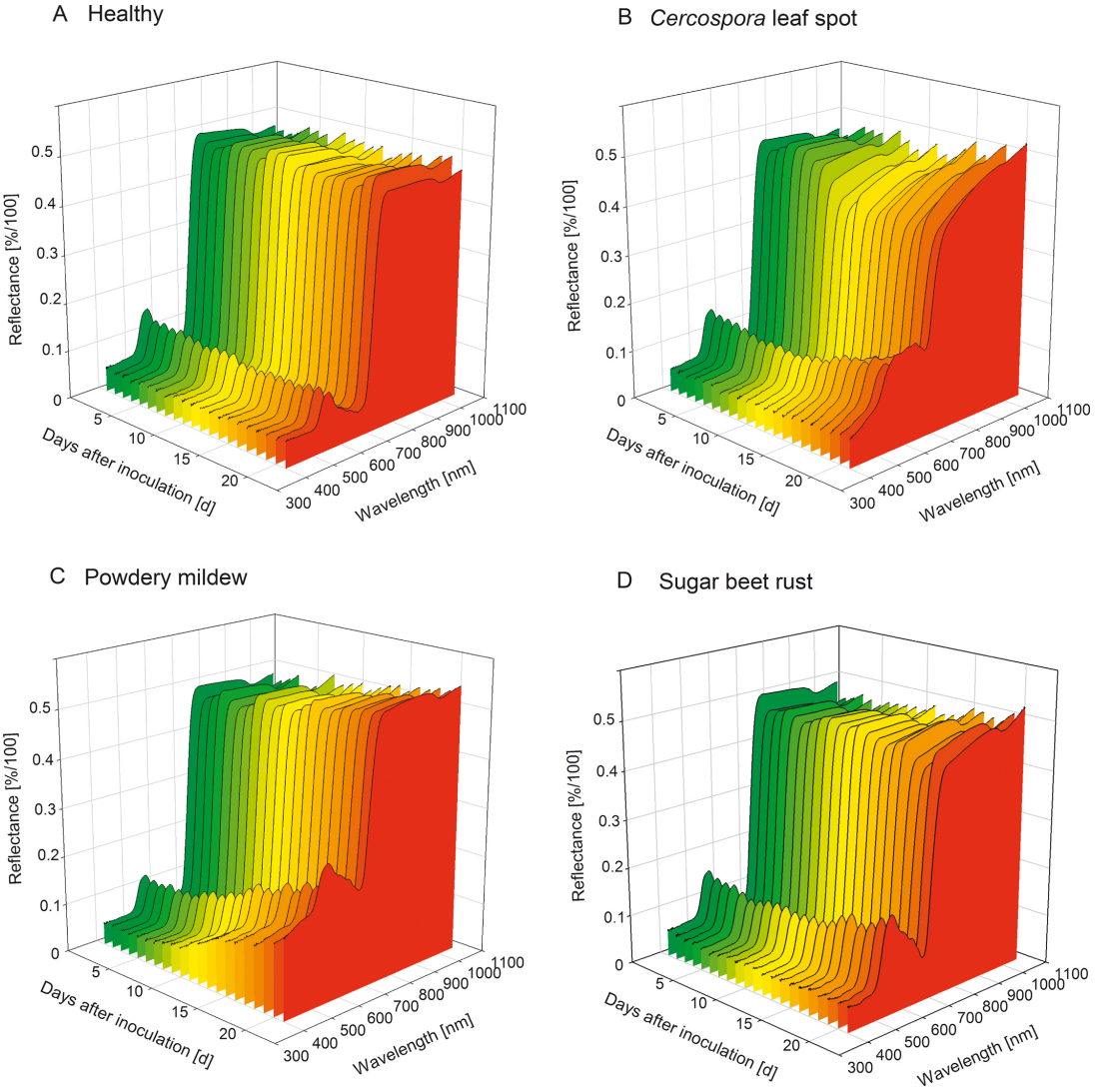

Figure 4.5: Spectral signatures of (A) healthy sugar beet leaves and sugar beet leaves affected with (B) *Cercospora* leaf spot, (C) powdery mildew, and (D) sugar beet rust from 0 to 21 dai.

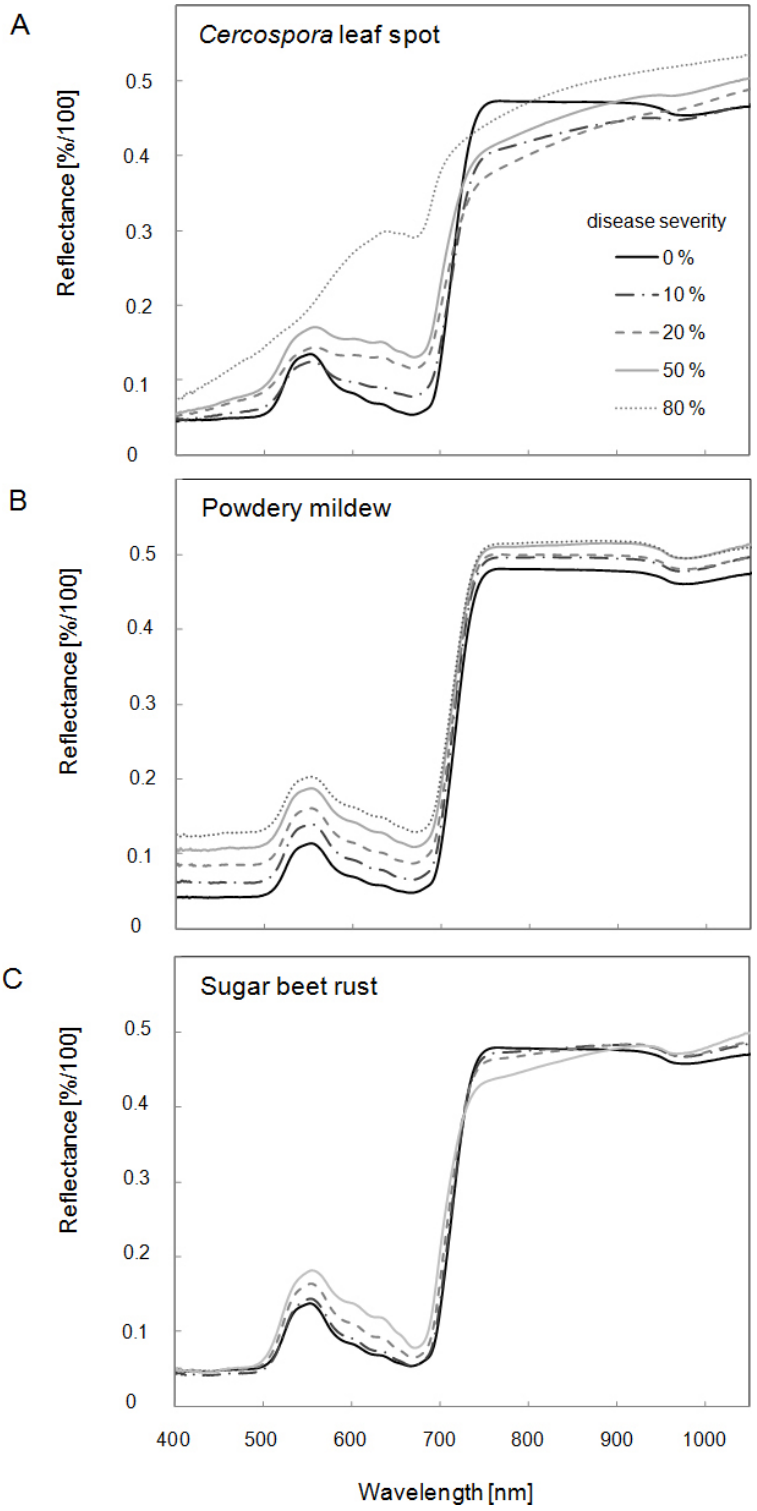

Figure 4.6: Spectral signatures of sugar beet leaves affected by (A) *Cercospora* leaf spot, (B) powdery mildew, and (C) sugar beet rust at different disease severities. Reflectance was measured under controlled conditions using an ASD FieldSpec FR.

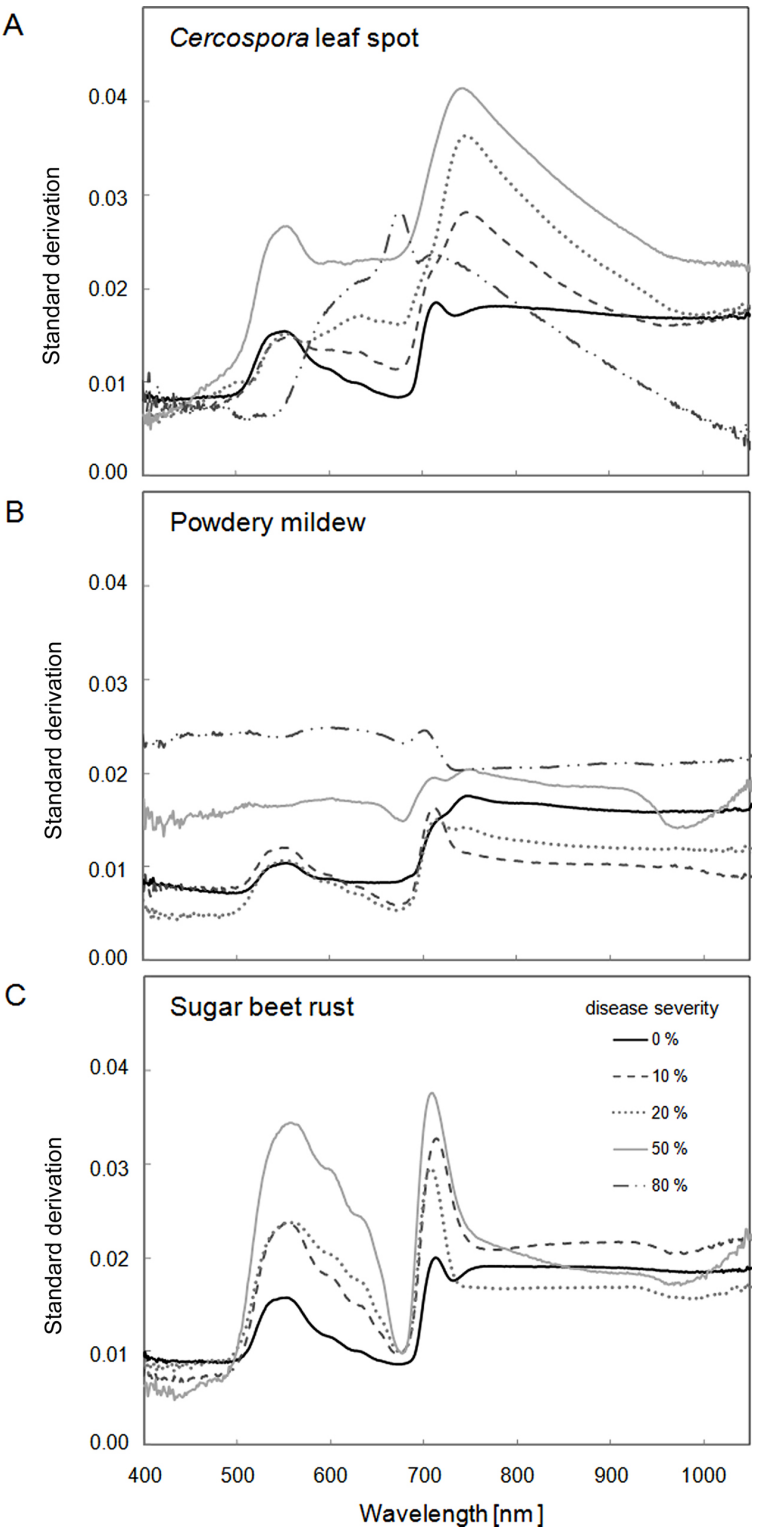

Figure 4.7: Standard derivation of spectral reflectance of sugar beet leaves affected by (A) *Cercospora* leaf spot, (B) powdery mildew, and (C) sugar beet rust at different disease severities. Reflectance was measured under controlled conditions using an ASD FieldSpec FR.

Correlation between spectral signatures and disease severity

The linear coefficient of correlation (r) for disease severity *versus* reflectance considerably varied with the wavebands. Strong differences were detected among the diseases (Fig. 4.8). The correlation between *Cercospora* leaf spot severity and reflectance was positive in the VIS range, with high values from 430 nm to 520 nm and from 570 nm to 710 nm (Fig. 4.8 A). In the NIR the correlation was negative with a maximum at 740 nm. For powdery mildew the severity was highly correlated to all wavelengths (Fig. 4.8 B). The coefficient of correlation was best in the VIS region and reached r = 0.85. Displaying the correlation between sugar beet rust disease severity and reflectance, Fig. 4.8 C indicated that wavelengths from 510 nm to 700 nm grade a strong positive correlation. In contrast to the other diseases, the correlation for sugar beet rust and wavelengths from 400 nm to 500 nm was weak. Similar to *Cercospora* leaf spot, a negative correlation was detected for sugar beet rust in the NIR.

Spectral reflectance in the SWIR

In addition to regular measurements of leaf reflectance in the range 400 nm to 1050 nm, reflectance spectra were recorded with a non-imaging spectroradiometer in the range 400 nm to 2500 nm, 0, 7, 14, and 21 days after inoculation at different disease severities (Fig. 4.9, Fig. 4.10).

The spectral signature of healthy sugar beet leaves in the SWIR is dominated by strong water absorption bands at 1200, 1400, 1940, and 2400 nm (Fig. 4.10). Two reflectance peaks occurred around 1650 nm and 2200 nm. Likewise, the absorption of structural compounds like cellulose, lignin, starch, and protein influences leaf reflectance in the SWIR.

Cercospora leaf spot

For sugar beet leaves with *Cercospora* leaf spot obvious changes in SWIR reflectance were assessed already 7 dai, at a mean disease severity of 1.3% (Fig. 4.9 A), while changes in the VIS and NIR were minor (Fig. 4.10 A). With increasing disease severity, this effect steadily proceeded. Changes next to the water

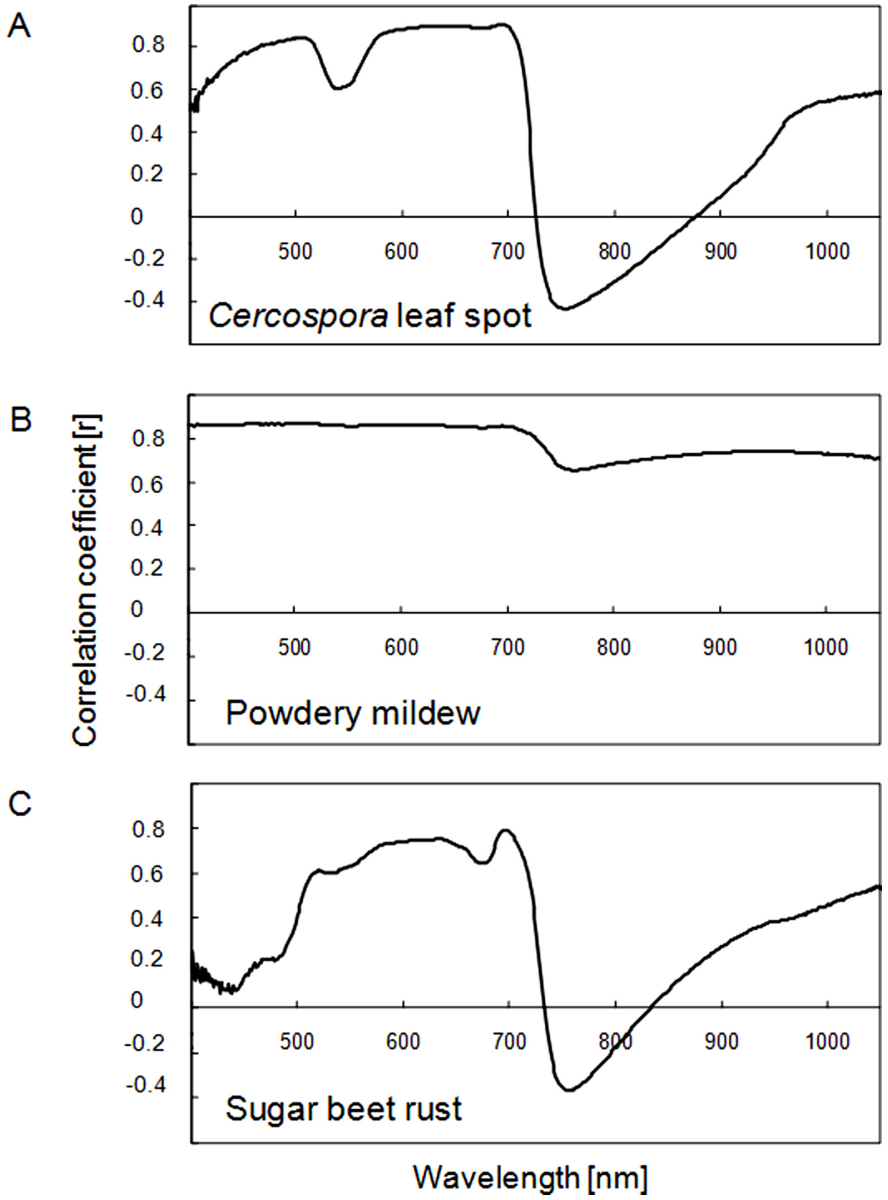

Figure 4.8: Diagram of coefficient of correlation (r) for the linear correlation between spectral reflectance of sugar beet leaves and disease severity in relation to wavelength for (A) *Cercospora* leaf spot, (B) powdery mildew, and (C) sugar beet rust.

absorption bands at 1400 nm and 1940 nm were most obvious 14 and 21 dai (disease severity: 14.7% and 57.9%, respectively). Changes in the SWIR were greater than those in the VIS and NIR.

Powdery mildew

Powdery mildew caused distinctive changes in the SWIR from 14 dai and later on (Fig. 4.10 B). With 2.5% disease severity 7 dai, reflectance curve of pow-

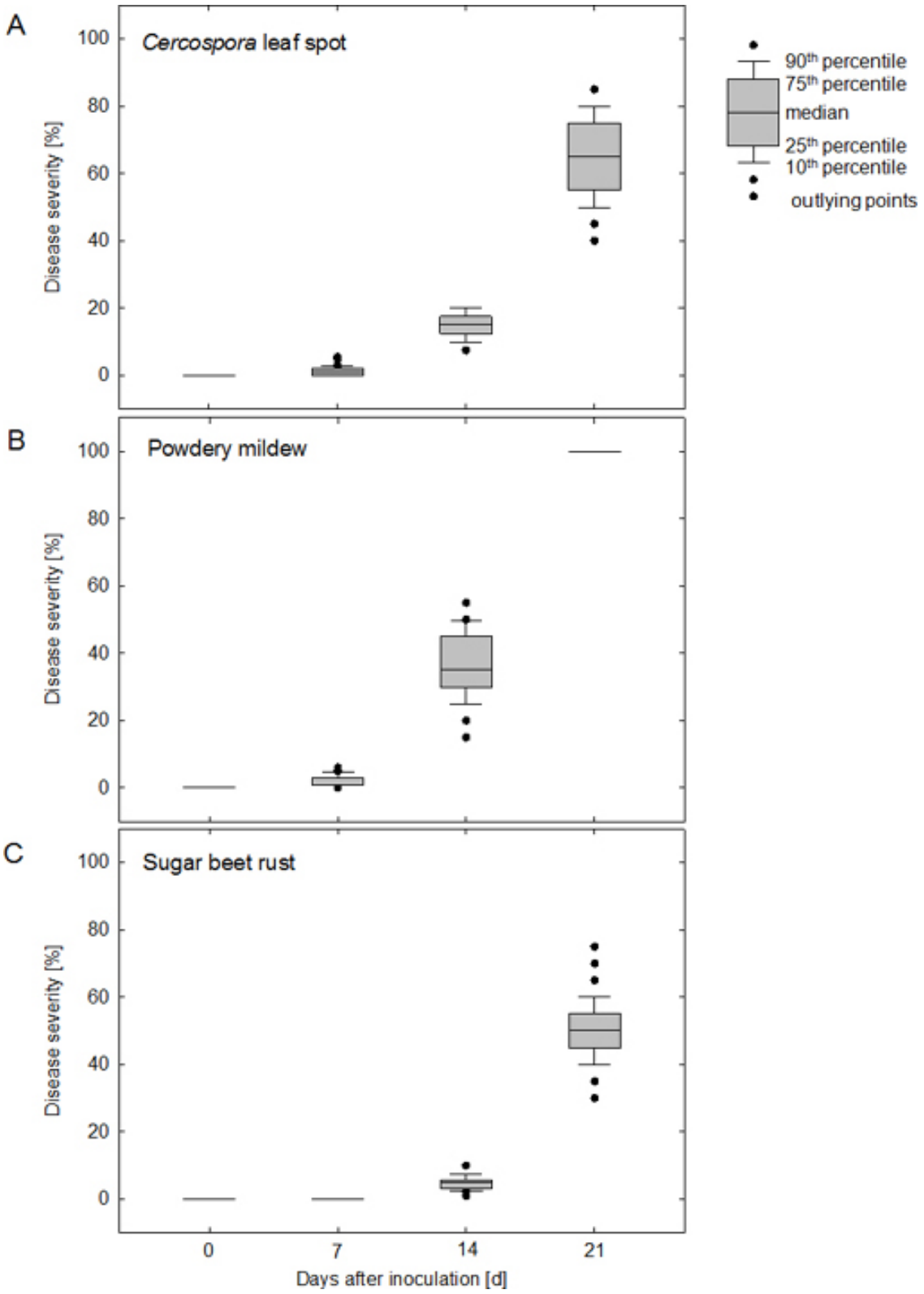

Figure 4.9: Disease severity of (A) *Cercospora* leaf spot, (B) powdery mildew and (C) sugar beet rust on sugar beet leaves at times of full range hyperspectral measurements in the VIS, NIR, and SWIR,0, 7, 14, and 21 days after inoculation (dai).

dery mildew interfered with reflectance of non diseased leaves. With increasing disease severity, reflectance in the SWIR rose slightly 14 and 21 dai (36.2% and 100%, respectively; Fig. 4.9 B). Similar to changes in the VIS and NIR, powdery mildew influenced more the absolute SWIR reflectance values than the shape of the spectrum.

Sugar beet rust

Contrary to the other two foliar diseases, increasing disease severity of sugar beet rust caused a decline of reflectance in the SWIR (Fig. 4.10 C). This effect was already detectable 7 dai, before visible symptoms occurred, and remained stable during the measurements until 14 dai with a disease severity of 4.9% and 21 dai with a disease severity of 42.5% (Fig. 4.9 C, Fig. 4.10 C).

Canopy reflectance

Canopy reflectance is influenced by several factors as leaf geometry, leaf angle and shadow effects. Thus, disease-specific effects may be covered. High variation in NIR reflectance during the measuring period was caused by the growth of sugar beet plants and leaves, and thus by changes in the sugar beet canopy. Plant growth influenced the canopy density, plant height, and soil cover as well as the relation between leaf area, petioles, and vegetative plant organs. Reflectance measurements on the canopy scale during disease progress gave similar effects with minor peculiarity (Fig. 4.11). Reflectance in the VIS of healthy leaves remained constant during the measuring period (Fig. 4.11 A). Reflectance of canopies of *Cercospora* leaf spot diseased sugar beet plants revealed a steady increase in reflectance between 550 and 700 nm, similar to measurements on the leaf scale (Fig. 4.11 B).

An impact of diseased leaves on canopy reflectance in the NIR was not detected. Canopy reflectance of powdery mildew diseased plants rose in the VIS. Variation in NIR reflectance was higher than in healthy leaves (Fig. 4.11 C). Significant changes in canopy reflectance due to sugar beet rust symptoms were not recorded (Fig. 4.11 D). Minimal reflectance deviation around the green peak

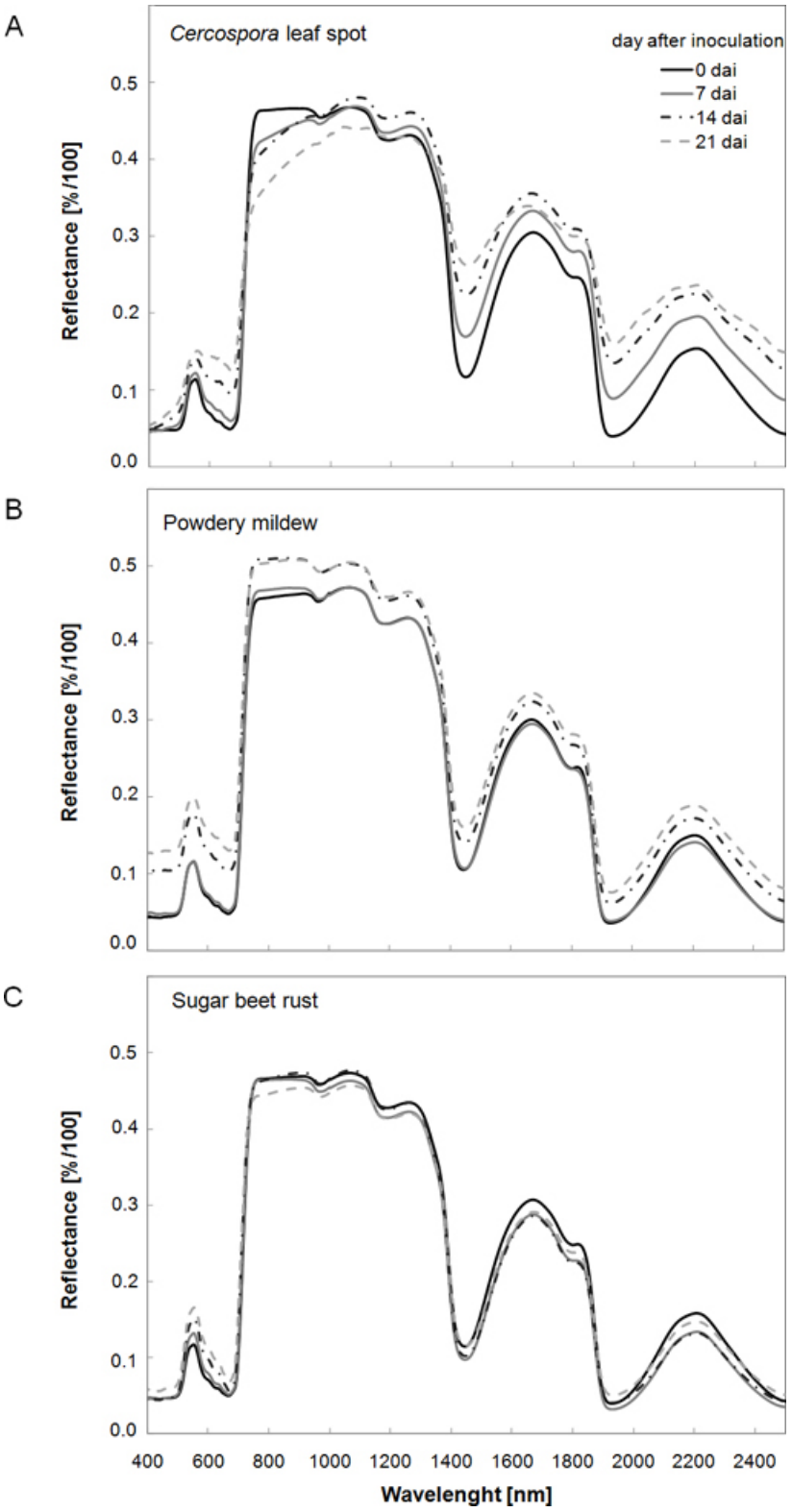

Figure 4.10: Spectral reflectance in the VIS, NIR and SWIR of healthy sugar beet leaves and leaves affected by (A) *Cercospora* leaf spot, (B) powdery mildew, and (C) sugar beet rust, 0, 7, 14, and 21 dai (ASD FieldSpec JR).

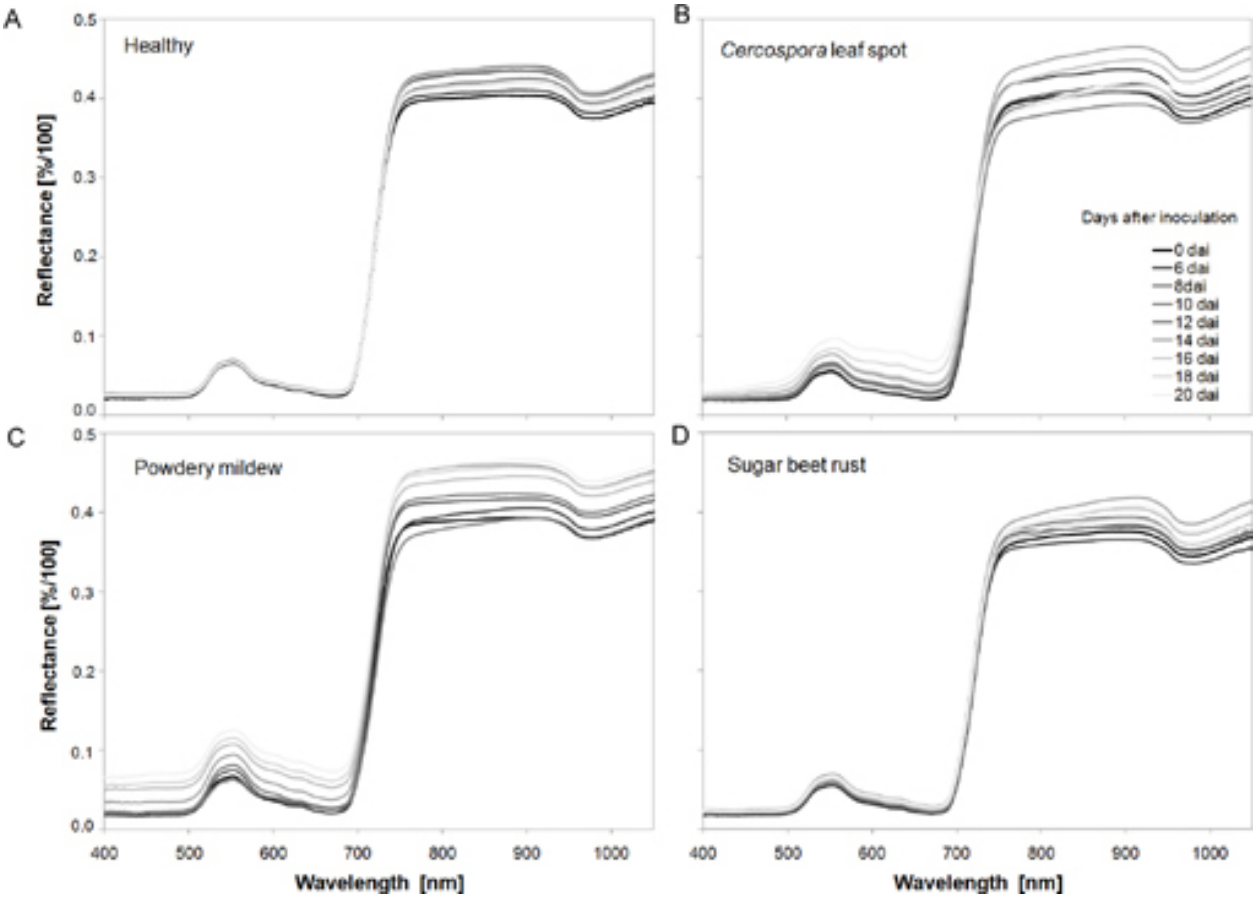

Figure 4.11: Spectral signature of (A) healthy sugar beet canopy and affected by (B) *Cercospora* leaf spot, (C) powdery mildew, and (D) sugar beet rust, measured on the canopy level in the VIS and NIR at different days after inoculation.

and between 550 to 700 nm occurred during the measuring period. In fact of the small symptom size and the leaf area to symptom relation, it was not feasible to assure a sugar beet rust infestation using a hyperspectral non-imaging spectroradiometer on canopy scale.

4.2.2 Selection of disease-specific wavelengths

An appropriate way to enhance differences between spectral signatures and to determine sensitive and significant wavelengths for a disease is the calculation of difference and ratio spectra.

Cercospora leaf spot

Maximal differences between healthy and *Cercospora* leaf spot diseased leaves over all disease severity levels were in the VIS at 510 nm and 690 nm. A maximal negative value was in the NIR at 740 nm (Fig. 4.12 A). High differences could be generally denoted between 600 to 700 nm. The wavelengths of maximum reflectance sensitivity to *Cercospora* leaf spot were predominant in the VIS between 450 to 500 nm and 600 to 700 nm, with maximal values at 480 nm and 665 nm (Fig. 4.13 A). In contrast to reflectance differences, sensitivities were low in the NIR.

Powdery mildew

For powdery mildew diseased leaves, reflectance differences were on a constant level between 400 to 700 nm, with a small peak at 700 nm and minor distinctive values between 720 to 1050 nm (Fig. 4.12 B). Maximal reflectance sensitivity was between 400 to 530 nm and 570 to 700 nm (Fig. 4.13 B). Sensitivity had a local minimum in the range from 530 to 570 nm.

Sugar beet rust

Comparatively minor differences and sensitivity values were estimated for spectral reflectance characteristic for sugar beet rust. Maximum differences occurred in the wavelengths of from 500 to 670 nm with an additional peak at 700 nm (Fig. 4.12 C). In the NIR, differences from 720 nm to 800 nm were negative. Sensitivity curve analysis indicated that wavelength most sensitive were from 500 to 670 nm and near 700 nm (Fig. 4.13 C).

The information from spectral reflectance measurement and their related parameters were combined in a table, summarising the principal impact of each disease on sugar beet reflectance (Tab. 4.2). Similarities and differences between the different diseases became obvious. *Cercospora* leaf spot increased reflectance in the blue, green, and red region and decreased reflectance in the NIR. Reflectance in the SWIR increased significantly, reflectance in the SWIR was decreasing with increasing disease severity.

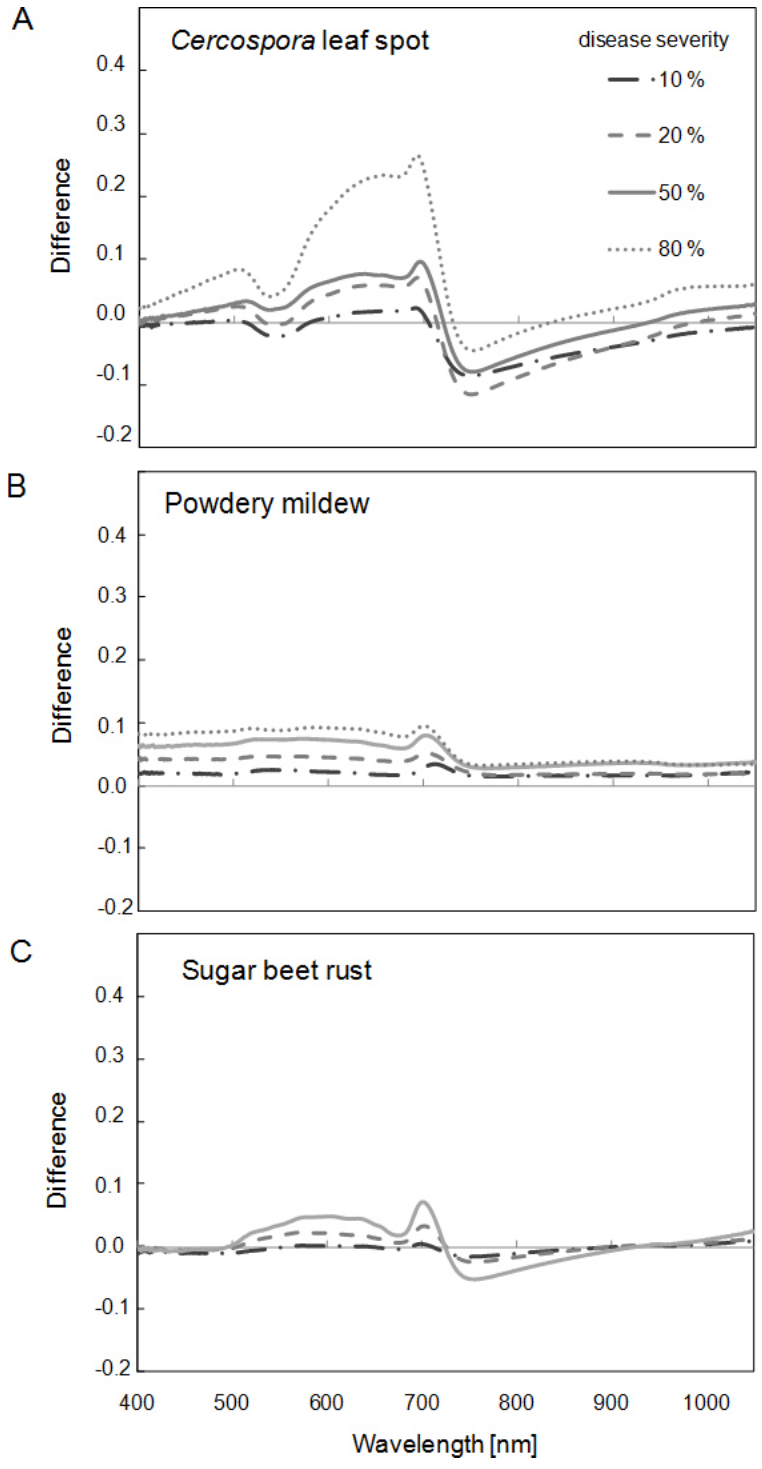

Figure 4.12: Difference spectra of sugar beet leaves affected by (A) *Cercospora* leaf spot, (B) powdery mildew, and (C) sugar beet rust at different disease severities. Non-dimensional differences were computed by subtracting reflectance of healthy leaves from that of diseased leaves.

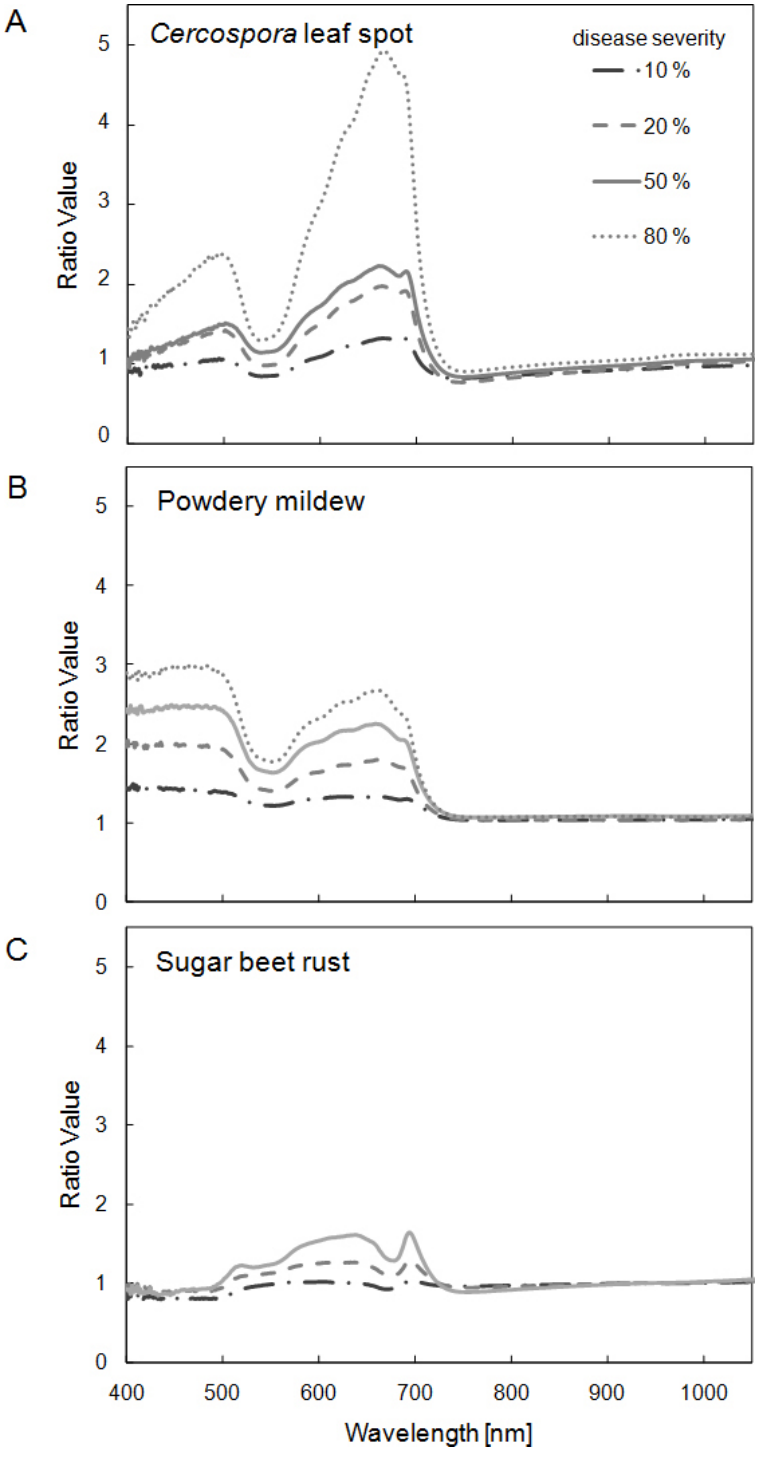

Figure 4.13: Ratio values of sugar beet leaves affected by (A) *Cercospora* leaf spot, (B) powdery mildew, and (C) sugar beet rust at different disease severities. Non-dimensional ratio-values were computed by dividing reflectance of diseased leaves by reflectance of healthy leaves.

Table 4.2: Summary of the effects of *Cercospora* leaf spot, powdery mildew, and sugar beet rust, respectively, on spectral reflectance, ratio value, reflectance difference, and correlation between reflectance and disease severity.

	Spectral reflectance					Ratio		Difference		Correlation	
	400–550 nm **Blue**	550–650 nm **Green**	650–700 nm **Red**	700–1200 nm **NIR**	1200-2500 nm **SWIR**	**Min**	**Max**	**Min**	**Max**	**Min**	**Max**
CLS	increase	increase	high	decrease	increase	550 nm	481 nm 665 nm	524 nm	688 nm	725 nm	495–514 nm 499 nm 581–704 nm 694 nm
PM	high	high	high	increase	increase	< 700 nm	500 nm 675 nm	754 nm 965 nm	694 nm	764 nm	400–700 nm 585 nm
SBR	low	decrease	low	decrease	decrease	720 nm	698 nm	488 nm 723 nm 921 nm	695 nm 747 nm	732 nm	629–638 nm 634 nm 688–704 nm 695 nm

Wavelengths around the green peak region, next to 690 nm as well as the slope at the red edge position were highly correlated to disease severity. Higher reflectance over the whole spectrum was characteristic for powdery mildew infestations. In general, wavelengths in the VIS were stronger correlated to powdery mildew disease severities than reflectance in the NIR and SWIR. The influence of sugar beet rust on reflectance parameters was minor; no change of spectral reflectance in the blue region, slight increase at the green peak region, and decrease in the NIR were characteristic. In contrast to the other pathogens, reflectance in the SWIR was decreasing with increasing disease severity.

4.3 Spectral vegetation indices as indicators of plant status and their correlation to diseases

Twenty-one SVIs related to physiological plant parameters were calculated for each treatment and every day. Their suitability to distinguish between healthy and diseased sugar beets was proven. Regarding the biochemical modifications of diseased plants, some SVIs were more sensitive to detect changes in plant health than others (Tab. 4.3, Tab. 4.4).

4.3.1 Effect of disease progression on spectral vegetation indices

The correlation between SVIs and disease severity varied among the different diseases (Tab. 4.3). Disease severity of *Cercospora* leaf spot was strongly correlated to vitality and leaf area related SVIs ND and NDVI (r = -0.89; r = -0.89), to the chlorophyll related spectral vegetation indices PSNDa and PSNDb (r = -0.89, r = - 0.90), as well as to PRI (r = -0.88) as an indicator for photosynthetic radiation use efficiency. Spectral vegetation indices highly correlated to powdery mildew were the pigment specific indices SIPI (r = -0.88), PSNDa, PSNDb, and PSNDc (r = -0.88, r = -0.89, r = -0.88), the NDVI (r = -0.88), and the SumGREEN index (r = -0.86), which is related to reflectance between 500 to 600 nm. Correlations between sugar beet rust disease severity and the SVIs was generally minor. Good correlations were found for the PRI (r = -0.82) and for the anthocyanin specific ARI (r = 0.79). The mCAI (r = -0.74) as an indicator for chlorophyll content and the ND (r = - 0.75) were also correlated to sugar beet rust infestation.

Cercospora leaf spot

The PSRI was most sensitive to increases in disease severity of *Cercospora* leaf spot (Tab. 4.4). Significant differences during the measuring period could be detected 7 dai and later, according to the occurrence of first symptoms. Significant changes were found for the BGI2, the ARI and the WI 8 dai, however, the

correlation to these indices was lower. The WI was significantly affected only by *Cercospora* leaf spot pathogenesis, while the impact of powdery mildew and sugar beet rust was not significant. Chlorophyll related spectral vegetation indices like SR, ND, NDVI, PRI, PSSRa, and PSSRb were able to detect changes within the pathogenesis of *C. beticola* 9 dai. The mSR was not suitable for the detection of physiological changes from *Cercospora* leaf spot. Significant differences occurred only from 14 dai to 18 dai. Likewise, REP, SumGREEN, and SumVIS were not appropriate to detect early changes caused by *Cercospora* leaf spot (significant differences were measured only after 16 dai).

Table 4.3: Coefficients of correlation between disease severity and spectral vegetation indices for the three leaf diseases of sugar beet.

Index	**Cercospora leaf spot**	**Powdery mildew**	**sugar beet rust**
SR	-0.85*[1]	-0.85*	-0.71*
mSR	-0.85*	-0.60*	-0.70*
ND	-0.89*	-0.86*	-0.75*
NDVI	-0.89*	-0.88*	-0.70*
PRI	-0.88*	-0.77*	-0.82*
SIPI	-0.86*	-0.88*	-0.51*
PSSRa	-0.81*	-0.85*	-0.64*
PSSRb	-0.81*	-0.85*	-0.61*
PSSRc	-0.74*	-0.83*	-0.23*
PSNDa	-0.89*	-0.88*	-0.64*
PSNDb	-0.90*	-0.89*	-0.72*
PSNDc	-0.81*	-0.88*	-0.22*
ARI	0.73*	0.51*	0.79*
mCAI	-0.84*	-0.78*	-0.74*
REP	-0.76*	-0.55*	-0.62*
PSRI	0.86*	-0.27*	0.64*
WI	-0.68*	-0.01	-0.59*
MCARI	-0.30*	-0.39*	0.61*
SumGREEN	0.80*	0.86*	0.60*
SumVIS	0.87*	0.86*	0.59*
BGI2	0.42*	0.82*	-0.44*

[1] correlation was calculated as Pearsons coefficient of correlation (r); asterisks denote significant correlation with p = 0.01, n = 630

Note: highlighted SVIs indicate high correlation to disease severity

Powdery mildew

Although first symptoms appeared 5 dai, significant changes in SVIs from powdery mildew were detected 8 dai (Tab. 4.4), the SumVIS index changed significantly to the initial value of the measuring period. The sensitivity of the SumVIS index, similar to the SumGREEN index differed strongly to the diseases, significant differences occurred 9 dai. An impact of *Cercospora* leaf spot and sugar beet rust were detectable by these indices only 16 dai and later. The SVIs - mSR, NDVI, PSSRa, PSSRb, PSNDa, and PSNDb – assessing the chlorophyll content, were sensitive to powdery mildew 10 dai, whereas the mCAI index was significant already 9 dai. Other pigment-specific SVIs like the carotenoid specific SIPI, PSSRc, and PSNDc and the anthocyanin-indicating ARI showed significant differences 10 dai and later. The REP seems as well appropriate to detect powdery mildew diseased sugar beet leaves. Significant differences in the red edge position were detected 10 dai for powdery mildew and only 16 dai for *Cercospora* leaf spot and sugar beet rust. The WI and the MCARI were less qualified to detect powdery mildew.

Sugar beet rust

Changes between rust-infected and healthy plants were recorded for the PRI linked to photosynthetic radiation use efficiency and for the senescence-indicating PSRI 10 dai (Tab. 4.4). These results coincided with the first occurrence of rust-specific symptoms on sugar beet leaves. All other vegetation indices were less suitable to distinguish between healthy and rust-diseased sugar beet leaves; significant differences occurred not earlier than 16 dai. No significant differences among SVIs were found for the carotenoid specific indices PSSRc and PSNDc. Although the non-inoculated plant remained healthy during the measuring period, statistically significant differences were measured within this treatment by SR, MCARI, BGI2, PSSRa, PSSRb, and PSNDa. In most of the cases these significances were recorded 14 to 20 dai, when senescence effects the healthy sugar beet leaves.

Table 4.4: Coefficients of correlation between disease severity and different spectral vegetation indices for the three leaf diseases of sugar beet.[1]

Index[2]	Treatment	Days after inoculation												
		0	5	6	7	8	9	10	11	12	14	16	18	20
SR	Healthy	2.49	2.82	2.89	2.97	2.96	2.99	2.99	2.99	3.08	**3.12***	3.07	3.07	3.02
	CLS	2.48	2.72	2.78	2.76	2.61	2.42	2.22	**2.16***	**2.24**	**1.97**	**1.69**	**1.61**	**1.50**
	PM	2.98	2.90	2.87	2.91	2.77	**2.66***	**2.50**	**2.44**	**2.34**	**2.19**	**2.10**	**2.01**	**1.88**
	SBR	2.48	2.65	2.75	2.73	2.73	2.73	2.62	2.70	2.72	2.60	**2.17***	**2.04**	**1.83**
mSR	Healthy	3.03	3.51	3.63	3.77	3.65	3.79	3.81	3.81	3.98	**4.03***	**4.01**	**4.04**	3.98
	CLS	3.00	3.43	3.55	3.38	3.25	2.99	2.75	2.63	2.72	**2.35***	**1.95**	**1.83**	**1.69**
	PM	3.73	3.65	3.57	3.73	3.52	3.44	**3.16***	**3.31**	**3.21**	**3.23**	**3.18**	**3.03**	**2.94**
	SBR	3.07	3.22	3.34	3.34	3.36	3.35	3.22	3.32	3.30	3.16	**2.49***	**2.31**	**2.03**
ND	Healthy	0.43	0.48	0.49	0.50	0.50	0.50	0.50	0.50	0.51	0.51	0.51	0.51	0.50
	CLS	0.43	0.46	0.47	0.47	0.45	0.42	0.38	0.37	**0.38***	**0.33**	**0.26**	**0.23**	**0.20**
	PM	0.50	0.49	0.48	0.49	0.47	**0.45***	**0.43**	**0.42**	**0.40**	**0.37**	**0.36**	**0.33**	**0.30**
	SBR	0.42	0.45	0.47	0.46	0.46	0.46	0.45	0.46	0.46	0.44	**0.37***	**0.34**	**0.29**
NDVI	Healthy	0.78	0.80	0.80	0.81	0.81	0.80	0.80	0.80	0.80	0.81	0.81	0.81	0.81
	CLS	0.79	0.79	0.79	0.80	0.77	**0.75***	**0.71**	**0.70**	**0.70**	**0.64**	**0.58**	**0.56**	**0.51**
	PM	0.81	0.81	0.81	0.80	0.80	0.78	**0.77***	**0.73**	**0.70**	**0.64**	**0.62**	**0.59**	**0.54**
	SBR	0.78	0.80	0.80	0.80	0.80	0.80	0.79	0.79	0.80	0.79	0.76	**0.75***	**0.72**
PRI	Healthy	0.02	0.03	0.03	0.02	0.02	0.03	0.03	0.03	0.02	0.02	0.03	0.03	0.03
	CLS	0.02	0.02	0.02	0.02	0.02	**0.01***	**-0.01**	**-0.01**	**-0.01**	**-0.02**	**-0.03**	**-0.04**	**-0.05**
	PM	0.03	0.02	0.03	0.02	0.03	0.03	0.02	0.02	**0.01***	**0.01**	**0.01**	**0.01**	**-0.01**
	SBR	0.03	0.03	0.02	0.02	0.02	0.03	**0.02***	**0.01**	**0.01**	**0.01**	**-0.01**	**-0.01**	**-0.03**
SIPI	Healthy	0.79	0.81	0.81	0.81	0.82	0.81	0.81	0.81	0.81	0.81	0.81	0.81	0.81
	CLS	0.79	0.80	0.80	0.81	0.78	0.77	**0.74***	**0.74**	**0.74**	**0.70**	**0.67**	**0.65**	**0.62**
	PM	0.82	0.81	0.82	0.80	0.80	0.78	**0.77***	**0.73**	**0.70**	**0.64**	**0.62**	**0.59**	**0.54**
	SBR	0.78	0.81	0.81	0.81	0.80	0.81	0.79	0.80	0.81	0.80	0.79	0.78	**0.76***
BGI2	Healthy	0.36	0.37	0.37	0.38	0.36	0.39	0.39	0.39	**0.42***	**0.41**	**0.43**	**0.44**	**0.43**
	CLS	0.34	0.39	0.40	0.36	**0.40***	**0.41**	**0.45**	**0.44**	**0.43**	**0.44**	**0.42**	**0.43**	**0.45**
	PM	0.38	0.39	0.38	0.42	0.40	0.42	0.43	**0.50***	**0.53**	**0.59**	**0.62**	**0.64**	**0.67**
	SBR	0.37	0.34	0.35	0.36	0.35	0.35	0.36	0.36	0.34	0.35	**0.29***	**0.30**	**0.29**

Tab. 4.4 continued

Index[2]	Treatment	Days after inoculation												
		0	5	6	7	8	9	10	11	12	14	16	18	20
PSSRa	Healthy	7.47	8.22	8.51	8.82	8.59	8.24	8.25	8.25	8.52	8.56	8.56	**8.98***	**8.91**
	CLS	7.65	7.99	8.03	8.03	7.15	**6.47***	**5.52**	**5.33**	**5.37**	**4.36**	**3.59**	**3.39**	**2.95**
	PM	8.72	8.49	8.95	8.23	8.03	7.48	**7.12***	**6.00**	**5.41**	**4.35**	**4.12**	**3.72**	**3.25**
	SBR	7.50	8.16	8.40	8.23	8.21	8.20	7.63	7.97	8.49	7.77	6.77	**6.55***	**5.63**
PSSRb	Healthy	6.54	7.42	7.61	7.82	8.18	7.94	7.94	7.94	8.01	**8.39***	**8.10**	**8.26**	**8.19**
	CLS	6.55	6.99	7.12	7.32	6.44	**5.73***	**4.93**	**4.77**	**5.02**	**4.06**	**3.31**	**3.10**	**2.70**
	PM	8.05	7.98	7.87	7.64	7.32	6.80	**6.39***	**5.50**	**4.98**	**4.10**	**3.81**	**3.48**	**3.03**
	SBR	6.45	7.21	7.54	7.25	7.19	7.18	6.71	6.94	7.23	6.60	**5.46***	**4.99**	**4.24**
PSSRc	Healthy	8.86	9.94	10.14	10.35	11.29	10.47	10.12	10.12	10.20	10.64	10.07	9.74	9.57
	CLS	9.01	9.16	9.28	10.29	9.07	8.20	**7.24***	**7.40**	**7.75**	**6.73**	**6.08**	**5.86**	**5.25**
	PM	10.76	10.45	10.39	9.74	9.48	8.41	**8.25***	**6.53**	**5.91**	**4.61**	**4.27**	**3.94**	**3.42**
	SBR	8.46	9.90	10.36	10.15	9.98	9.81	9.33	9.78	10.65	9.66	9.82	9.35	8.88
PSNDa	Healthy	0.76	0.78	0.79	0.80	0.79	0.78	0.78	0.78	0.79	0.79	0.79	**0.80***	**0.80**
	CLS	0.77	0.78	0.78	0.78	0.75	0.73	**0.69***	**0.68**	**0.69**	**0.63**	**0.56**	**0.54**	**0.49**
	PM	0.79	0.79	0.80	0.78	0.78	0.76	**0.75***	**0.71**	**0.69**	**0.63**	**0.61**	**0.58**	**0.53**
	SBR	0.76	0.78	0.79	0.78	0.78	0.78	0.77	0.78	0.79	0.77	0.74	0.74	**0.70***
PSNDb	Healthy	0.73	0.76	0.77	0.77	0.78	0.78	0.78	0.78	0.78	0.79	0.78	0.78	0.78
	CLS	0.74	0.75	0.75	0.76	0.73	0.70	**0.66***	**0.65**	**0.67**	**0.60**	**0.54**	**0.51**	**0.46**
	PM	0.78	0.78	0.77	0.77	0.76	0.74	**0.73***	**0.69**	**0.67**	**0.61**	**0.58**	**0.55**	**0.50**
	SBR	0.73	0.76	0.77	0.76	0.76	0.76	0.74	0.75	0.76	0.74	0.69	**0.67***	**0.62**
PSNDc	Healthy	0.80	0.82	0.82	0.82	0.84	0.83	0.82	0.82	0.82	0.83	0.82	0.81	0.81
	CLS	0.80	0.80	0.81	0.82	0.80	0.78	**0.76***	**0.76**	**0.77**	**0.74**	**0.72**	**0.71**	**0.68**
	PM	0.83	0.83	0.82	0.81	0.81	0.79	**0.78***	**0.73**	**0.71**	**0.64**	**0.62**	**0.60**	**0.55**
	SBR	0.79	0.82	0.82	0.82	0.82	0.82	0.81	0.81	0.83	0.81	0.82	0.81	0.80
mCAI	Healthy	-33.9	-31.2	-30.6	-29.9	-29.0	-30.5	-30.4	-30.4	-28.6	-28.2	-28.8	-28.0	-30.2
	CLS	-33.1	-31.6	-31.0	-29.8	-31.0	-30.7	-30.4	-30.1	-31.8	-33.1	**-38.5***	**-39.0**	**-42.2**
	PM	-30.1	-29.7	-29.2	-29.9	-32.5	**-33.3***	**-33.8**	**-36.4**	**-37.3**	**-43.6**	**-44.2**	**-47.4**	**-51.6**
	SBR	-31.6	-31.1	-29.8	-30.7	-31.6	-32.0	-32.4	-31.6	-31.8	-31.8	**-35.8***	**-35.6**	**-37.8**
ARI	Healthy	-0.35	-0.53	-0.62	-0.73	-0.46	-0.45	-0.49	-0.49	-0.34	-0.25	-0.34	-0.42	-0.48
	CLS	-0.47	-0.55	-0.52	-0.30	**0.07***	**0.39**	**0.92**	**1.15**	**1.04**	**1.47**	**1.48**	**1.57**	**1.69**
	PM	-0.39	0.04	-0.32	-0.14	-0.14	-0.24	**0.13***	**0.05**	**0.15**	**0.03**	**0.09**	**0.18**	**0.15**

Tab. 4.4 continued

Index[2]	Treatment	Days after inoculation												
		0	5	6	7	8	9	10	11	12	14	16	18	20
	SBR	-0.48	-0.56	-0.57	-0.55	-0.74	-0.77	-0.49	-0.50	-0.55	-0.43	**0.02***	**0.26**	**0.67**
REP	Healthy	716.3	717.9	718.2	718.5	717.9	718.2	718.2	718.2	718.8	718.6	718.6	718.6	718.4
	CLS	716.2	717.7	718.1	717.5	717.7	717.4	717.1	717.0	716.9	716.2	**714.1***	**713.1**	**712.1**
	PM	718.3	718.0	717.9	718.2	717.5	717.3	**716.8***	**717.0**	**716.7**	**716.3**	**716.5**	**716.1**	**716.1**
	SBR	716.5	717.0	717.4	717.5	717.3	717.2	717.0	717.3	717.3	717.1	**714.7***	**713.9**	**711.9**
PSRI	Healthy	0.011	0.014	0.012	0.009	0.020	0.018	0.015	0.015	0.015	0.019	0.013	0.009	0.011
	CLS	0.009	0.008	0.008	**0.017***	**0.017**	**0.017**	**0.031**	**0.038**	**0.042**	**0.064**	**0.089**	**0.099**	**0.124**
	PM	0.013	0.017	0.010	0.014	0.011	0.008	0.012	**0.008***	**0.009**	**0.004**	**0.003**	**0.008**	**0.006**
	SBR	0.004	0.014	0.016	0.014	0.011	0.009	**0.017***	**0.015**	**0.014**	**0.016**	**0.030**	**0.030**	**0.045**
WI	Healthy	1.04	1.04	1.04	1.04	1.04	1.03	1.04	1.04	1.03	1.04	1.03	1.03	1.03
	CLS	1.04	1.03	1.04	1.03	**1.02***	**1.01**	**1.00**	**0.99**	**1.00**	**0.99**	**0.98**	**0.98**	**0.98**
	PM	1.04	1.04	1.03	1.03	1.03	1.04	1.03	1.04	1.03	1.04	1.03	1.03	1.04
	SBR	1.04	1.04	1.04	1.04	1.04	1.04	1.04	1.04	1.04	1.03	1.03	1.03	**1.02***
MCARI	Healthy	0.24	0.18	**0.17***	**0.16**	**0.17**	**0.17**	**0.16**	**0.16**	**0.14**	**0.15**	**0.15**	**0.16**	**0.17**
	CLS	0.24	0.19	**0.17***	**0.18**	**0.17**	**0.16**	**0.14**	**0.14**	**0.15**	**0.14**	**0.15**	**0.16**	**0.14**
	PM	0.17	0.18	0.19	0.17	0.20	0.20	0.21	0.17	0.16	0.15	**0.14***	**0.14**	**0.13**
	SBR	0.24	0.22	0.20	0.20	0.21	0.21	0.21	0.20	0.22	0.21	**0.30***	**0.31**	**0.33**
SumGREEN	Healthy	0.11	0.10	0.09	0.09	0.09	0.09	0.09	0.09	0.08	0.08	0.09	0.08	0.09
	CLS	0.11	0.10	0.10	0.09	0.10	0.10	0.10	0.10	0.10	0.11	**0.13***	**0.13**	**0.14**
	PM	0.09	0.09	0.09	0.09	0.10	**0.11***	**0.11**	**0.12**	**0.13**	**0.16**	**0.16**	**0.18**	**0.20**
	SBR	0.12	0.10	0.09	0.10	0.10	0.10	0.11	0.10	0.10	0.10	0.12	0.12	**0.13***
SumVIS	Healthy	0.08	0.07	0.07	0.07	0.06	0.07	0.07	0.07	0.06	0.06	0.06	0.06	0.07
	CLS	0.08	0.07	0.07	0.07	0.08	0.08	0.08	0.08	0.08	0.09	**0.11***	**0.11**	**0.12**
	PM	0.07	0.07	0.07	0.07	**0.09***	**0.09**	**0.09**	**0.10**	**0.10**	**0.13**	**0.14**	**0.15**	**0.18**
	SBR	0.08	0.07	0.07	0.07	0.07	0.07	0.08	0.07	0.07	0.08	**0.09***	**0.09**	**0.10**

[1] for each index within a row, bold letters indicate significant differences to the initial value and asterisk marks denote first occurrence of significant differences during the measuring period, according to general linear model GLM and Bonferroni-test (p = 0.01; n= 60)

[2] CLS = Cercospora leaf spot, PM = powdery mildew, SBR = sugar beet rust

Note: From day 1 to day 6 there were no significant differences between healthy and diseased treatments;
highlighted date indicates first appearance of visible disease symptom

4.3.2 Combination of spectral vegetation indices for disease identification

The results presented above allow only a classification between healthy and diseased plants. In a second approach, index combinations were tested to differentiate the diseases. Pair-wise correlation coefficients between the SVIs were calculated in a correlation matrix (Tab. 4.5). Low correlation coefficients indicated high dissimilarity of scatter-plots and thus a suitable index combination for disease detection and discrimination. Indices based on similar wavelength or similar regions of the spectrum like NDVI and PSNDa, ND and SR, or mCAI and SumGREEN, were not suitable for discrimination of healthy and diseased plants or among the diseases, as indicated by their high correlation coefficient (NDVI *vs.* PSNDa r= 0.99; ND *vs.* SR r = 0.98; mCAI *vs.* SumGREEN r = - 0.99). Combinations of SVIs like ARI and SIPI (r = -0.60), MCARI and SR (r= -0.21), BGI2 and PRI (r= -0.09), or WI and MCAI (r= -0.03) were weakly correlated or not correlated, which indicated suitable combinations for disease separation. Scatter matrixes for all index combinations were mapped and the best differentiating combinations were examined (Fig. 4.14, Fig. 4.15). Divergent scatter plots denoted robust index combinations to distinguish between the different diseases.

Plots of SIPI, PSSRa, PSSRb and NDVI, SumGREEN and SumVIS as well as REP, PSRI, PRI *versus* each other resulted in stacked scatter plots (Fig. 4.14). The discriminative potential of these combinations was low; the classes interfered with each other. Combinations including the ARI, except those with PSRI and PRI, respectively, showed obvious divergent scatter plots for diseased and healthy leaves, as well as among the diseases. Most pronounced differences were observed for the combination ARI *vs.* SIPI, ARI *vs.* NDVI, BGI2 *vs.* PRI. In particular similar results could be noticed for ARI *vs.* mCAI.

Table 4.5: Correlation[1] matrix between calculated spectral vegetation indices from healthy sugar beet leaves and sugar beet leaves affected with *Cercospora* leaf spot, powdery mildew, and sugar beet rust during measuring period. Low correlation coefficients (r) indicate high dissimilarity of scatter-plots and thus a robust index combination for disease detection and discrimination. High correlation coefficients and thus inappropriate index combinations are highlighted.

	SR	mSR	ND	NDVI	PRI	SIPI	PSSRa	PSSRb	PSSRc	PSNDa	PSNDb	PSNDc	ARI	mCAI	Rre	REP	PSRI	WI	MCARI	Sum Green	Sum VIS
mSR	.93*																				
ND	.98*	.92*																			
NDVI	.85*	.67*	.89*																		
PRI	.82*	.83*	.87*	.77*																	
SIPI	.77*	.52*	.79*	.96*	.59*																
PSSRa	.88*	.70*	.87*	.93*	.72*	.91*															
PSSRb	.95*	.80*	.93*	. 90*	.76*	.87*	.97*														
PSSRc	.74*	.47*	.72*	.86*	.49*	.92*	.92*	.88*													
PSNDa	.85*	.68*	.89*	.99*	.77*	.95*	.93*	.90*	.85*												
PSNDb	.92*	.77*	.95*	.98*	.82*	.92*	.93*	.94*	.84*	.98*											
PSNDc	.69*	.41*	.69*	.88*	.44*	.98*	.85*	.81*	.92*	.88*	.85*										
ARI	-.76*	-.73*	-.78*	-.75*	-.85*	-.60*	-.77*	-.73*	-.56*	-.76*	-.75*	-.47*									
mCAI	.78*	.59*	.80*	.85*	.55*	.89*	.81*	.82*	.79*	.85*	.88*	.88*	-.42*								
Rre	-.38*	-.14*	-.39*	-.58*	-.14*	-.71*	-.53*	-.49*	-.63*	-.57*	-.56*	-.76*	.03	-.85*							
REP	.78*	.81*	.83*	.60*	.77*	.46*	.57*	.66*	.40*	.60*	.72*	.37*	-.54*	.64*	-.27*						
PSRI	-.57*	-.63*	-.66*	-.65*	-.84*	-.42*	-.52*	-.49*	-.30*	-.66*	-.63*	-.26*	.77*	-.34*	.02	-.58*					
WI	.56*	.56*	.61*	.61*	.74*	.44*	.57*	.53*	.40*	.62*	.59*	.31*	-.84*	.20*	.17*	.41*	-.75*				
MCARI	-.21*	-.39*	-.17*	.26*	-.07*	.32*	.19*	-.01	.29*	.26*	.08*	.33*	-.16*	-.03	-.14*	-.46*	-.15*	.26*			
SumGreen	-.78*	-.58*	-.78*	-.82*	-.50*	-.87*	-.79*	-.82*	-.79*	-.81*	-.86*	-.88*	.37*	-.99*	.83*	-.61*	.23*	-.16*	.08*		
SumVIS	-.77*	-.53*	-.77*	-.88*	-.52*	-.94*	-.83*	-.83*	-.84*	-.88*	-.89*	-.95*	.44*	-.98*	.84*	-.55*	.30*	-.25*	-.10*	.97*	
BGI2	-.25*	.09*	-.25*	-.61*	-.09*	-.77*	-.59*	-.46*	-.77*	-.60*	-.50*	-.83*	.26*	-.55*	.65*	.09*	.02	-.17*	-.67*	.54*	.66*

1 correlation was calculated as Pearsons coefficient of correlation (r); asterisk marks denote significant correlation with p = 0.01, n = 2520; highlighted combination denote high correlation, with r $\geq$ 0.7

The combination between SumVIS and PSRI offers potential to discriminate between healthy, *Cercospora* leaf spot, and powdery mildew (Fig. 4.15). Scatter plots for the healthy class is aggregated on the left bottom of the graph, while powdery mildew scatter plots are orientated in a straight line to the upper left and *Cercospora* leaf spot scatter plots to the right middle. Sugar beet rust interferes with *Cercospora* leaf spot scatter plots and was not distinguishable by this combination.

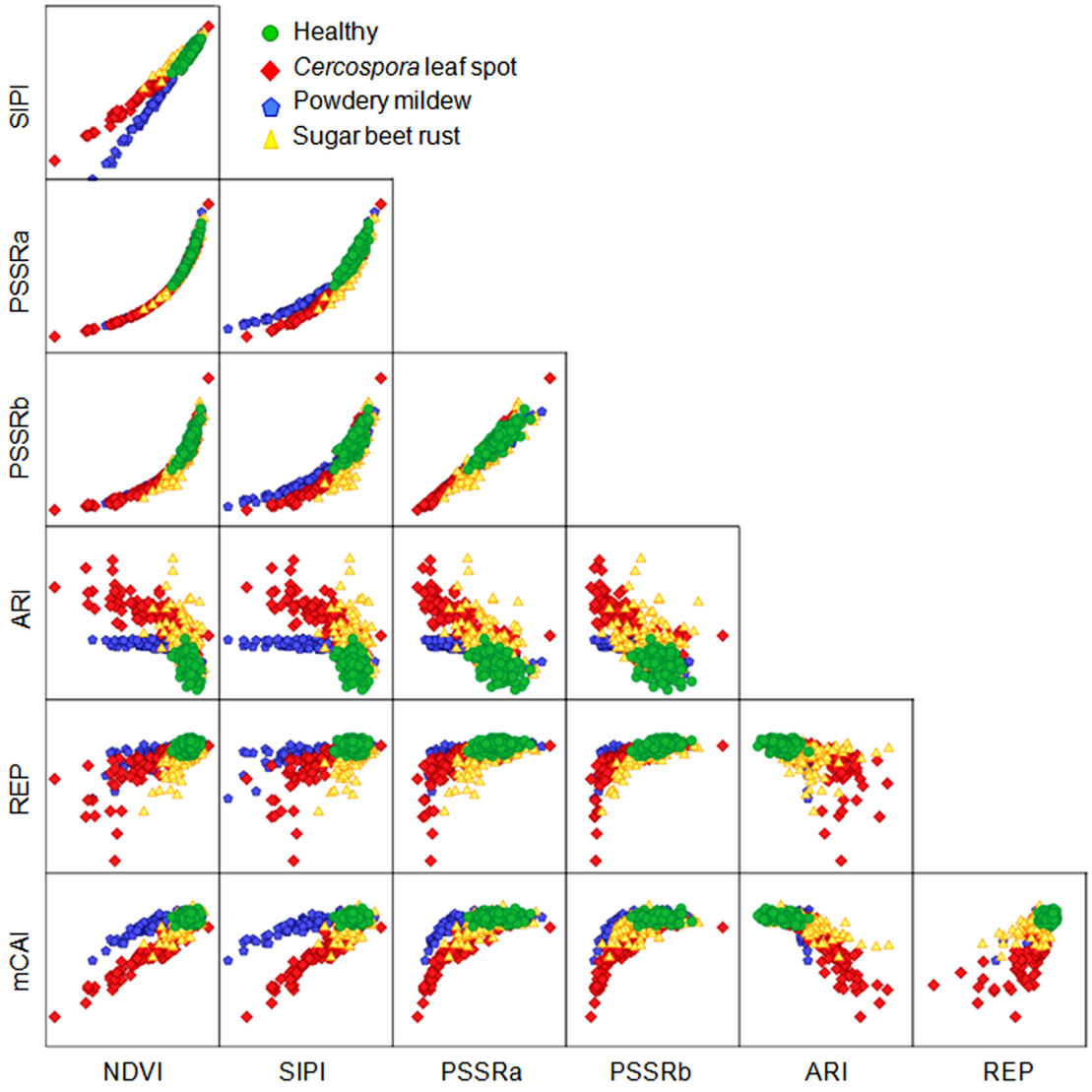

Figure 4.14: Scatter matrix of spectral vegetation indices combinations for the discrimination of three leaf diseases of sugar beet, divergent scatter-plots denote a robust index combination for disease detection and discrimination. Best divergent combinations were ARI *vs.* NDVI, ARI *vs.* SIPI, mCAI *vs.* ARI, and mCAI *vs.* SIPI.

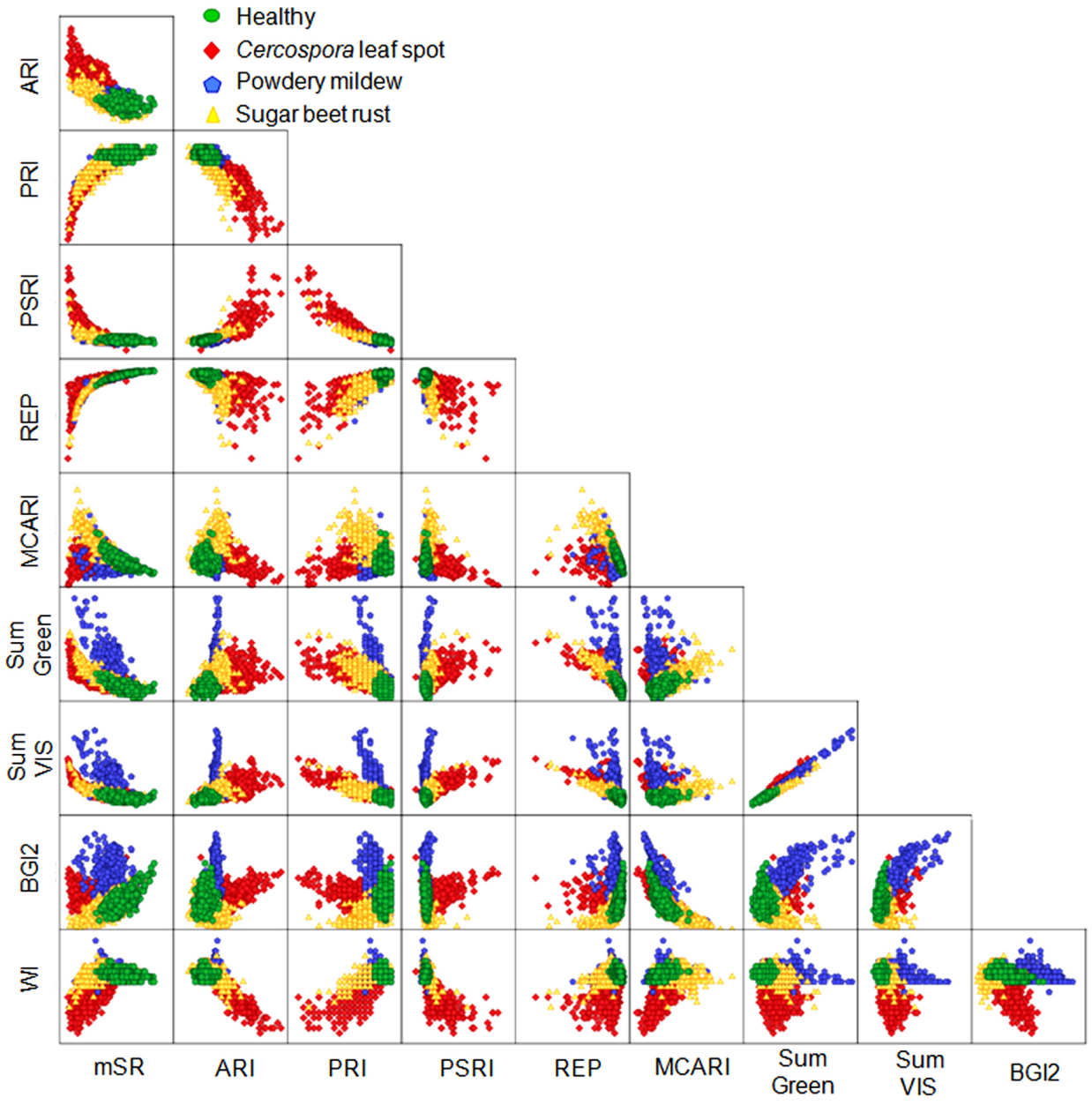

Figure 4.15: Scatter matrix continued. Best divergent combinations were SumVIS *vs.* ARI, BGI2 *vs.* PRI, and in particular to discriminate *Cercospora* leaf spot diseased plants from sugar beet rust diseased plants MCARI *vs.* ARI and MCARI *vs.* PSRI.

Studying the combination ARI *vs.* SIPI in more detail showed that the severity of diseases biased the scatter plots (Fig. 4.16). Values from leaves with low disease severity were placed in the same region of the plot, irrespective of the disease. With increasing disease severity, *Cercospora* leaf spot values changed to lower SIPI values and increasing ARI values. For higher sugar beet rust

severities only an increase in ARI values could be observed, whereas the SIPI remained constant. The distribution of powdery mildew values was highly divergent with constant ARI values, while SIPI values explicitly decreased with increasing disease severity.

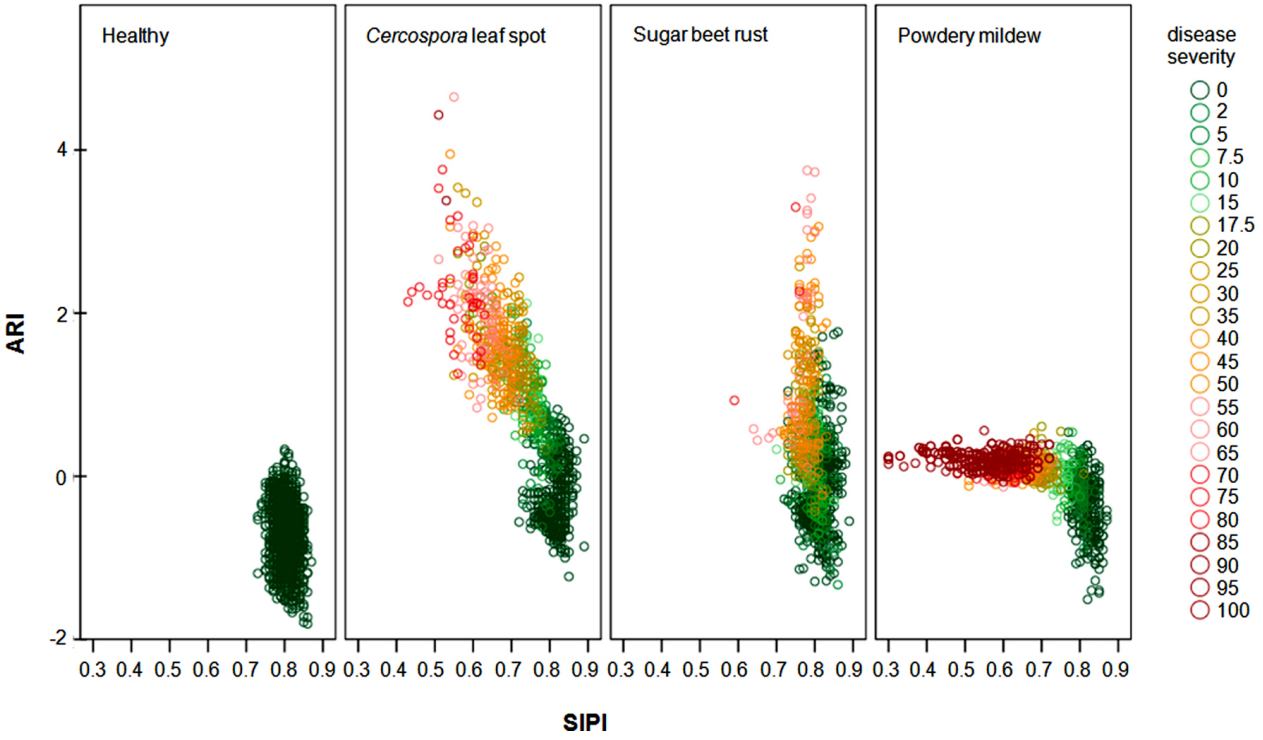

Figure 4.16: Scatter matrix between the spectral vegetation indices ARI and SIPI for healthy sugar beet leaves and diseased leaves. Colours display disease severity. Each treatment has a typical orientation in the coordinate system, thus a differentiation using this index combination seems feasible.

4.4 Detection and classification of plant diseases with Support Vector Machines based on spectral vegetation indices

The following results were achieved in cooperation with Till Rumpf, Institute of Geodesy and Geoinformation, Department of Geoinformation, University Bonn, using Support Vector Machines (SVMs) with SVIs as features for detection and classification of the diseases.

4.4.1 Dichotomous classification between healthy and diseased sugar beet leaves

In a first dichotomous approach Support Vector Machines were used for the differentiation between two classes, non-inoculated, healthy leaves and leaves, inoculated with one of the three leaf pathogens, respectively. Eight SVIs (NDVI, SR, SIPI, PSSRa, PSSRb, ARI, REP, mCAI) and SPAD-values were used as features for classification. The results showed that the specificity of classification was always above its sensitivity. Accuracy ranged from 93% to almost 97% (Tab. 4.6).

The classification accuracy increased with increasing disease severity (Fig. 4.17). Differences in the number of leaves per disease give additional information on the reliability of classification results. With only 1% to 2% diseased leaf area, the classification accuracy was about 65% for all diseases. The accuracy of differentiating between healthy leaves and leaves with *Cercospora* leaf spot symptoms rapidly increased with 3% to 5% disease severity. When more than 10% of the leaf area was covered by leaf spots, the classification accuracy reached 100% (Fig. 4.17). The accuracy of detecting symptoms of sugar beet rust and powdery mildew was lower at low disease severities. For sugar beet rust classification accuracy reached 95% when disease severity was above 6%. Leaves with powdery mildew could be differentiated from healthy leaves with an accuracy of about 95% when 10% to 15% of the leaf area was diseased (Fig. 4.17).

Table 4.6: Classification result of the dichotomous classification between healthy and diseased sugar beet leaves based on spectral vegetation indices using Support Vector Machines.

Leaf disease	Accuracy [%]	Specificity [%]	Sensitivity [%]
Cercospora leaf spot	96.68	97.84	95.45
Sugar beet rust	96.20	97.14	95.14
Powdery mildew	93.18	94.80	91.40

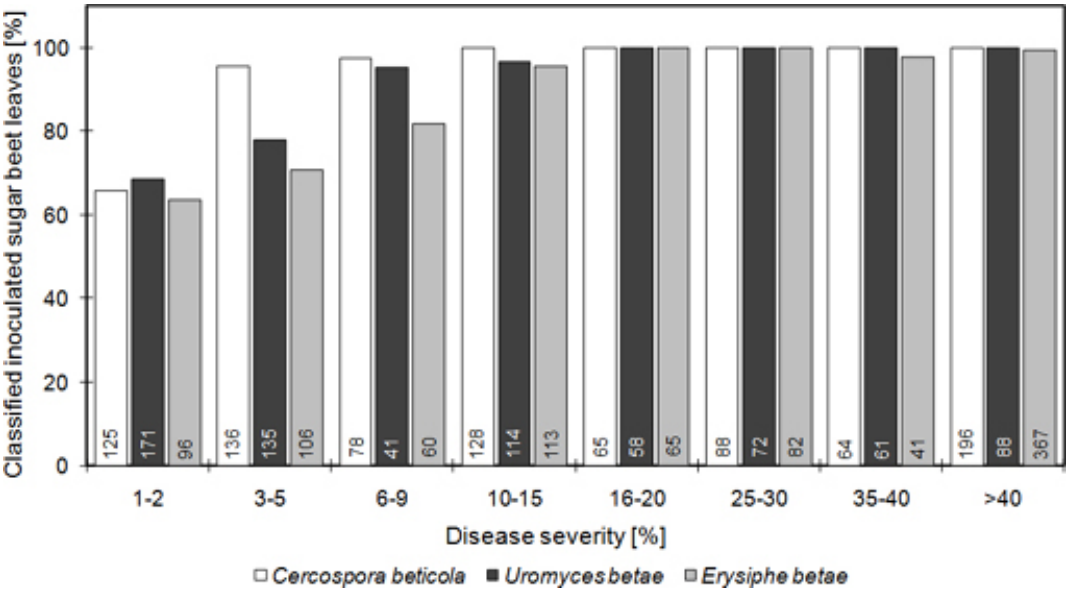

Figure 4.17: Classification result of non-inoculated sugar beet leaves and sugar beet leaves with three diseases depending on disease severity (numbers within bars denote class size).

4.4.2 Multi-class classification among healthy leaves and leaves with specific disease symptoms

Tab. 4.7 summarises the results of the model learned which classified healthy sugar beet leaves and leaves diseased with *Cercospora* leaf spot, sugar beet rust, and powdery mildew, respectively (multi-class classification). The overall classification accuracy was better than 88%, differences between the classes were low. The class recall of each class ranged between 84% and $>$ 92%. The class of healthy leaves was classified best. Classification difficulties occurred in separating between sugar beet rust and *Cercospora* leaf spot and also in the classification between powdery mildew and healthy sugar beet leaves.

4.4.3 Classification of healthy leaves and leaves inoculated with fungal pathogens at early stages of pathogenesis

For the differentiation between healthy sugar beet leaves and leaves inoculated with one of the pathogens before specific disease symptoms became visible, SVI data were used starting 3 dai. First symptoms of *Cercospora* leaf spot

Table 4.7: Classification results of the multi-class classification between healthy and diseased sugar beet leaves based on spectral vegetation indices using Support Vector Machines.

Prediction	**Ground truth**				
	Healthy	*Cercospora* leaf spot	Sugar beet rust	Powdery mildew	*Class precision*
Healthy	942	32	47	69	86.42%
Cercospora leaf spot	12	748	61	13	89.69%
Sugar beet rust	20	88	622	14	83.60%
Powdery mildew	46	12	10	834	92.46%
Class recall	92.35%	85.00%	84.05%	89.68%	**88.12%**

appeared 6 dai, rust 8 dai, and powdery mildew 5 dai. Leaves inoculated with *C. beticola* were correctly classified by SVMs with an accuracy range from 65% to 80%, even before symptoms became visible (Fig. 4.18 A). When specific symptoms occurred 6 dai, the classification accuracy increased until 12 dai when it converged at 100%. Throughout the 21 days of the experiment, the classification accuracy of the automatic procedure was consistent to visually classified *Cercospora* leaf spot-infected leaves. The classification accuracy of healthy leaves was almost 87% 3 dai and reached $>$ 95% 8 dai and later.

Although first symptoms of sugar beet rust appeared only 8 dai, a classification accuracy of 90% for *U. betae*-infected leaves was reached 3 to 5 dai (Fig. 4.18 B). One day before first rust symptoms became visible, the sensitivity decreased to about 71% and increased again 15 dai to $>$ 98%. The results of the automatic classification were inferior to visual ratings only between 12 and 14 dai. Healthy sugar beet leaves were classified with an accuracy of 72% at early stages of leaf colonization by *U. betae*, but from 10 dai the classification accuracy was always $>$ 95%.

Already 3 dai the classification accuracy of powdery mildew was $>$ 80% and increased to almost 92% 5 dai (Fig. 4.18 C). After the appearance of first visible colonies the classification rate decreased $<$ 70% 6 dai, and subsequently increased again from 10 to 20 dai $>$ 95%. In contrast to the results for the leaves colonized by the other pathogens the visual classification of *E. betae*-infected

leaves was superior (13% to 23%) to the automatic classification procedure from 6 to 9 dai. In the beginning of the experiment, the classification rate of healthy leaves was $> 91\%$; in the third week, however, it decreased to 77% 20 dai.

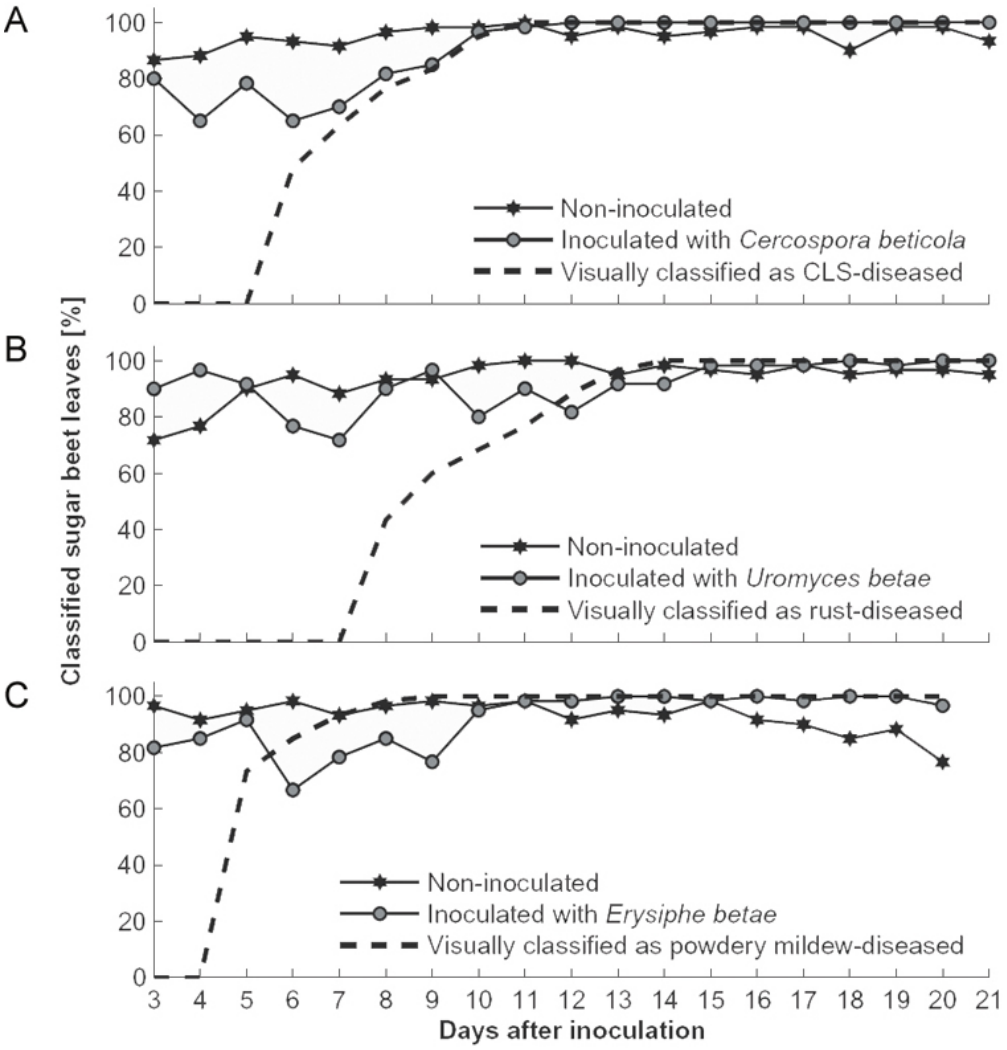

Figure 4.18: Effect of incubation time on the Support Vector Machines classification based on SVIs between healthy sugar beet leaves inoculated with *Cercospora beticola* (A), *Uromyces betae* (B), and *Erysiphe betae* (C), respectively.

4.5 Hyperspectral imaging for disease detection, identification, and quantification

Hyperspectral imaging data assessed with the hyperspectral camera ImSpector V10 enables – in contrary to non-imaging hyperspectral data – both, the spatial and temporal observation of disease development.

4.5.1 Pixel-wise attribution of spectral signatures during disease development

4.5.1.1 Spectral signatures of mature symptoms

Hyperspectral imaging enables the observation changes in sugar beet leaf tissue due to the foliar diseases *Cercospora* leaf spot, powdery mildew, and sugar beet rust on the pixel level. Changes in spectral reflectance of healthy leaf tissue due to growth and senescence processes can be recorded as well. The spectral signatures from a transect through healthy leave tissue is plotted in Fig. 4.19 A, where each spectrum belongs to one pixel from the transect. Spectral reflectance of healthy leaf tissue from adjacent pixels over a leaf segment was quite homogeneous. Minor variations can be explained by the natural heterogeneity of the surface, the surface structure of sugar beet leaves, and the interaction with incoming light.

Cercospora leaf spot
Spectral reflectance from a transect through a mature *Cercospora* leaf spot symptom showed obvious differences, depending to the region of the symptom (Fig. 4.19 B). Reflectance of tissue from the margin of a leaf spot increased in the VIS and decreased in the NIR. Spectra from the necrotic centre were characterized by increased reflectance in the VIS and NIR; the slope at the red edge position was lower.

Powdery mildew
Reflectance of leaf tissue diseased with powdery mildew was increasing, depending on the density of the mycelial cover of the leaf surface (Fig. 4.19 C). Spectral reflectance of the margin of a powdery mildew colony was characterized by an obvious increase of reflectance in the VIS and a minor increase in the NIR. With higher mycelia density in the centre of a colony, reflectance increase in the VIS and NIR became more pronounced.

Sugar beet rust
Changes in spectral signatures caused by sugar beet rust were less obvious, in fact of the small symptom size and the less destructive interaction with the host plant (Fig. 4.19 D). The margin from healthy tissue to a rust pustule was characterized by a general decrease in reflectance. The centre of rust pustules revealed inferior reflectance values around the green peak.

4.5.1.2 Changes in spectral signatures during pathogenesis

In addition to characteristic spectral signatures of distinctive regions of a symptom, the developmental stages had an effect on spectral reflectance (Fig. 4.20). Spectral signature of a one day-old *Cercospora* leaf spot symptom showed marginal differences to healthy leaf tissue (Fig. 4.20 A). With further symptom development, reflectance in the VIS increased most explicit between 580 to 700 nm. Reflectance in the NIR declined consistent with advanced age of symptoms and the slope at the red edge position became less steep.

For pixels representing powdery mildew, reflectance in the VIS and NIR increased with time. Reflectance of a three day-old symptom in the VIS was already 0.05%/100 higher than reflectance of an one day-old symptom (Fig. 4.20 B). Reflectance further increased with the maturation of powdery mildew colonies.

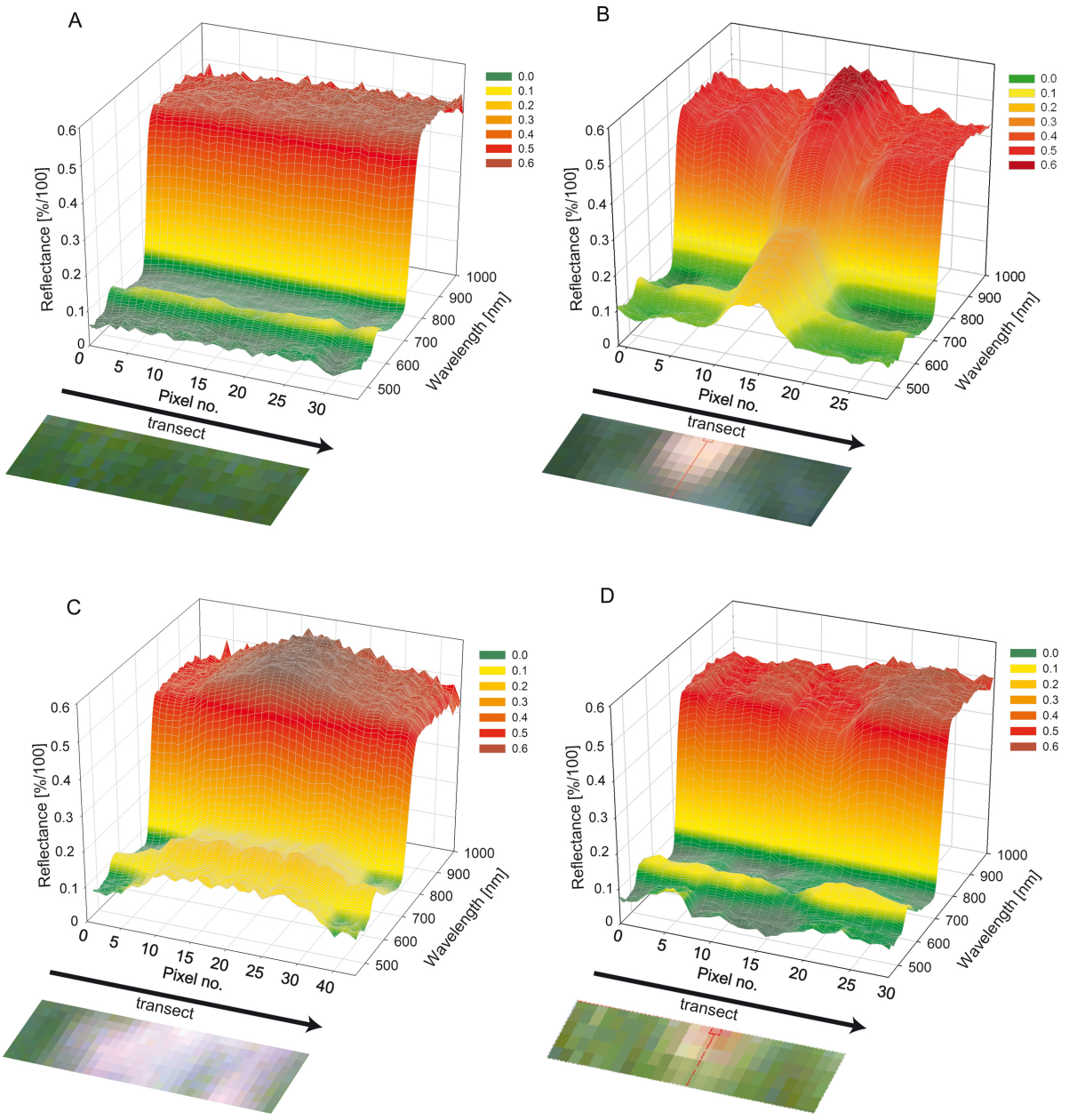

Figure 4.19: Impact of foliar diseases on the spectral reflectance of sugar beet leaves, pixel-wise reflectance spectra of a transect trough leaf tissue from hyperspectral imaging. (A) Healthy tissue and mature symptoms of (B) *Cercospora* leaf spot, (C) powdery mildew, and (D) sugar beet rust.

Single uredia of sugar beet rust occurred late in the measuring period. Hence, temporal evolution of the symptoms was monitored over five days only. Spectral reflectance of a one and a two day old symptom showed no significant difference to reflectance of healthy tissue (Fig. 4.20 C). Minor changes between healthy tissue and three day-old rust pustules were detected between 550 to

700 nm. Reflectance decrease of little account at 750 nm was observable for almost mature uredina.

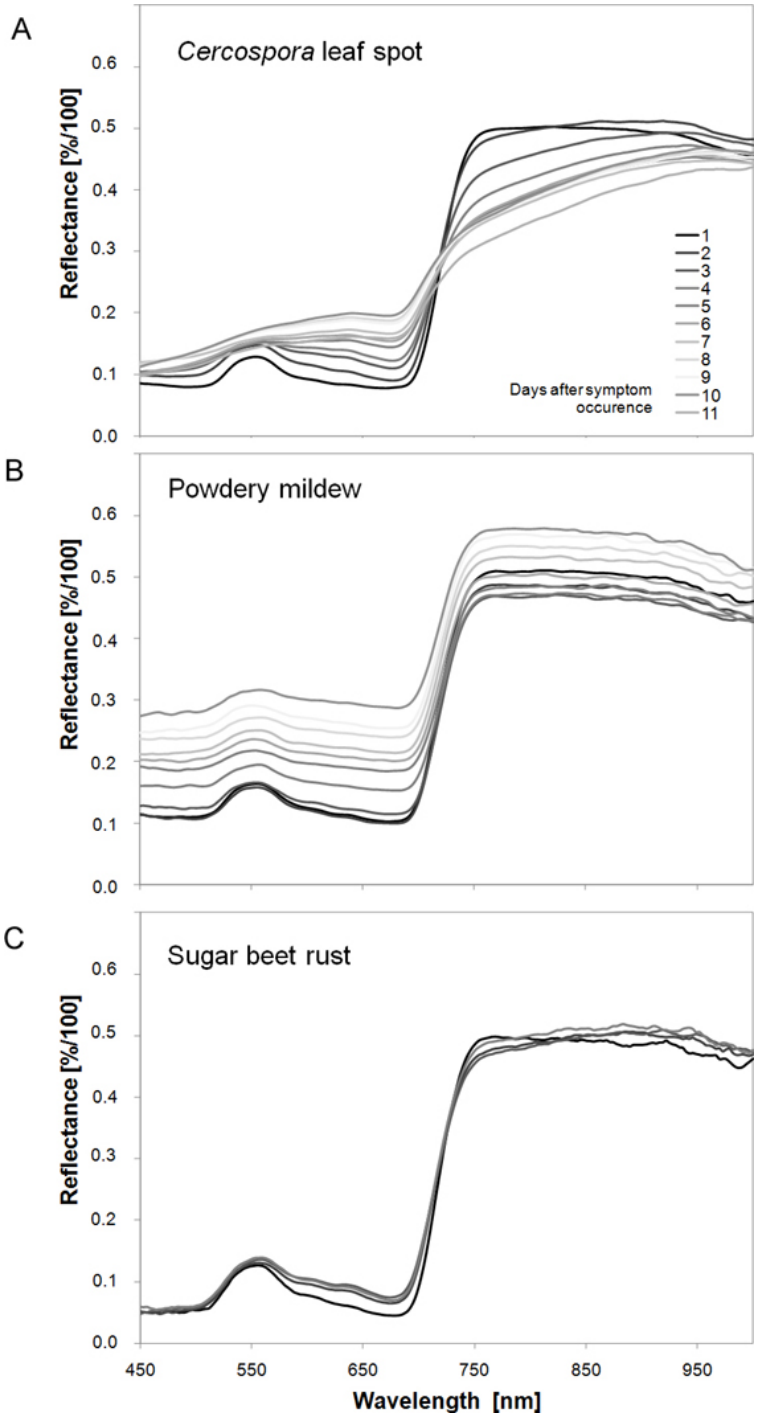

Figure 4.20: Changes in spectral signatures of sugar beet disease during maturation of symptoms, starting from the first appearance of symptoms. Reflectance spectra were obtained from imaging data by pixel-wise extraction from regions of interest. (A) *Cercospora* leaf spot, (B) powdery mildew, and (C) sugar beet rust.

4.5.2 Spatial illustration of vegetation indices during disease development

Spectral vegetation indices, calculated from hyperspectral imaging data, facilitate to highlight diseased leaf tissue and to discriminate among healthy and diseased leaf area on the spatial scale. The correlation of a SVI to a specific disease differs depending on the biochemical and biophysical parameters affected and described by SVIs.

Cercospora leaf spot

Fig. 4.21 visualizes eight spectral vegetation indices calculated from hyperspectral imaging data of a sugar beet leaf diseased by *Cercospora* leaf spot. The visual disease severity on the RGB image (R: 639 nm, G: 551 nm, B: 458 nm) of the sugar beet leaf was 20% 14 dai (Fig. 4.21 A). NDVI values enabled a clear separation of healthy leaf areas and area with *Cercospora* leaf spots by bright and dark pixels, respectively (Fig. 4.21 B). Similar results were obtained for SR and SIPI, but these SVIs were more sensitive to differences in leaf topography and different illumination conditions (Fig. 4.21 C, G). The use of SumGREEN, mCAI, and REP revealed a lower discriminating potential of the SVIs (Fig. 4.21 D, E, F). Values of REP from diseased leaf tissue appear as diffuse spots, not clearly distinguishable from healthy tissue (Fig. 4.21 F). Explicit visual differentiation of healthy and diseased leaf tissue by these SVIs seems not possible. As already proven on non-imaging hyperspectral data, the ARI was correlated positively to disease severity of *Cercospora* leaf spot. Hence, bright pixels in the false-colour image denote symptoms of *Cercospora* leaf spot and darker pixels denote healthy leaf tissue (Fig. 4.21 H). False-colour image of WI values highlighted a distinctive detection of the *Cercospora* leaf spot symptoms (Fig. 4.21 I). The WI was largely insensitive to differences in leaf topography and illumination conditions. The leaf was displayed as a homogenous, grey coloured plane with disease symptoms highlighted in black. Another advantage

of this index was the clear separation of healthy and diseased leaf tissue from leaf veins, which were coloured in white.

Powdery mildew

The same spectral vegetation indices calculated from hyperspectral imaging data revealed differences in their suitability to detect powdery mildew (Fig. 4.22). Fig. 4.22 A is a RGB image of a sugar beet leaf, with powdery mildew at 30% disease severity. Powdery mildew mycelium covered the middle part of the leaf and tissue around the leaf veins. A distinctive separation of healthy and diseased leaf parts was feasible calculating the NDVI (Fig. 4.22 B), SR (Fig. 4.22 C), and SIPI (Fig. 4.22 G). The SumGREEN index accentuated healthy, green parts by low values, displayed by dark pixels in the SVI false-colour image (Fig. 4.22 D). This SVI was therefore highly suitable to detect powdery mildew diseased areas of sugar beet leaves. The mCAI, REP, ARI, and WI were not convenient for the detection of powdery mildew (Fig. 4.22 E, F, H, I).

Sugar beet rust

The detection of sugar beet rust by the use of SVIs calculated from hyperspectral imaging data was most demanding. Due to the small symptom size, and thus the high amount of mixed pixel in hyperspectral data, only few SVIs highlighted symptoms caused by *U. betae* (Fig. 4.23). A magnified sub-square of a sugar beet rust diseased leaf and the use of different SVIs is illustrated in Fig. 4.23. The small, 0.5 to 1 mm sized rust pustule in the upper middle of the leaf segment was only detectable by the MCARI, PSRI, and ARI. However, a separation from heterogenic leaf tissue like leaf veins or leaf concavity was difficult.

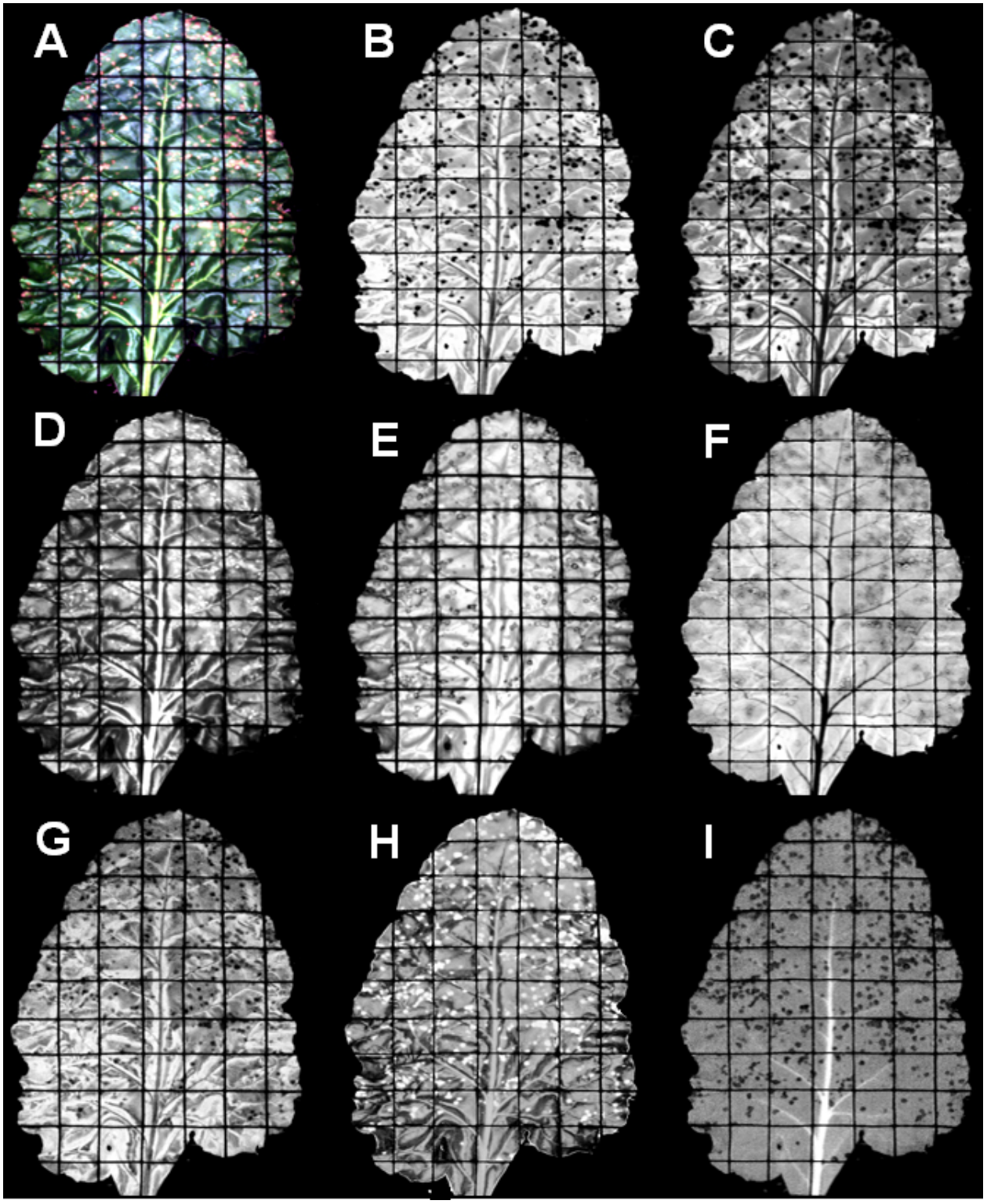

Figure 4.21: Use of spectral vegetation indices calculated from hyperspectral imaging data of a sugar beet leaf with *Cercospora* leaf spot, for the separation of healthy and diseased plant tissue 17 dai. (A) RGB image, (B) NDVI, (C) SR, (D) sumGREEN, (E) mCAI, (F) REP, (G) SIPI, (H) ARI, (I) WI. Spectral vegetation indices were visualized by a grey-scale false-colour image, black pixel denote lower SVI-values and white pixel higher SVI-values.

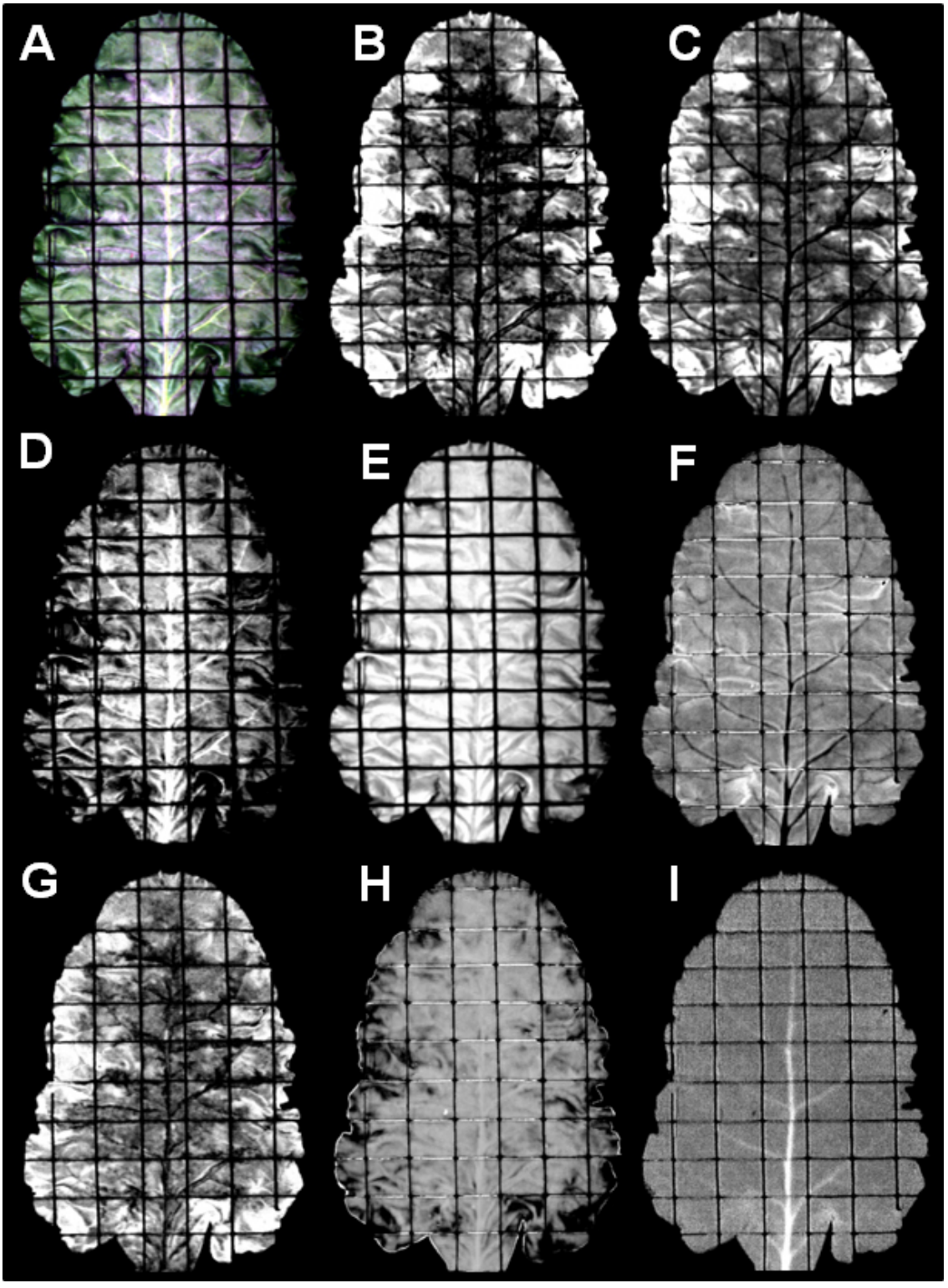

Figure 4.22: Use of spectral vegetation indices calculated from hyperspectral imaging data of a sugar beet leaf with powdery mildew. Separation of healthy and diseased plant tissue 14 dai. (A) RGB image, (B) NDVI, (C) SR, (D) sumGREEN, (E) mCAI, (F) REP, (G) SIPI, (H) ARI, (I) WI. Spectral vegetation indices are visualized by a grey-scale false-colour image, black pixel denote lower SVI-values and white pixel higher SVI-values.

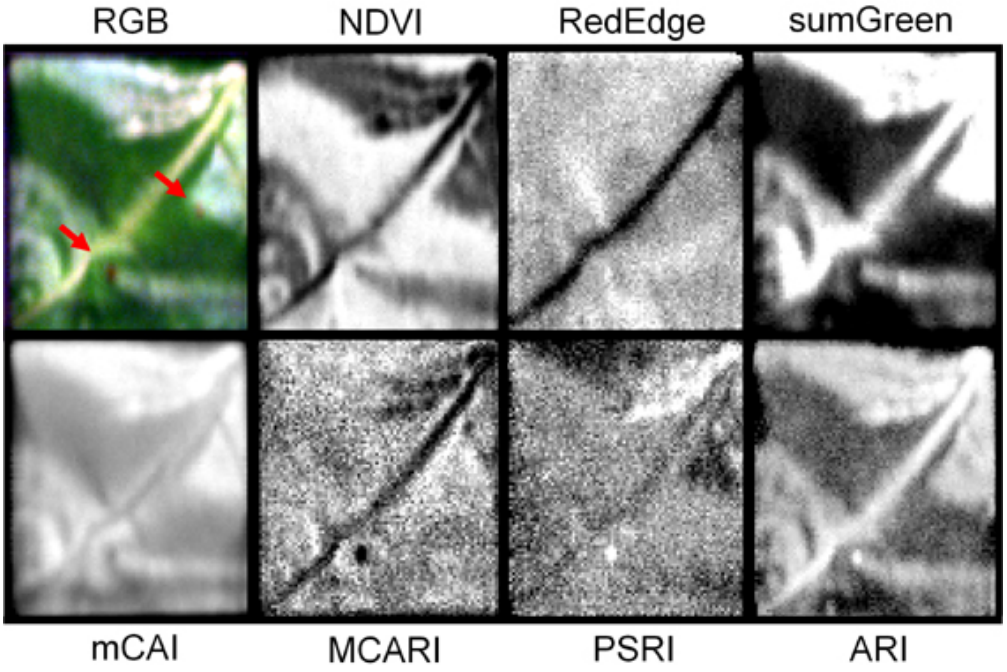

Figure 4.23: Use of spectral vegetation indices calculated from hyperspectral imaging data of a sugar beet leaf segment with sugar beet rust. Separation of healthy and diseased plant tissue 17 dai. (RGB image, SVIs calculated: NDVI, REP, sumGREEN, mCAI, MCARI, PSRI, ARI. SVIs are visualized by a grey-scale false-colour image, black pixel denote lower SVI-values and white pixel higher SVI-values).

4.5.2.1 Binary classification of healthy and diseased leaf tissue by spectral vegetation indices

Based on SVIs from hyperspectral imaging data, a binary classification model for each sugar beet disease was developed in coorporation with Thorsten Mewes, Centre for Remote Sensing and Land Surfaces, University of Bonn. Twenty-eight SVIs were calculated from hyperspectral imaging data. Values of SVIs were visualized in false-colour images (Fig. 4.24; Fig. 4.25). In a next step disease responsive SVIs were determined manually and threshold-values of SVIs were defined for each disease and each spectral vegetation index, respectively (Tab. 4.8). SVIs values greater or lower than threshold-values were displayed in a binary disease image with black (non-diseased) and white (diseased) pixels (Fig. 4.24; Fig. 4.25).

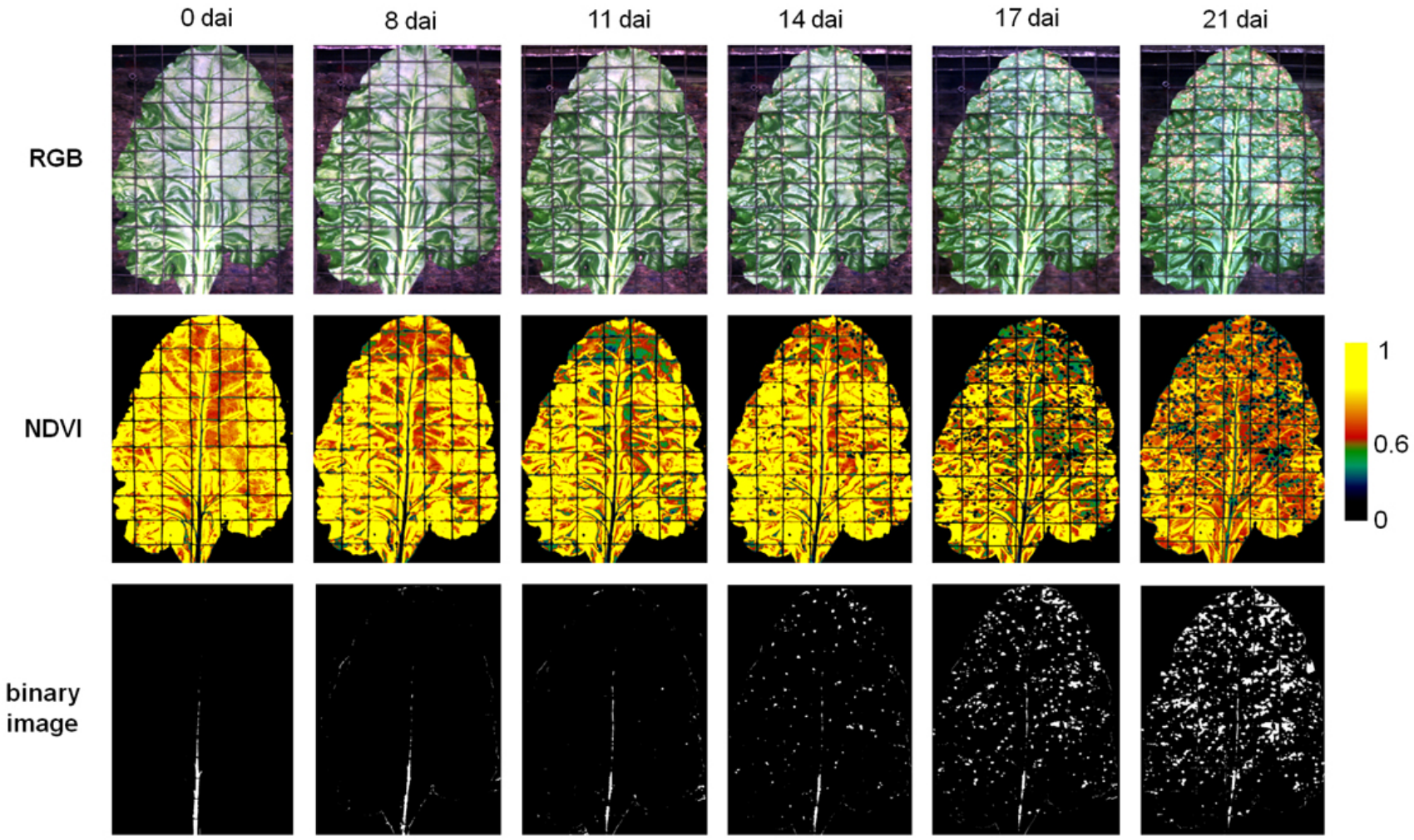

Figure 4.24: Differentiation of healthy and diseased sugar beet leaf tissue by calculating spectral vegetation indices and creating binary images, 0, 8, 11, 14, 17, and 20 days after inoculation. Pixels representing *Cercospora* leaf spot were assessed using the NDVI with a threshold of < 0.6. For the binary images, white pixel denote diseased leaf tissue, black pixel denote healthy leaf tissue.

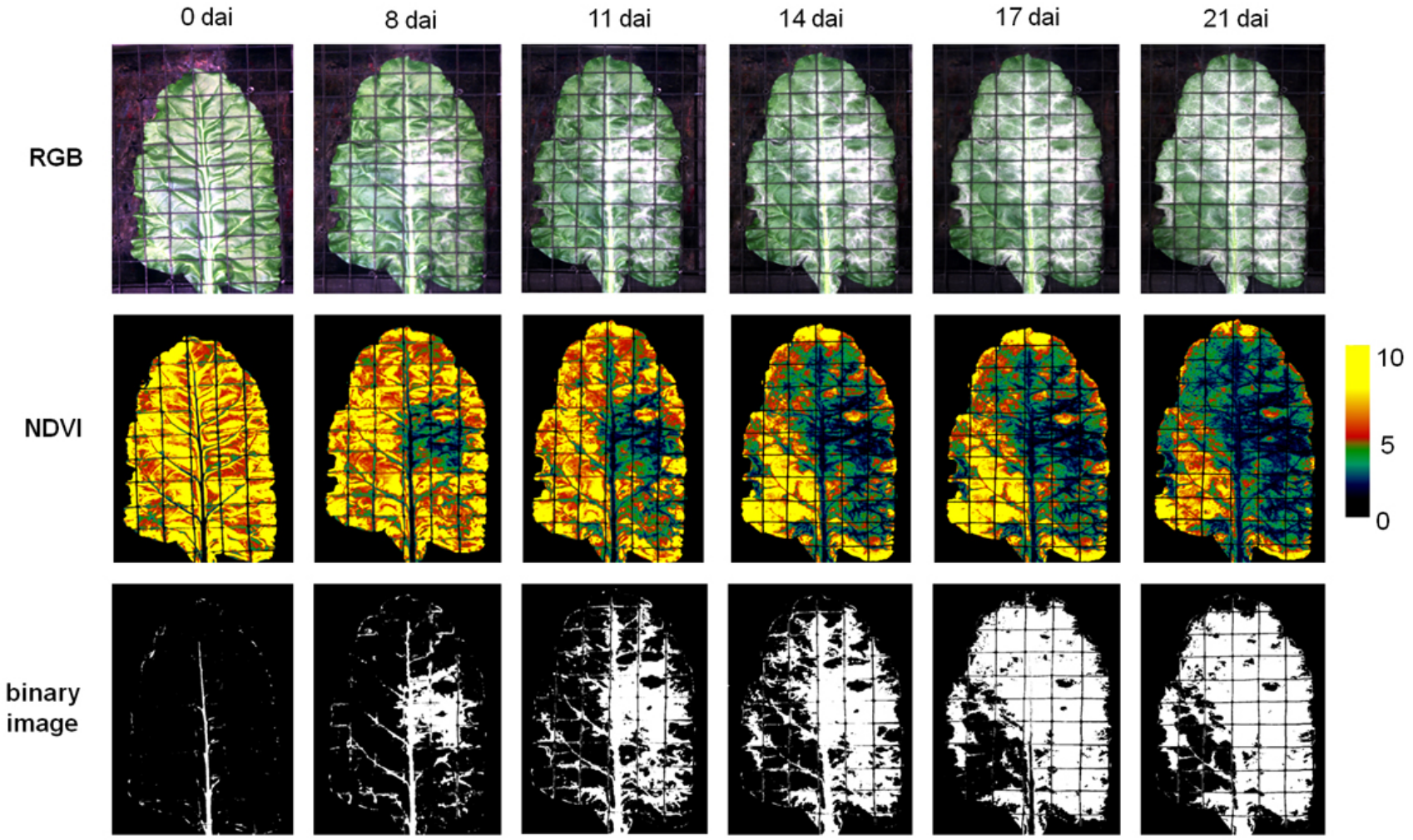

Figure 4.25: Differentiation of healthy and diseased sugar beet leaf tissue by calculating spectral vegetation indices and creating binary images, 0, 8, 11, 14, 17, and 20 days after inoculation. Pixels representing powdery mildew were assessed using the PSSRb with a threshold of < 5. For the binary images, white pixel denote diseased leaf tissue, black pixel denote healthy leaf tissue.

Table 4.8: Threshold values to distinguish healthy and diseased tissue of sugar beet leaf to create binary images of diseased leaf tissue and coefficient of determination of visually assessed disease severity and automatically classified disease severities by different vegetation indices.

		Disease[2]		
Index	**Threshold**[1]	**CLS**	**PM**	**SBR**
SumGreen	> 0.2	0.44	0.57	0.01
NDVI	< 0.6	**0.98**	0.69	0.06
SR	< 2	**0.96**	0.36	0.31
SIPI	< 0.6	0.37	0.68	0.19
PSSRa	< 0.5	0.89	**0.87**	0.14
PSSRb	< 0.5	0.77	**0.93**	0.07
PSSRc	< 0.5	0.46	**0.86**	0.11
PSNDa	< 0.6	**0.98**	0.68	0.06
PSNDb	< 0.55	**0.97**	0.64	0.06
PSNDc	< 0.55	0.75	0.50	0.17
ARI	< 0.1	0.95	0.45	**0.67**

[1] pixels with spectral vegetation indices values greater/or lower than threshold values were classified as diseased
[2] correlation was calculated as Pearsons coefficient of correlation (r), asterisk marks denote significant correlation with ** p = 0.01, and * p = 0.05, n=50; bold numbers indicate high correlation

Conformance of visible symptoms in the RGB image with parts of the leaves classified as *Cercospora* leaf spot or powdery mildew diseased was obvious (Fig. 4.24; Fig. 4.25). Because of low correlation, images for sugar beet rust are not shown.

Quantification of diseased and healthy leaf area from binary disease images was possible in a next step. High coefficients of determination could be obtained for the relationship between SVIs-based automatically classified disease severity and visually assessed disease severity (Fig. 4.26). For *Cercospora* leaf spot detection, the NDVI $\left(R^2 = 0.98\right)$, PSNDa/b $\left(R^2 = 0.98\right)$, and SR $\left(R^2 = 0.96\right)$ showed best correlation (Tab. 4.8). The PSSRa, b, and c fitted best for powdery mildew $\left(R^2 = 0.87, R^2 = 0.93, R^2 = 0.86, \text{respectively}\right)$. The quantification of sugar beet rust by the ARI gave lower correlation to visual assessment $\left(R^2 = 0.67\right)$. All other SVIs were not significantly correlated to the results of automatic disease severity classification of sugar beet rust.

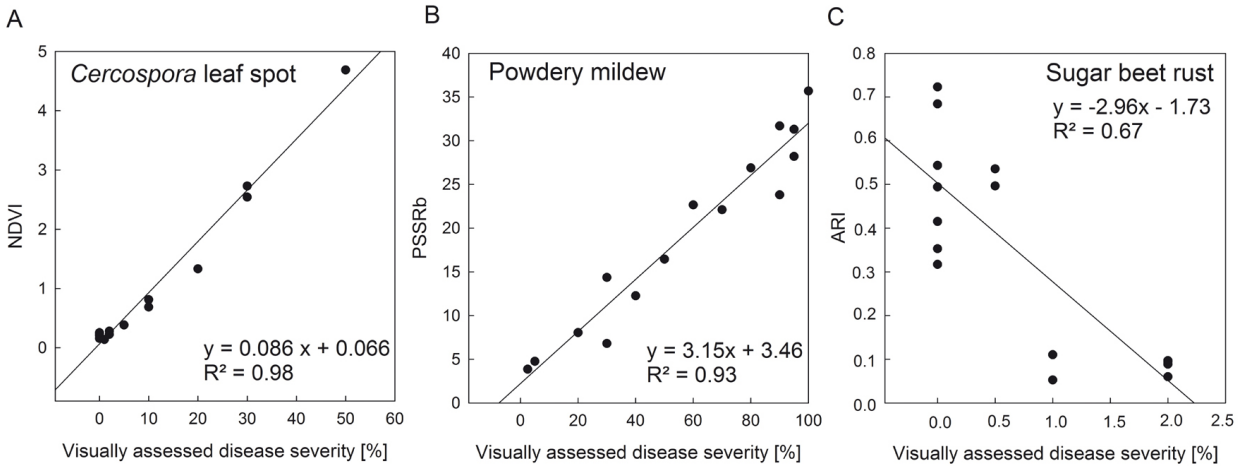

Figure 4.26: Correlation between spectral vegetation index based *versus* visually disease assessment.

4.5.3 Spectral angle mapper classification for the assessment of foliar leaf diseases from hyperspectral images and its ability to distinguish multiple disease symptoms

Based on hyperspectral imaging data the SAM was used to distinguish healthy and diseased sugar beet tissue and to detect disease specific symptoms of different peculiarities. Characteristic endmember spectra from healthy tissue and disease symptoms were extracted from hyperspectral imaging data and stored in a spectral library. Each endmember represents a to distinguish class. Background, grid wire, and leaf veins were masked out and coloured in black.

Cercospora leaf spot

For *Cercospora* leaf spot classification, the three classes 'healthy' sugar beet tissue, 'margin' of *Cercospora* leaf spots, and their necrotic 'centre' were chosen. The SAM classification resulted in false-colour class images (Fig. 4.27), where green colour denote 'healthy' leaf tissue, red pixels belong to the class 'margin', and yellow pixels denote 'necrotic' centre of *Cercospora* leaf spots. The first row of Fig. 4.27 shows RGB images of the classified hyperspectral data cube. No visible symptoms of *Cercospora* leaf spot occurred 0 dai and 8 dai. The result of the SAM, shown in the second row, was similar; the whole leaf area was classified as healthy leaf tissue. Eleven days after inoculation first sporadic

symptoms became visible as sunken necrotic leaf tissue. Early symptoms of *Cercospora* leaf spot were classified as margin of *Cercospora* leaf spot with high reliability. However, non-diseased leaf tissue next to the grid wire and leaf veins was inaccurately classified as margin of *Cercospora* leaf spot. Symptoms of different development stages were found on the RGB images 14 dai. Fully developed *Cercospora* leaf spots next to emerging spots were assessed. False-colour SAM classification gave similar images to the ground truth RGB image. Healthy leaf tissue appeared as green pixels, the margin was correctly classified in red, and scattered necrotic centres were displayed as yellow pixels. Minor misclassified pixels around the grid wire and leaf border were visual. Healthy and diseased leaf tissue was reliably detected by the SAM classifier also 17 dai, when larger, coalescing necrotic areas due to *Cercospora* leaf spot appeared.

Classification results of the SAM algorithm were validated using a confusion matrix (Tab. 4.9). On the first day of the measuring period, 99.89% of the total leaf area was classified as healthy leaf tissue (overall accuracy of 99.88%). Only 0.11% of the healthy leaf tissue remained unclassified. The very high kappa coefficient of 0.99 underlines the agreement between ground truth data and classification result. Similar results were obtained 8 dai. Only 1.1% of the healthy leaf tissue was unclassified with an overall classification accuracy of 98.9% and a kappa coefficient of 0.99. Classification accuracy decreased to 89.58% with a kappa coefficient of 0.52, 11dai; 11.2% of healthy area was classified as margin of a *Cercospora* leaf spot, whereas 9% of the margin was unclassified or classified as healthy tissue. With higher disease severity and mature symptoms, classification accuracy increased to 96.58% and a kappa coefficient of 0.92, 14 dai. Differentiation between healthy leaf tissue and the margin of *Cercospora* leaf spots and between the margin of a *Cercospora* leaf spot and the necrotic centre was demanding. At this time of disease progress the diseased leaf area was classified as 7.61%. Seventeen days after inoculation the SAM classification resulted in 20.95% leaf area diseased by *Cercospora* leaf spot (overall accuracy = 99.73, kappa coefficient = 0.98).

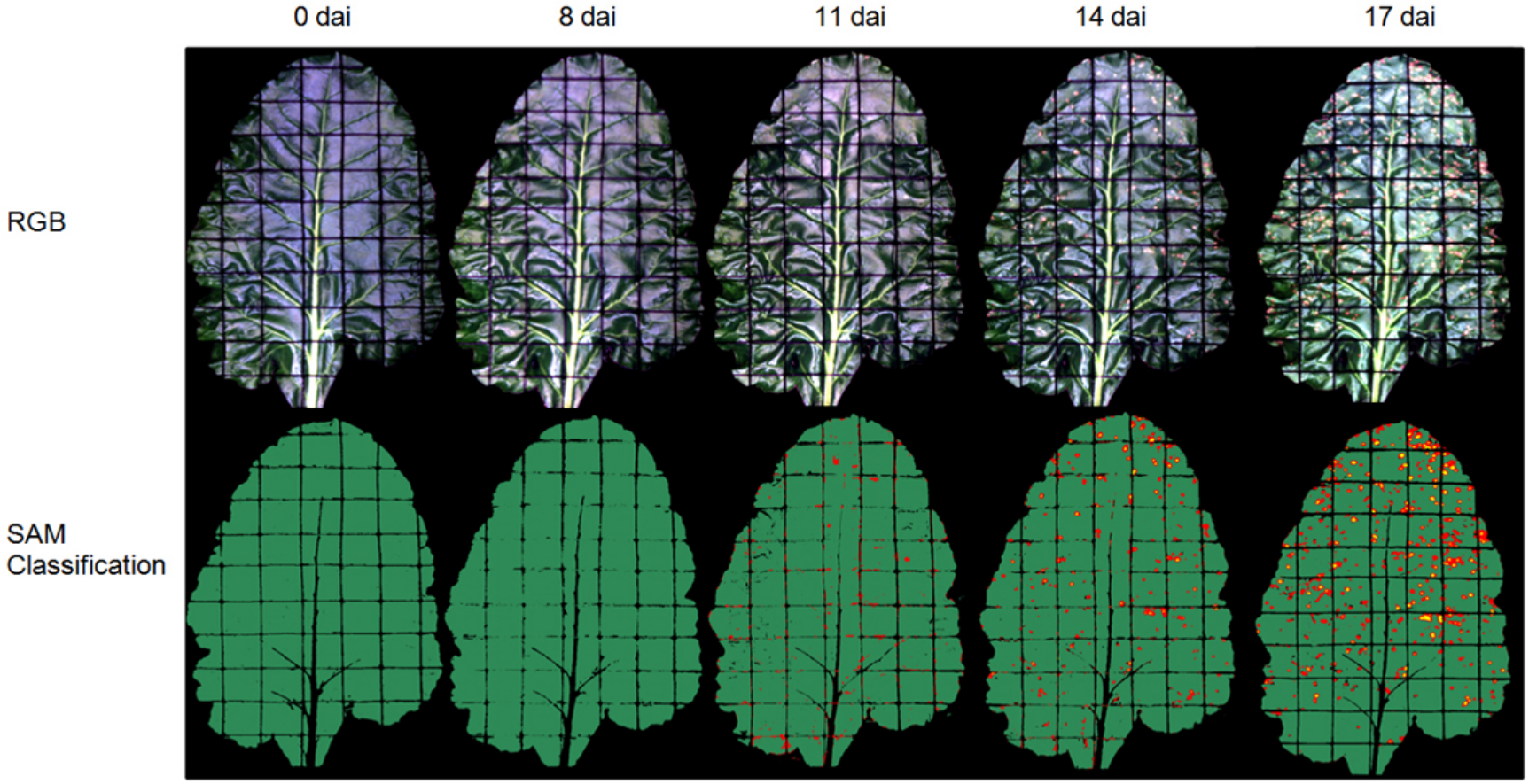

Figure 4.27: Automatic classification of *Cercospora* leaf spot using spectral angle mapper (SAM) algorithm. The three classes 'healthy' (green), 'margin' of *Cercospora* leaf spots (red), and 'necrotic centre' of *Cercospora* leaf spot (yellow) were separated at different disease severity stages with a maximum angle threshold of 0.1°.

Table 4.9: Classification accuracy of spectral angle mapper classification of *Cercospora* leaf spot diseased leaves during disease progress.

Days after inoculation 0				
	Ground truth			
Class	Healthy	Margin	Centre	Total
unclassified	0.11	0	0	0.11
Healthy	99.89	0	0	99.89
Margin	0	0	0	0
Centre	0	0	0	0
	Overall = 99.88,		**Kappa = 0.99**	
Days after inoculation 8				
	Ground truth			
Class	Healthy	Margin	Centre	Total
unclassified	1.1	0	0	1.1
Healthy	98.9	0	0	98.9
Margin	0	0	0	0
Centre	0	0	0	0
	Overall = 98.90,		**Kappa = 0.99**	
Days after inoculation 11				
	Ground truth			
Class	Healthy	Margin	Centre	Total
unclassified	0	6.67	0	0.53
Healthy	88.82	2.22	0	92.91
Margin	11.18	91.11	0	6.56
Centre	0	0	0	0
	Overall = 89.01,		**Kappa = 0.53**	
Days after inoculation 14				
	Ground truth			
Class	Healthy	Margin	Centre	Total
unclassified	0	0	0.1	0
Healthy	100	4.78	0	92.39
Margin	0	93.53	16.07	6.18
Centre	0	1.79	83.82	1.43
	Overall = 96.58,		**Kappa = 0.92**	
Days after inoculation 17				
	Ground truth			
Class	Healthy	Margin	Centre	Total
unclassified	0	0	0	0
Healthy	87.5	1.08	0	79.05
Margin	12.5	98.92	0	15.01
Centre	0	0	100	5.94
	Overall = 98.73,		**Kappa = 0.98**	

Powdery mildew

For powdery mildew classification, the classes 'healthy' sugar beet tissue, 'light mycelium', and 'dense mycelium' of powdery mildew were chosen. When the entire tissue was healthy, the total leaf area was classified as healthy leaf tissue by the SAM algorithm 0 dai (Fig. 4.28). A visible powdery mildew mycelium colony appeared 8 dai in the right middle of the sugar beet leaf and next to the branching leaf veins. These parts were coloured in yellow and red in the classification image, according to the chosen endmembers. The powdery mildew coverage enlarged with time, first over the entire right leaf side, followed by the upper left leaf area. SAM classification images were in accordance with visually assessed disease symptoms. Verifying the classification accuracy using a confusion matrix, high classification accuracies $> 94\%$ were reached over the measuring period (Tab. 4.10). A classification accuracy of 100% and a perfect agreement (kappa coefficient = 1) between classification result and ground truth data was reached. An overall classification accuracy of 94.3% and a kappa coefficient of 0.88 was computed 8 dai.

Minor difficulties in separating between healthy tissue and tissue covered by light mycelium occurred; some parts of the dense mycelium remained unclassified. 12.6% misclassification of light mycelium as healthy leaf tissue resulted in a 96.8% classification accuracy (kappa coefficient = 0.91), 11 dai. With further disease development a distinctive separation between healthy and diseased sugar beet leaf tissue was possible, 100% of the ground truth class 'healthy' were classified correctly 14 dai and 17 dai, respectively.

The separation between light and dense powdery mildew mycelium resulted in 6% misclassification 14 dai and reduced overall classification accuracy to 97.2% (kappa coefficient = 0.95). Seventeen days after inoculation, 11.9% of the light mycelium was classified as dense mycelium, and 25% *vice versa*. The higher rate of misclassification caused a comparatively lower classification accuracy of 90.11% (kappa coefficient = 0.84).

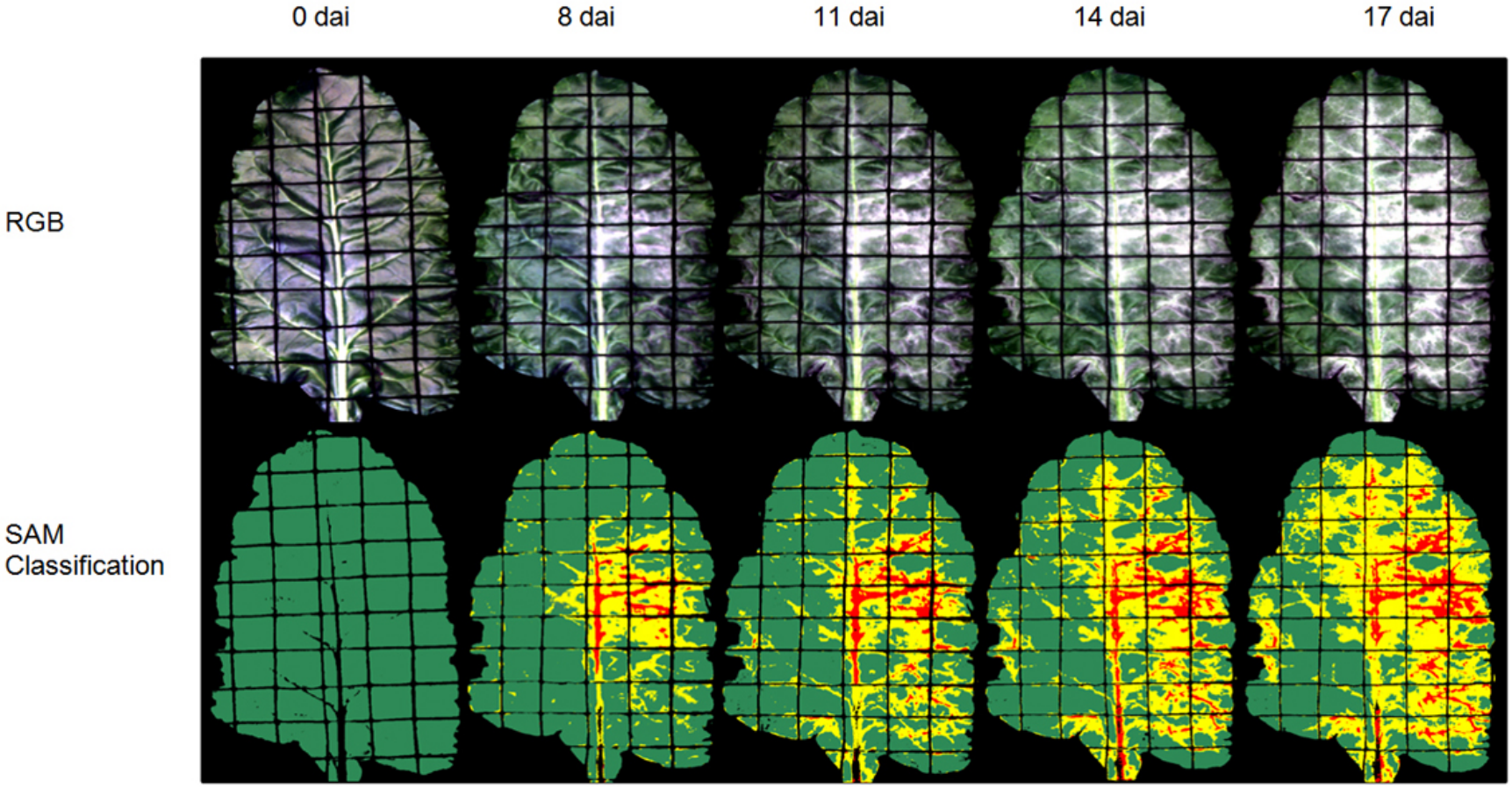

Figure 4.28: Automatic classification of powdery mildew using spectral angle mapper (SAM) algorithm. The three classes 'healthy' (green), 'light mycelium' of powdery mildew (yellow), and 'dense mycelium' of powdery mildew (red) were separated at different disease severity stages with a maximum angle threshold of 0.1°.

Table 4.10: Classification accuracy of spectral angle mapper classification of powdery mildew diseased leaves during disease progress.

Days after inoculation 0				
	Ground truth			
Class	Healthy	Light mycelium	Dense mycelium	Total
unclassified	0	0	0	0
Healthy	100	0	0	100
Light mycelium	0	0	0	0
Dense mycelium	0	0	0	0
			Overall = 100,	**Kappa = 1**
Days after inoculation 8				
	Ground truth			
Class	Healthy	Light mycelium	Dense mycelium	Total
unclassified	0	0	3.49	0.41
Healthy	94.04	4.44	0	85.16
Light mycelium	5.96	94.07	0	9.69
Dense mycelium	0	1.48	96.51	4.74
			Overall = 94.34,	**Kappa = 0.88**
Days after inoculation 11				
	Ground truth			
Class	Healthy	Light mycelium	Dense mycelium	Total
unclassified	0	0	0	0
Healthy	99.92	12.62	0	80.63
Light mycelium	0.08	77.1	0	10.65
Dense mycelium	0	10.28	100	8.72
			Overall = 96.79,	**Kappa = 0.91**
Days after inoculation 14				
	Ground truth			
Class	Healthy	Light mycelium	Dense mycelium	Total
unclassified	0	0	0	0
Healthy	100	0	0	58.06
Light mycelium	0	93.63	6.82	20.38
Dense mycelium	0	6.37	93.18	21.56
			Overall = 97.23,	**Kappa = 0.95**
Days after inoculation 17				
	Ground truth			
Class	Healthy	Light mycelium	Dense mycelium	Total
unclassified	0	0	0.29	0.09
Healthy	100	0	0	49.87
Light mycelium	0	88.07	25	25.71
Dense mycelium	0	11.93	74.71	24.33
			Overall = 90.18,	**Kappa = 0.84**

Sugar beet rust

The small size of *U. betae* uredia and the low disease severity complicated classification of sugar beet rust by the SAM algorithm. Additionally, the spatial resolution of the camera system limited the detection of rust pustules and resulted in high amount of mixed pixels. First rust pustules became visible 20 days after inoculation. Before this day, no classification of sugar beet rust inoculated sugar beet leaves was possible. Fig. 4.29 illustrates the difficulties of classifying sugar beet rust pustules based on hyperspectral data.

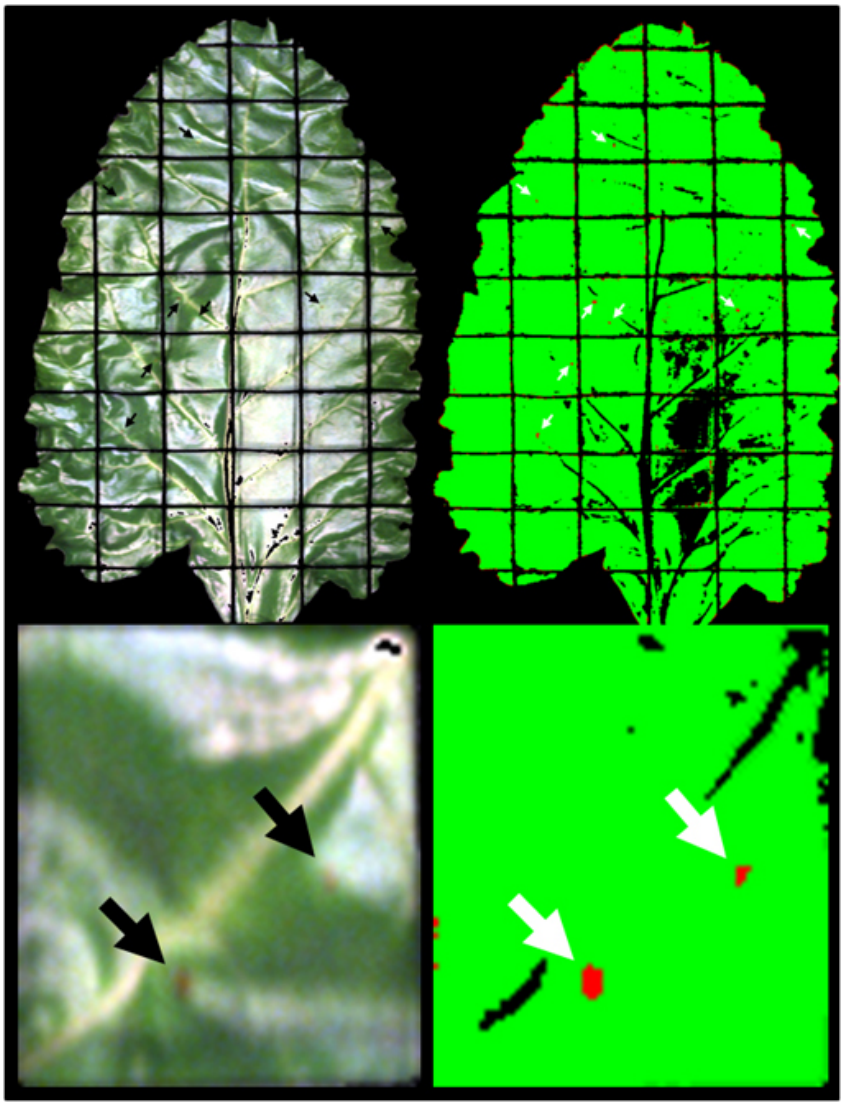

Figure 4.29: Automatic classification of sugar beet rust using spectral angle mapper algorithm on leaf scale and zoom into one sub-square. Mature symptoms (red) were separated from healthy leaf tissue (green), 20 days after inoculation. Black pixel denote unclassified pixel.

In the RGB image sugar beet rust uredia, marked by black arrows, were hardly detectable by the naked eye. The high magnification of one leaf sub-square, containing characteristic sugar beet rust pustules is shown on the bottom left of Fig. 4.29. Structures were diffuse without distinctive separation of the various components. However, nearly all rust pustules were detected by the SAM algorithm correctly, but there was a high amount of misclassified pixels (Fig. 4.29, right side). Numerous pixels next to the grid wire and along the leaf border were classified as sugar beet rust. Likewise, it was not possible to assign the entire healthy leaf parts to the class 'healthy'. As a consequence, the post classification based on ground truth data yielded in an overall classification accuracy of 61.7% with a low kappa coefficient of 0.56 (Tab. 4.11), with 15.98% unclassified healthy leaf area and 15.12% unclassified symptoms of sugar beet rust. Differentiation between healthy leaf parts and symptoms of sugar beet rust was also not fulfilling; 20.67% of the rust pustules were classified as healthy and 4% of the healthy tissue was classified as rust.

Table 4.11: Classification accuracy of spectral angle mapper classification of sugar beet rust diseased leaves with mature symptoms.

Days after inoculation 20			
	Ground truth		
Class	Healthy	Rust	Total
unclassified	15.98	15.12	15.98
Healthy	80.02	20.67	82.13
Rust	4.00	64.21	2.89
Overall = 61.70,		**Kappa = 0.56**	

4.6 Monitoring of plant diseases on the field scale using remote sensing technologies

The temporal and spatial disease development on the field scale was observed by different hyperspectral airborne and handheld sensors at different times during vegetation period, at the experimental station Klein-Altendorf 2008.

4.6.1 Spatial soil heterogeneity

The EM 38 measurements of the area showed only marginal variability of the apparent electrical conductivity (ECa, Fig. 4.30). With ECa values from 23.5 to 46.5 mS m^{-1} the soil texture was quite heterogeneous, indicating loamy silt at high field moisture capacity. However, most parts of the field had ECa values from 23.5 to 30.2 mS m^{-1}, indicating a rather homogeneous soil texture.

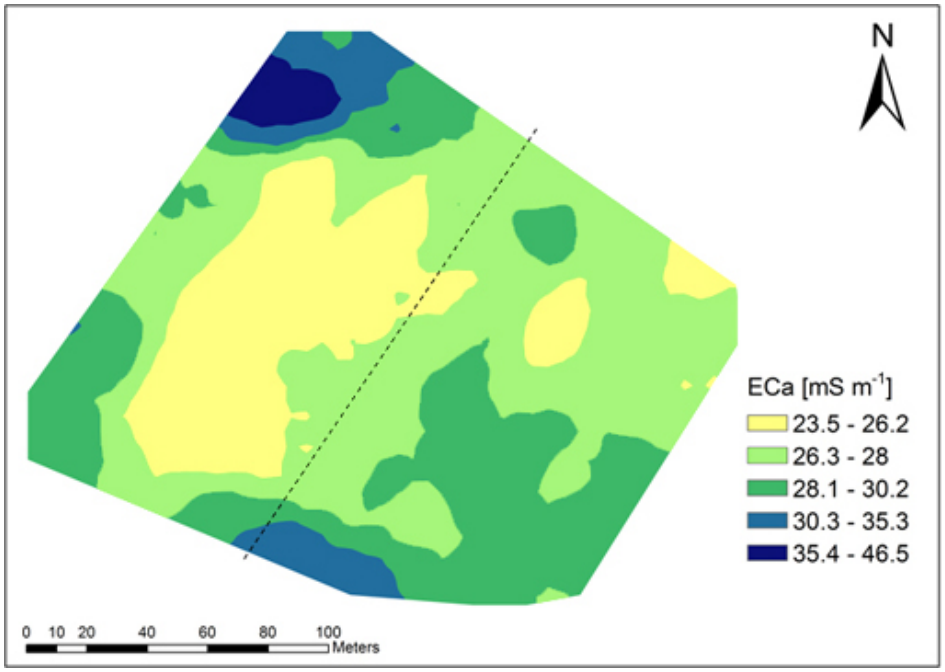

Figure 4.30: Variability of the apparent electrical conductivity (ECa) at the field site Klein-Altendorf, measured with EM38 soil sensor on 15th of April 2008.

4.6.2 Progress of *Cercospora* leaf spot and powdery mildew

At the field site Klein-Altendorf 2008, powdery mildew was the dominant foliar sugar beet disease (Fig. 4.31 B). In July sugar beet plants were healthy throughout the field, diseased sugar beet plants could not be monitored in the two plots. In early August, average disease severity of *Cercospora* leaf spot and powdery mildew in the untreated plot were 0.3% and 5% diseased leaf area, respectively (Fig. 4.31 A, B). Only a few clusters of *Cercospora* leaf spot diseased plants were detected in the untreated plot (Fig. 4.32 A). Two *Cercospora* leaf spot patches with disease severity up to 7% were identified. Around these disease centres, single plants infested with *Cercospora* leaf spot were monitored. Fungicide-treated sugar beet plants remained almost healthy, solitary plants with single *Cercospora* leaf spot spots were detected in the southern part of the fungicide-sprayed plot. Plants with higher intensity of powdery mildew were aggregated in the western part of the untreated plot (Fig. 4.32 C).

From this part of the field declining powdery mildew severity declined towards the fungicide-treated plot. In September, increasing disease severity of both diseases was visually assessed in both plots (Fig. 4.31 A, B). *Cercospora* leaf spot appeared in patches with 12% disease severity in the untreated plot and 2% diseased leaf area in the fungicide treated plot, respectively. In general, only few plants with *Cercospora* leaf spot ratings up to 35% diseased leaf area could be monitored in the northern part of the non-treated plot (Fig. 4.32 B).

Sugar beet plants with high *Cercospora* leaf spot infection exhibited lower powdery mildew infection and *vice versa* (Fig. 4.32 B, D). Mean disease severity of powdery mildew increased to 67% over the area in the untreated plot, and uniformly to 22% diseased leaf area in the fungicide-treated plot (Fig. 4.31 B). In the untreated plot, higher powdery mildew disease severities were monitored in the western and southern part (Fig. 4.32 D).

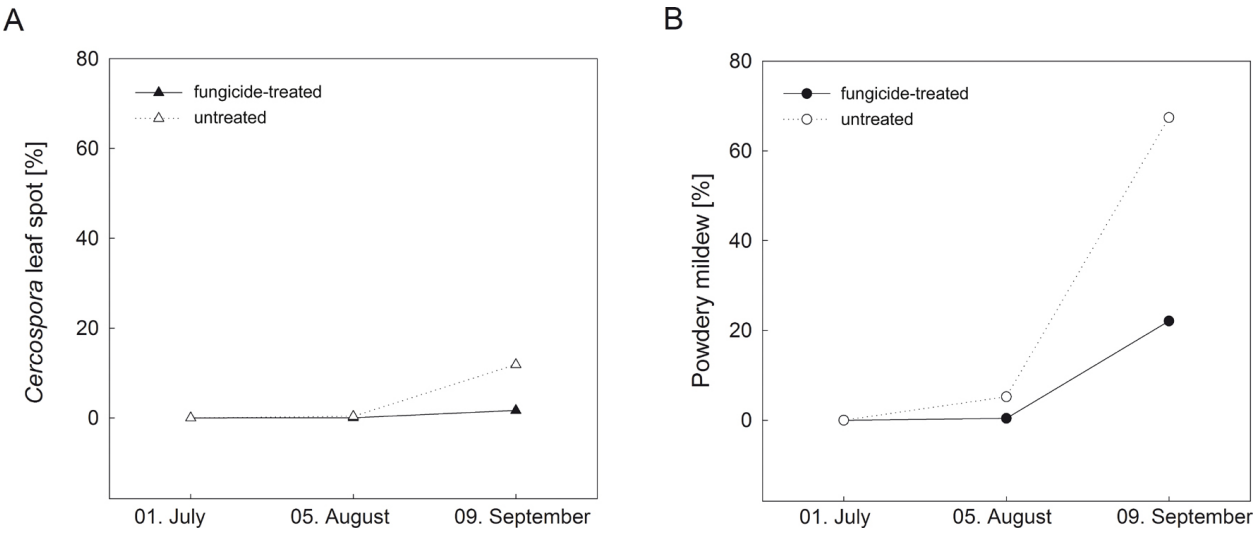

Figure 4.31: Disease progress of *Cercospora* leaf spot (A) and powdery mildew (B) on sugar beet, Klein-Altendorf 2008.

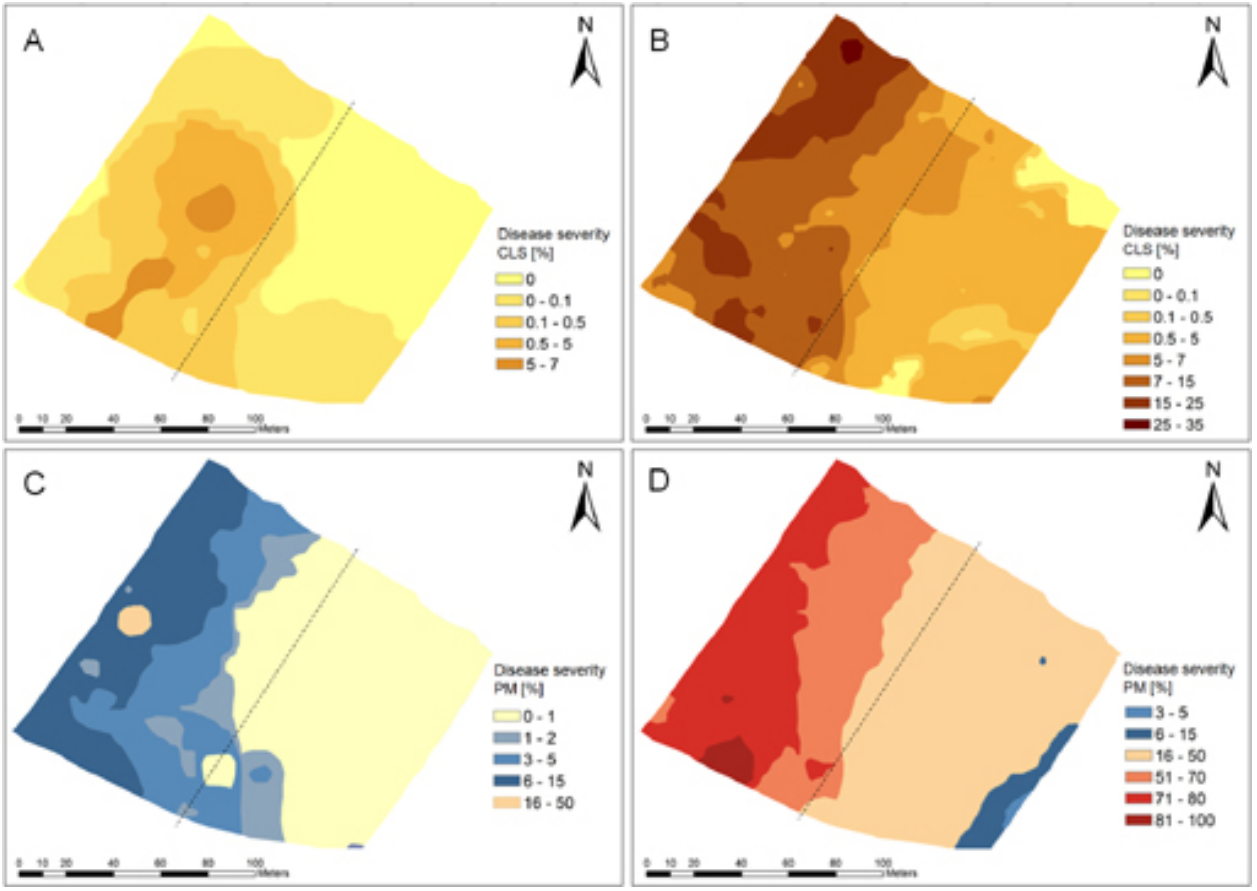

Figure 4.32: Spatial distribution of disease severity of *Cercospora* leaf spot (A, B) and powdery mildew on 6th of August (A,C) and 9th of September (B,D), Klein-Altendorf 2008.

4.6.3 Impact of plant diseases on sugar beet biomass

Significant differences in plant biomass, assessed as leaf dry matter were detected in the growth period (Fig. 4.33). In early July mean leaf biomass of 20 sugar beets, from 5 sampling points in the plots, did not vary significantly. Overall biomass of sugar beet leaves increased from July to August. In August, dry matter of fungicide-treated sugar beet leaves was higher than that from non-treated plants, although without statistically significances. Leaf biomass in September was lower than in August, with a significantly lower dry matter of untreated sugar beets compared to sugar beet leaves from the fungicide-treated plot.

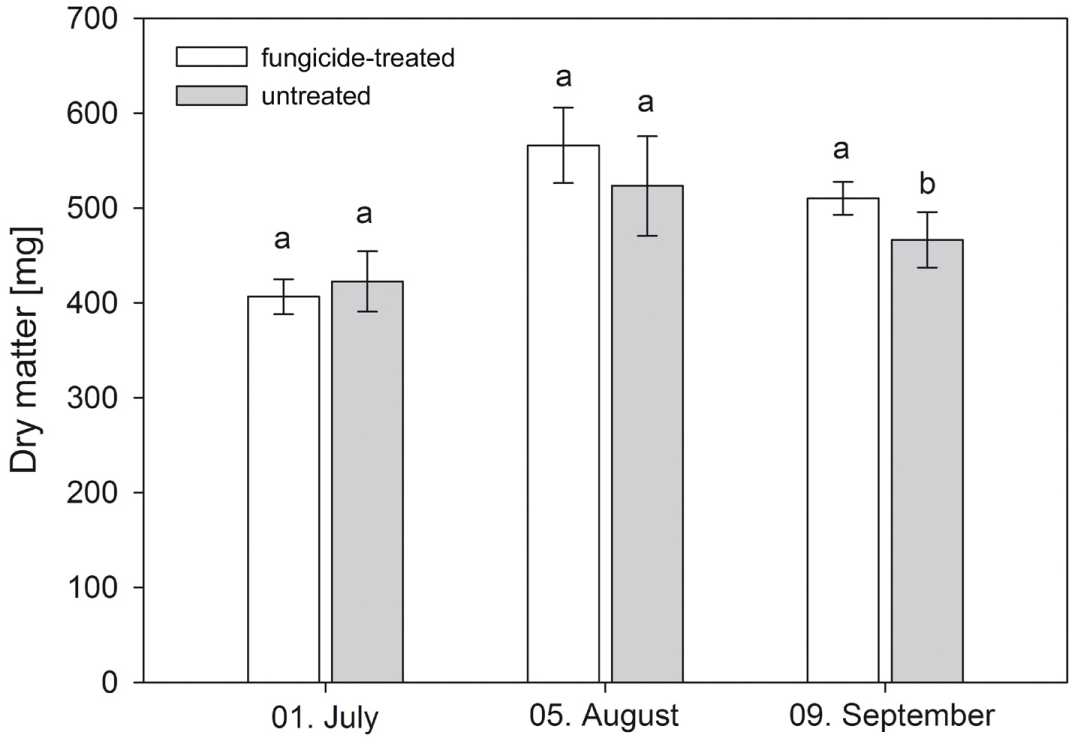

Figure 4.33: Impact of fungicide treatment on plant biomass from sugar beet canopy, sampled at different measuring dates during growth period of sugar beet, Klein-Altendorf 2008 (bars denote standard derivation, dry matter values within one sampling date with different letters are significantly different according to Students t-test, p = 0.5).

4.6.4 Multi-temporal and multi-sensoral monitoring of diseases

The NDVI is the most common vegetation index in remote sensing and gives information on crop biomass and plant vitality. Therefore, NDVI values were calculated pixel-wise for the classification of the ROSIS and HyMap images (Fig. 4.34). In July, NDVI values were distributed homogeneously over the experimental field; no significant differences could be detected at this early stage of the growth period (Fig. 4.34 A). By this time no fungicide treatment had been applied and no fungal infection of sugar beet plants could be assessed visually.

In early August, however, NDVI values showed a general spatial trend. NDVI values in the untreated plot were obviously lower than in the fungicide-treated plot. Because the NDVI is negatively correlated to disease severity, this sensor based information coincided with early infection patterns in the field (Fig. 4.31 B; Fig. 4.35). A cluster of lower NDVI values appeared in the south western part of the field (Fig. 4.34 B). A coefficient of determination of $R^2 = 0.69$ was calculated for the NDVI with incidence of powdery mildew symptoms and powdery mildew disease severity. NDVI values of the sprayed plot were around 0.9, while NDVI values of the untreated plot declined to 0.88. Due to low *Cercospora* leaf spot disease severity, *Cercospora* leaf spot and NDVI were not correlated.

From non-imaging hyperspectral data, measured with the ASD FieldSpec in September, various spectral vegetation indices were calculated. All SVIs were significantly correlated to disease severity of *Cercospora* leaf spot and powdery mildew, respectively (Tab. 4.12). The NDVI showed a strong negative correlation to powdery mildew severity (r = -0.71). Due to the overall low incidence, the correlation to *Cercospora* leaf spot was lower (r= -0.48). The mCAI, related to leaf chlorophyll content, was highly correlated to the disease severity of powdery mildew (r = -0.72) and also showed a correlation to *Cercospora* leaf spot (r = -0.60). In this field study, the ARI, an indicator of pigment modifications,

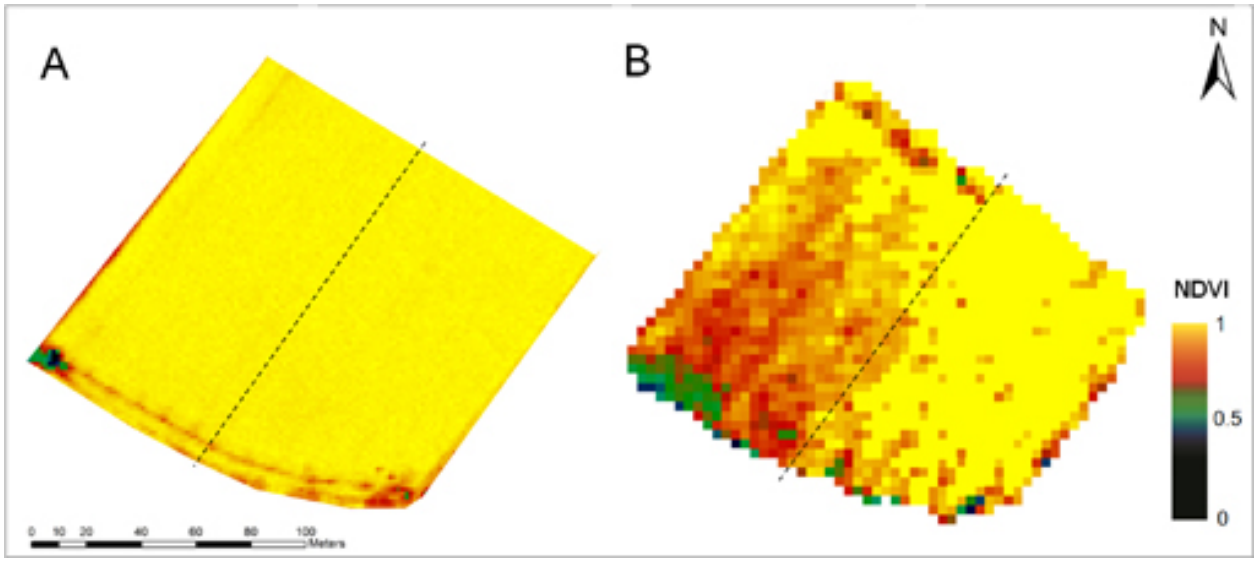

Figure 4.34: Classified NDVI images calculated from airborne hyperspectral ROSIS data from 1th July, and HyMap image from 6th August, Klein-Altendorf 2008.

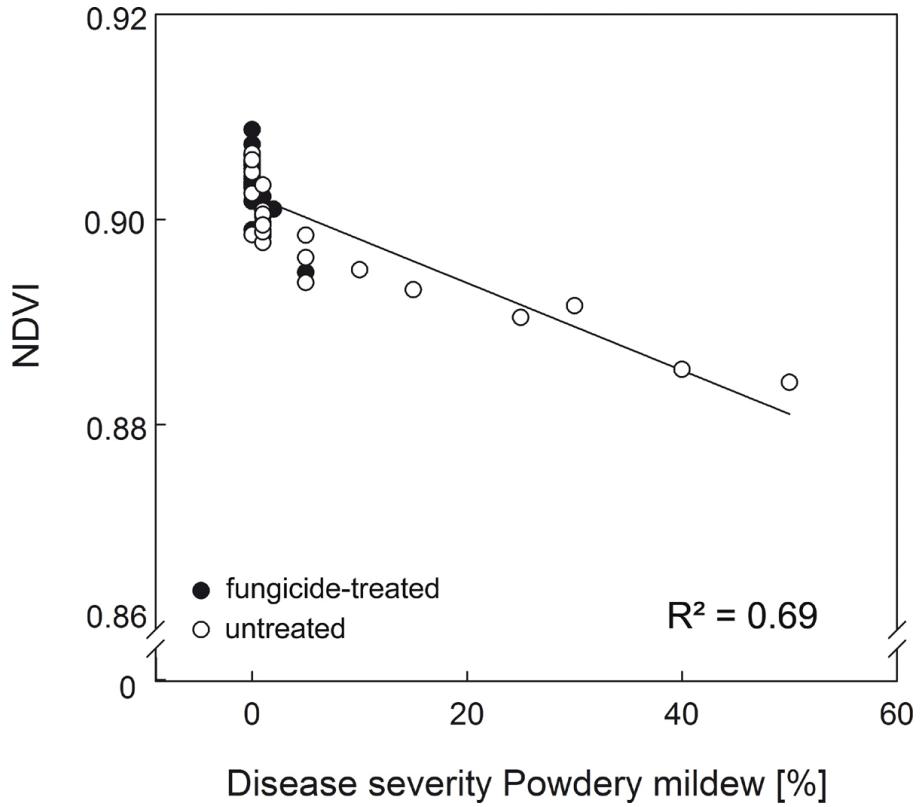

Figure 4.35: Relationship between disease severity of powdery mildew and NDVI calculated from HyMap scene on 6th August, Klein-Altendorf 2008.

Table 4.12: Coefficients of correlation between disease severity and spectral vegetation indices for the leaf diseases of sugar beet on the canopy scale, Klein-Altendorf 2008.

Index	Cercospora leaf spot	Powdery mildew
NDVI	-0.48**[1]	-0.71**
REP	-0.29*	-0.54**
SR	-0.45**	-0.64**
PSSRa	-0.45**	-0.65**
PSSRb	-0.44**	-0.64**
SIPI	-0.44**	-0.69**
ARI	0.73**	0.79**
mCAI	-0.60**	-0.72**
MCARI	-0.49**	-0.63**
OSAVI	-0.53**	-0.59**
MCARI/OSAVI	0.56**	0.73**

[1] correlation was calculated as Pearsons coefficient of correlation (r) asterisk marks denote significant correlation with ** p = 0.01, and * p = 0.05, n = 50

gave the best correlation between index values and disease severity, for both powdery mildew (r = 0.79) and *Cercospora* leaf spot (r = 0.73). Also the soil effect minimizing index combination between MCARI and OSAVI was highly correlated to powdery mildew (r = 0.73), but lower to severity of *Cercospora* leaf spot (r = 0.56). The chlorophyll specific indices PSSRa and PSSRb, MCARI as well as the additionally tested vegetation indices REP, SR, SIPI, and OSAVI were lower correlated to pathogen incidence of powdery mildew and *Cercospora* leaf spot (Tab. 4.12). Because powdery mildew was the predominant disease in this growing season, indices highly correlated to powdery mildew severity were selected and plotted to examine their potential for discriminating the untreated and fungicide-treated plots (Fig. 4.36). A general gradient between sprayed and non-sprayed sugar beets was detected. Scatter plots of SVIs from the fungicide-treated plot could be separated from scatter plots relating to spectral vegetation indices from the untreated plot.

Comparing the spatial pattern of these index values with that of visual assessed disease severity levels (Fig. 4.37), the lower NDVI and mCAI values and higher

ARI and MCARI/OSAVI values followed the spatial distribution of disease severity for powdery mildew and *Cercospora* leaf spot. Significant lower NDVI values have been measured in the untreated plot compared to the sprayed part of the field (Fig. 4.37 A). A clear differentiation of the treatments by calculating mCAI and ARI values as well as by the ratio between MCARI and OSAVI seems possible (Fig. 4.37 B, C, D).

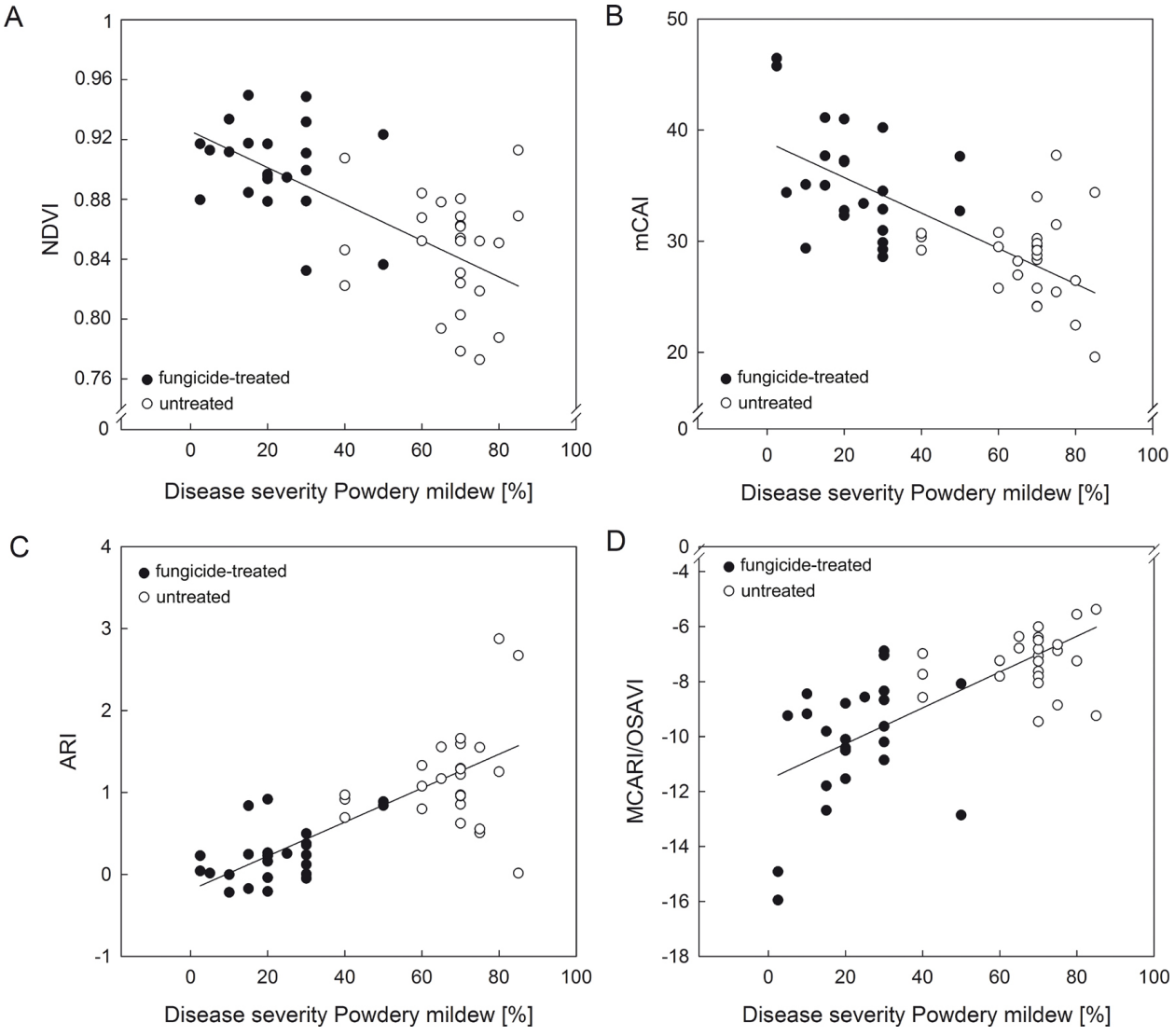

Figure 4.36: Scatter plots displaying the relationship between disease severity of powdery mildew and spectral vegetation indices NDVI, mCAI, ARI, and MCARI/OSAVI of sugar beet canopy, measured at growth stage 49, 9th September, Klein-Altendorf 2008.

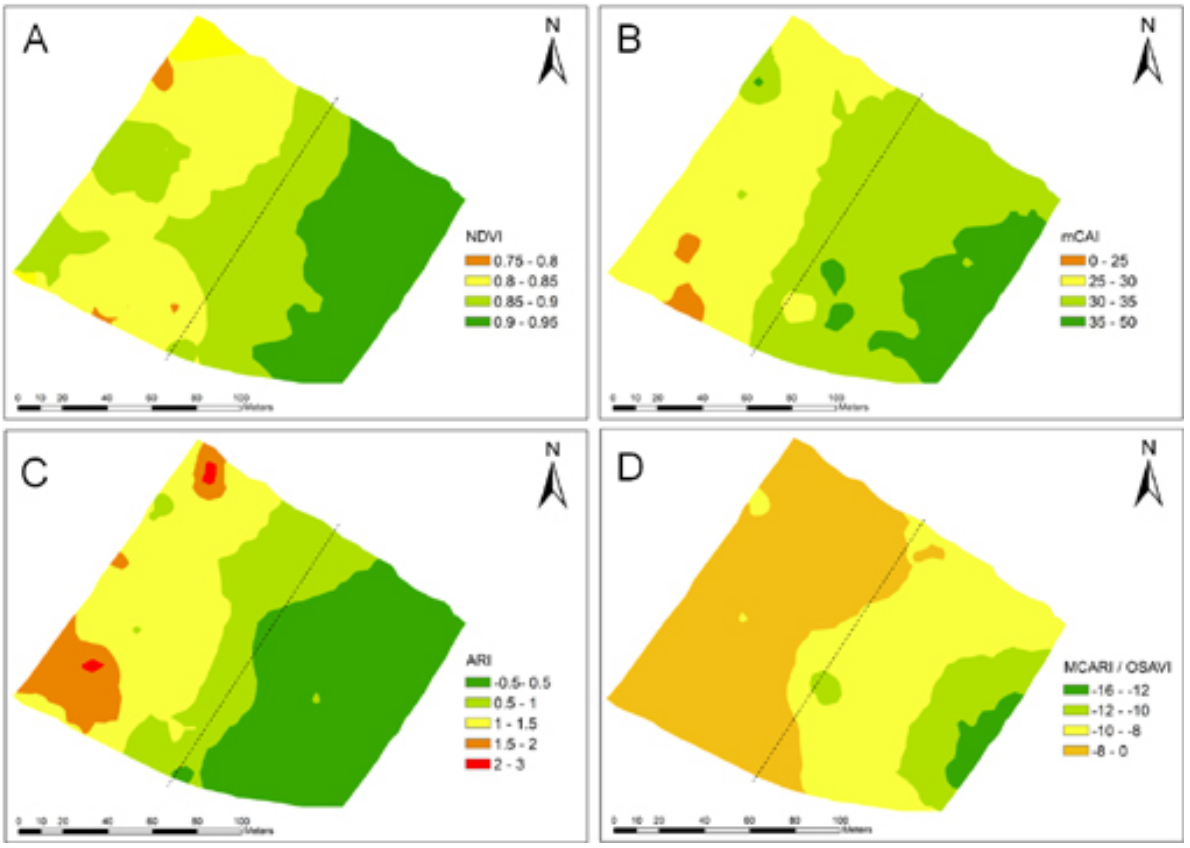

Figure 4.37: Classified maps of spectral vegetation indices of sugar beet canopy reflectance, measured by ASD-FieldSpec at growth stage 49, 9th September, Klein-Altendorf 2008 (n = 50).

5. DISCUSSION

The main emphasis of this work was to investigate the potential of hyperspectral sensors for applications in plant pathology and precision crop protection. Reliable detection and identification of plant diseases and precise and reproducible quantification of disease severity are important for predicting yield loss, monitoring and forecasting of epidemics, phenotyping for disease resistance breeding, and for the understanding of fundamental biological processes during disease progress. In this work high attention has given to the three key points, whether the detection, identification, and quantification of fungal diseases can be implemented by hyperspectral sensors. Knowledge of how solar radiation interacts with vegetation is necessary to interpret and process reflectance data (Knipling, 1970). The interactions between the host plant sugar beet and the fungal pathogens *Cercospora beticola*, *Erysiphe betae*, and *Uromyces betae* influence the reflectance of solar radiation of the plant during disease development in different ways. Resulting spectral signatures, unique for the diseases may be useful for detection and identification of the plant diseases. The quality and quantity of information of spectral signals depend on several factors like the sensor system (spectroradiometer, hyperspectral camera, or airborne sensor), the measuring scale (leaf, plant, canopy, or field), and on data analysis and interpretation. Limitations and difficulties in the detection of foliar diseases due to different scales and measuring conditions – controlled conditions in a laboratory, under greenhouse conditions, and in the field – should be revealed.

Effect of diseases on reflectance

The investigations were based on the hypothesis that reflectance of diseased plants differs from that of healthy leaf tissue. An optical differentiation of healthy and diseased plants may be based on spectral measurements of different wavebands or on a combination of wavebands (West *et al.*, 2003). The identification of a specific disease or stress using remote sensing techniques is still a significant challenge in vegetation monitoring. Wavelengths in the VIS range are largely absorbed by pigments. The reflectance of NIR radiation depends on leaf structure and multiple scattering within the leaf related to the fraction of air spaces. Reflectance in the SWIR is highly influenced by the absorption of water, proteins, and other carbon constituents (Asner, 1998; Ceccato *et al.*, 2001; Curran, 1989; Jacquemoud and Ustin, 2001; Jensen, 2002). To classify various fungal diseases, multi-temporal approaches on different scales were chosen under controlled conditions and in the field to collect and compare spectral signatures of foliar sugar beet diseases.

Changes in reflectance result from modifications of biophysical and biochemical characteristics of plant tissue. The recording of changes caused by the development of fungal diseases may allow disease discrimination by hyperspectral sensing. Diseases may cause changes in tissue colour and leaf shape, transpiration rate, crop canopy morphology and density as well as variation in the interaction of solar radiation with plants (West *et al.*, 2010). This results in modified optical properties of leaf tissue. Reflectance of leaves has been shown to be sensitive to plant stress due to changes in pigmentation, hypersensitive reaction and cell wall degradation (Blackburn, 2007; Carter and Knapp, 2001; Chaerle *et al.*, 2004; Lenk *et al.*, 2006). Disease-specific symptoms like chloroses, necroses or fungal structures may be also detectable (Bravo, 2006; West *et al.*, 2003).

Physiological interactions between diseases and crops depend on the pathogen and its host plant (Glazebrook, 2005; Jones and Dangl, 2006; Knogge, 1996;

Mendgen and Hahn, 2002; Van Kan, 2006). Primary symptoms of leaf diseases often are associated with the formation of chlorotic or necrotic tissue. The pattern of responses and the degree of up- and down-regulation of physiological processes are related to the type of the host-pathogen relationship. Perthotrophs like *C. beticola* rapidly kill plant cells to feed subsequently on the nutrients released from the dead tissue, biotroph pathogens like *E. betae*, and *U. betae* form haustoria to take up nutrients from living cells. As characteristic symptoms differ as well, different wavebands are suitable for the detection of different diseases (Nutter and Littrell, 1996).

Composition and content of leaf pigments change when plants are exposed to pathogens that induce chlorotic and necrotic symptoms (Carter and Knapp, 2001; Coops *et al.*, 2003; Jing *et al.*, 2007; Pietrzykowski *et al.*, 2006). Pigment content of sugar beet leaves inoculated with *C. beticola*, *E. betae* or *U. betae* was slightly decreasing during disease progress. However, the development of disease specific symptoms had only a small effect on leaf total chlorophyll content. This effect was only significant to a decrease in pigment content at high infection rates with mature symptoms. Trends were also evident in accessory pigment content; chlorophyll a and b, and carotenoids decreased. Levall and Bornmann (2000) came to comparative results. Due to high variation between sampled leaves infected with *C. beticola*, no significant differences in pigment content were reported in their study. However, according to Malthus and Madeira (1993), a slight increase in pigment content has been observed at early infection stages. This effect was most evident for the biotroph diseases powdery mildew and sugar beet rust from 5 to 8 days after inoculation.

Symptoms of infections by *C. beticola* are a consequence of the biological activity of cercosporin in the host cells and the intracellular growth of the fungal mycelia (Daub and Ehrenshaft, 2000; Feindt *et al.*, 1981). The fungal toxin causes membrane damage and cell death after the fungus has penetrated the leaf through stomata (Daub and Ehrenshaft, 2000; Knogge, 1996; Weiland *et al.*,

2010). The toxin is produced during vegetative growth of the fungus in the light, relevant for virulence and pathogenicity of *C. beticola*. Intracellular growth and colonization of leaf tissue by the pathogen is facilitated by leakage of nutrients into the intercellular spaces where fungal colonization occurs (Daub *et al.*, 2010; Goodwin and Dunkle, 2010). Electron microscopic observations visualized the cell collapse and the sharp discrimination between symptomatic and healthy tissue. Differences in symptom expression, particularly colouration of the margin of *Cercospora* leaf spots were observed under different cultivation and light conditions. The characteristic reddish brown border was formed under natural sunlight illumination in the field, whereas it appeared pale brown under artificial illumination in the greenhouse. The link between light exposure and development of the necrotic spot and red margin typical of *Cercospora* leaf spot is consistent with cercosporin's mode of action as a photosensitizer (Daub and Ehrenshaft, 2000).

Changes in spectral signature of *Cercospora* leaf spot resulted from necrotic areas that enlarged with time. These localized, in early infection stage non-uniform patches of necrotic tissue, are surrounded by healthy tissue. Due to tissue degradation and the accumulation of brown and reddish brown pigments, reflectance spectra of *Cercospora* leaf spot significantly increase in the complete VIS, especially between 600 and 700 nm. Decreasing reflectance in the NIR and increasing reflectance in the SWIR is due to the effect of the invasive growth of *C. beticola* on the tissue structure of sugar beet leaves. With further symptom development the colonized tissue degrades more and more; collapse of parenchyma and epidermal cells, decrease of cell water content, and increased lignifications are the consequences (Feindt *et al.*, 1981; Steinkamp *et al.*, 1979). Changes in sugar beet leaf reflectance in the NIR and SWIR were most pronounced for *Cercospora* leaf spot than for the other diseases.

In early disease stages the impact of powdery mildew on the chlorophyll content is rather low, since the biotrophic fungus on the plant surface relies on the

photosynthetic activity of the host tissue (Francis, 2002; Glawe, 2008; Mendgen and Hahn, 2002). Significant changes in the chlorophyll absorption bands of powdery mildew diseased leaves could be detected neither early after inoculation nor at moderate disease severities. Coverage of the leaf surface by white mycelia generally increased reflection, especially in the VIS and less marked, but still obvious, in the NIR and SWIR. The increase in the NIR and SWIR may be due to direct reflectance of fungal hyphae on the leaf surface and to changes in water content of the host cell wall due to activities of the fungus.

Similar to *E. betae*, *U. betae* the causal agent of sugar beet rust is a biotrophic pathogen, colonising living plant cells and not apparently triggering any obvious adverse plant response (Heath, 1997). The very small uredinia surrounded by a chlorotic halo were scattered on the leaf surface and resulted only in minor reflectance changes between 550 and 700 nm. In contrast to the other diseases, sugar beet rust did not increase leaf reflectance in the violet-blue region. Also the effect on NIR and SWIR was low, although sugar beet rust generally decreased reflectance in the SWIR.

Disease detection and its assessment by reflectance spectra are feasible for diseases causing changes in pigments – VIS range – or cell structure – NIR range (Malthus and Madeira, 1993). The authors described a flattening of the reflectance in the VIS and a decrease in the NIR reflectance shoulder at 800 nm for leaves infected by the necrotrophic pathogen *Botrytis fabae*. These responses may correspond to the collapse of tissue structure due to pathogen spread. Reflectance of cucumber leaves infected by *Colletotrichum orbiculare* was affected in the violet-blue region and the NIR (Sasaki *et al.*, 1998). Comparing different disease assessment methods for downy mildew in quinoa, reflectance measurement in the red in the NIR provided highest correlation with yield loss (Danielsen and Munk, 2004).

In situ leaf reflectance measurements indicated specific spectral signatures for sugar beet leaves, respectively diseased with *C. beticola*, *E. betae*, and *U. betae*.

The intensity of physiological changes and the extent of the symptoms influenced changes in spectral reflection of sugar beet. Similar trends with minor exiguous impact on spectral reflectance have been observed on the canopy and field scale. Specific effects of some diseases, specific effects of disease stages, and the impact of disease severity on spectral characteristics of plants are sophisticated, but may be also used for the characterization of host-pathogen interactions. Hyperspectral measurements of diseased sugar beet leaves revealed that spectral response of early symptoms or low disease severity differs from that from mature symptoms or high disease severity. Furthermore specific regions of the spectrum seem to have higher potential for discrimination of diseases than only one or few wavelengths.

The spectral response of plants to different stress factors may be similar (Bock *et al.*, 2010; Stafford, 2000). Plant stress begins with a constraint or highly unpredictable fluctuations imposed on regular metabolic patterns, which cause tissue injury, disease or aberrant physiology. According to Gaspar *et al.* (2002), plant stress is the altered physiological condition caused by factors that tend to alter an equilibrium. Plant growth, productivity, and reproductive capacity generally are influenced negatively (Rhodes and Nadolska-Orczyk, 2001). Most abiotic stress factors like water deficiency, nutrient deficiency, solar radiation, and temperature as well as pathogens affect the photosynthetic apparatus and its functions (Carter and Miller, 1994; Chapin, 1991; Stafford, 2000). Associated response to different kinds of stress in reflectance spectra by minor reflectance around 700 nm and 550 to 575 nm have been measured by Carter and Knapp (2001).

Stress-induced physiological consequences are highly variable (Balachandran *et al.*, 1997). Plant fungus interactions and the resulting disease symptoms are influenced by various external factors and thus are variable as well (Dangl *et al.*, 1996). The spatial and temporal distribution of stress symptoms caused by pathogens is different from those caused by abiotic factors (Vollenweider and

Günthard-Georg, 2005). Nutrient deficiencies, drought stress, or temperature stress cause relative uniform patterns, whereas foliar diseases are associated mostly with localized, discrete lesions. This has to be considered for disease detection.

Comparison of hyperspectral non-imaging and imaging sensing
The sensitivity of hyperspectral sensing systems to changes in plant reflectance largely depends on sensor technology and the measuring scale. Spectroradiometers average the reflection in several narrow wavebands of light within the field of view of the sensor (West *et al.*, 2003, 2010). Measurements with the non-imaging spectroradiometer gave a good correlation of reflectance to diseases regardless to spatial information. But as the portion of diseased tissue in the mixed signal decreases with disease severity, the sensitivity and specificity of the non-imaging spectroradiometer was limited at low disease severities. Reflectance curves measured with non-imaging systems always represent the mean of the reflectance of healthy and diseased tissue. This results in a number of problems, typical for single point measurements (Scholten *et al.*, 2005). The effect of small or a few disease symptoms, e.g. sugar beet rust on spectral reflectance of the field-of-view was low. The spectra include a high percentage of reflectance from healthy tissue and only a low portion of reflectance from symptomatic tissue.

Hyperspectral imaging systems, in contrast, record leaf reflectance in several narrow wavebands for each pixel, forming a focussed image (Bock *et al.*, 2010; West *et al.*, 2010). Spatial and spectral information can be acquired simultaneously (Fitzgerald, 2004). It is expected that hyperspectral imaging can improve disease detection through a better examination of the host pathogen interactions (Bock *et al.*, 2010; Chaerle and van der Straeten, 2001). Imaging sensor systems allows a pixel-wise attribution of disease-specific symptoms and healthy tissue (Steiner *et al.*, 2008) and improves both, the specificity and sensitivity of hyperspectral disease detection. Some diseases and their symptoms can only

be distinguished from other diseases and stresses when hyperspectral imaging with high spatial resolution is used (West *et al.*, 2010). Using the example of sugar beet uredinia, pure spectral signatures could be extracted pixel-wise from hyperspectral imaging data. Nevertheless, the small size of uredinia and limited spatial resolution of the sensor resulted in a strong influence of neighbouring pixels and a high amount of mixed pixels.

Hyperspectral imaging enabled the detailed description and comparison of leaf reflectance during the development of the diseases. The three sugar beet diseases differed in their temporal and spatial development. On the leaf scale *Cercospora* leaf spot formed fast growing leaf spots, finally resulting in necrotic areas. On the canopy scale the disease often were accumulated in clusters. Sugar beet rust mainly appeared in singular uredinia over a leaf, and on single plants on the field scale. The small size of rust colonies impeded the classification in early stages or at low disease severity. Similarly, an unambiguous detection of powdery mildew in early stages is challenging. First symptoms are fluffy white mycelia covering the leaf surface which affects the spectral signature like a dusty coat. But unique for powdery mildew is its plane colonization of the leaf tissue and the fast spread and infestation inside crop stands. Similar differences were monitored for leaf rust and powdery mildew in wheat crops (Franke *et al.*, 2009). Leaf rust appeared mainly in stable patches, whereas powdery mildew exhibited a more dynamic distribution within the field and over time. The development of patterns in time and space may help to identify the disease or stress influencing the crop canopy (Nutter *et al.*, 2010).

Besides analysing the temporal development of the pathogenesis and disease-specific symptoms, also spatial patterns of discrete symptoms of sugar beet diseases could be investigated. The results revealed parallels between temporal and spatial disease characteristics. Modifications of spectral reflectance at different developmental stages were reproduced in spectral signatures of different regions of the symptom. For instance, reflectance of the necrotic

centre of *Cercospora* leaf spot was consistent with overall reflectance of mature symptoms, whereas reflectance of new, immature symptoms was similar to that from the margin of fully developed lesions. Similar results were obtained for different developmental stages and different regions of mature symptoms of powdery mildew and sugar beet rust. These observations derived from hyperspectral imaging clearly demonstrate the gradual transition from healthy to diseased tissue for all diseases in both, time and space. Based on hyperspectral image data cubes, pure spectral signatures from healthy tissue and areas with *Cercospora* leaf spot, powdery mildew, and sugar beet rust can be extracted. However, there is always a gradient in reflectance between symptomatic and symptom-less/healthy leaf tissue and a clear classification between healthy and diseased is difficult. This phenomenon has not been described in literature by now and may be investigated even at smaller scales at the cellular level.

The potential of hyperspectral imaging for the detection of diseases in crops was shown convincingly only in few studies. In most of these studies hyperspectral imaging was used for the detection of one disease in a crop. Disease quantification or the differentiation among several diseases or stress symptoms have been reported only in very few studies. In an early attempt, Coops *et al.* (2003) categorized the severity of needle blight in Australian Pine from airborne hyperspectral imagery and reached a classification accuracy of $> 70\%$ for the three classes low, medium, and high infection as compared to ground truth data. Bravo *et al.* (2003) successfully implemented a hyperspectral line scanning system to detect yellow rust in wheat fields. The hyperspectral camera system was mounted on a hand pushed cart, 1 m above the ground. Detection accuracy of 96% was realized using four selected wavelengths from the range of 460 to 900 nm. Polder *et al.* (2010) compared hyperspectral imaging to colour and fluorescence imaging for the detection of tulip breaking virus (TBV) in tulips. Best results were obtained from the spectral camera system in the VIS and gave results similar to that of visual assessment by experts. The authors aim to develop an autonomous robot equipped with a hyperspectral camera

for the detection of diseased tulips. Insect-induced stress has been detected by hyperspectral data cubes in wheat plants. According to Nansen *et al.* (2009) the main advantages of hyperspectral detection systems are I) fast data collection, II) the potential of a real-time data analysis, and III) non-destructive data collection enable repeated measurements on the same individuals.

Extraction and use of disease relevant parameters

Next to the technical specifications of hyperspectral sensor systems for data recording, data analysis is essential to extract suitable results without losing important information. According to Carter and Knapp (2001), who linked spectral characteristics to stress and chlorophyll concentration, the subtraction of spectra from healthy leaves from those representing diseased leaves revealed the responses of significant spectral regions. For sugar beet diseases, the correlation in the different ranges was tributary to disease specific symptoms, and the sensitivity was regulated by disease severity. As wavelengths near 700 nm have the strongest linear relationship to total chlorophyll content (Carter and Knapp, 2001; Gitelson *et al.*, 2003), the response of leaves diseased with *Cercospora* leaf spot and sugar beet rust in this range was more pronounced than the response to powdery mildew. Reflectance in the VIS from 450 to 520 nm and from 570 to 710 nm was highly correlated to severity of these diseases. This is in contrast to results from Steddom *et al.* (2005), who measured *Cercospora* leaf spot with a multispectral radiometer in the field. The deviation is likely to result from differences in the sensor systems (hyperspectral with 1 nm resolution *vs.* multispectral with 9 bands) and in measuring conditions (lab *vs.* field; constant light conditions *vs.* sunlight). Jing *et al.* (2007) estimated a strong linear correlation between chlorophyll a concentration and yellow rust severity in wheat at around 700 nm. Similar results were obtained for spectral sensitivity of *Eucalyptus globules* foliage in response to *Mycosphaerella* leaf disease (Pietrzykowski *et al.*, 2006). In further data analyses, wavelengths with highest correlations may be used for ratio development according to Carter and Knapp

(2001), Carter and Spiering (2002), Richardson *et al.* (2001), and Yang *et al.* (2007).

From the different methods for waveband selection used in this study it can be concluded, that not a single wavelength can be used to detect or to identify a disease. The combination of specific spectral regions or broad spectral bands improves the detection accuracy. Variability of reflectance among the three sugar beet diseases exceeded intradisease variability. Nevertheless, there are still some difficulties. E.g., it is still under examination in which way mixed infections of plants with two or more diseases affect spectral reflectance signature.

Many data analysis methods for hyperspectral application aim to reduce data dimensionality. Redundant information from narrow bands is removed and the computation time may be reduced. A common method is the calculation of SVIs. For early detection and for site-specific plant protection, SVIs have to be sensitive to changes in the reflection caused by diseases. Similarly, they have to be specific for diseases/stress.

The potential of SVIs for early disease detection has been investigated in several studies (e.g. Delalieux *et al.*, 2009; Graeff *et al.*, 2006; Naidu *et al.*, 2009; Steddom *et al.*, 2003, 2005). Most of the developed indices are highly correlated to the content of pigments, biomass, or leaf area (Le Maire *et al.*, 2004; Thenkabail *et al.*, 2000). Different changes in spectral reflectance not only denoted the occurrence of a disease, but also provided information on the developmental stage and severity of the disease. Delalieux *et al.* (2009) demonstrated that the discriminatory performance of SVIs for apple scab depends on the infection stage and the phenological stage of apple leaves. Indices commonly used in remote sensing, however, lack disease specificity. Nevertheless, SVIs gave promising results in studies assessing only one disease. A binary classification into healthy and diseased plants using single SVIs was feasible. The three diseases affected

leaf reflectance assessed with non-imaging and imaging sensors – and SVIs – of sugar beet in different ways.

SVIs highly correlated to chlorophyll, anthocyanin, and water content showed a high sensitivity to different stages of *Cercospora* leaf spot (e.g. NDVI, ARI, WI). The anthocyanin specific ARI was developed by Gitelson *et al.* (2001) to retrieve anthocyanin content from reflectance. Anthocyanins are water-soluble pigments with a absorption peak around 550 nm, responsible for red coloration of plant tissue. Depending on the sugar beet variety and illumination intensity the boundary zone of *Cercospora* leaf spots is coloured from pale brown to deep-wine red as a result of betacyanin accumulation (Steinkamp *et al.*, 1979). Betacyanins are highly water-soluble pigments, present in the cell vacuole. Similar to anthocyanins, the absorption maximum of betacyanins is from 538 nm to 550 nm (Frank *et al.*, 2005; Kobayashi *et al.*, 2000; Piatelli and Minale, 1964). Although reddish brown symptoms of *Cercospora* leaf spot result from betacyanin accumulation, the ARI based on reflectance at 550 nm is useful for the detection of disease symptoms not related to anthocyanins.

For powdery mildew detection, however, carotenoid-specific indices and SVIs combining the information from absolute reflectance over a spectral range (e.g. SIPI, PSSRc, SumGREEN, BGI2) were more suitable. In contrast to the other diseases, powdery mildew affected reflectance also in the violet-blue region of the spectrum where absorption of carotenoids is maximal. This effect may be explained by the overall reflection increase due to powdery mildew as the disease had no significant effect on the level of carotenoids.

For sugar beet rust the photochemical reflection index (PRI) was most sensitive. The PRI was developed to estimate photosynthetic light use efficiency (Gamon *et al.*, 1997; Rascher *et al.*, 2010). The basic wavelength of PRI is 531 nm correlated to the composition of xanthophylls, pigments involved in non-photochemical quenching (Gamon *et al.*, 1992). An effect of rust infection on non-photochemical quenching has been described for oat and beans.

Scholes and Rolfe (1996) investigated the efficiency of photosynthesis in localised regions of oat leaves infected by crown rust (*Puccinia coronata*). Non-photochemical quenching was low within diseased regions, but much higher, compared to healthy leaves, in uninfected regions of diseased leaves. Similar results have been obtained for *Phaseolus vulgaris* infected by *Uromyces appendiculatus* (Peterson and Aylor, 1995).

SVIs, calculated on hyperspectral imaging data revealed the potential for discriminating among healthy and diseased tissue on the leaf scale. Besides the detection of the three diseases, *Cercospora* leaf spot and powdery mildew could be quantified and the results were highly correlated to visual disease assessment. Due to the small symptom size and exiguous infestation severity, quantification of sugar beet rust was not feasible. With *Cercospora* leaf spot and powdery mildew diseased tissue of sugar beet leaves were accurately recognized and visualized in binary images. This simple, threshold-based analysis seems suitable for an automatic disease detection and quantification for many fields of application. Compared to the approach of Camargo and Smith (2009b), who developed an algorithm for automatically identification of visual symptoms on RGB images, hyperspectral images offers a surplus on information, which is required for high sensitivity. The origin and quality of the sensor data is essential for the success of any system for disease and pattern recognition. Shafri and Ezzat (2009) and Shafri and Hamdan (2009) applied SVIs on airborne hyperspectral images to map and quantify *Ganoderma* disease on oil palms. With and accuracy of 82.8% in their study, the NDVI fitted best for disease detection in forests, regardless of disease specificity.

Analysis of non-imaging hyperspectral data showed that the use of more than just one SVI improves the sensitivity and specificity for disease detection and identification. As the correlation between disease severity and SVIs differs significantly among diseases, it can be concluded that combinations of SVIs have a high potential for hyperspectral disease detection and discrimination. First

analyses confirmed this idea and demonstrated that diseases may be detected and identified in very early stages (Rumpf *et al.*, 2010). Thereby it is crucial to combine SVIs based on different wavelength of the hyperspectral spectrum. SVIs related to different physiological parameters showed divergent scatter plots for healthy plants and mapped each disease separately. SVIs based on similar wavelengths of the spectrum are highly correlated to each other, and hence not feasible for discrimination.

Powerful data processing methodology is required to utilize the full potential of combined SVIs, given that sensor-based disease detection allows automatic classification of diseases for precision crop protection applications. Data mining techniques, the process of extracting important and useful information from a large set of data (Mucherino *et al.*, 2009; Wu *et al.*, 2008b), and in particular SVMs seem to be able to solve this complex problem. Different techniques have been proposed for mining data in terms of disease detection. All solved a dichotomous problem, i.e. the classification between healthy and plants with mature disease symptoms. Bravo *et al.* (2003) investigated the difference in spectral reflectance between healthy and rust-diseased wheat. Using a quadratic discrimination model based on the reflectance of four wavebands, they correctly differentiated spectra of diseased and healthy crops at a classification accuracy of 96%. In a next step they successfully applied the neural network Self-Organizing Maps (SOM) to discriminate between healthy plants, nitrogen deficiency, and diseased wheat plants in the field (Moshou *et al.*, 2006). Wang *et al.* (2008) spectrally predicted late blight infections on tomatoes using artificial neural networks (ANNs).

Wu *et al.* (2008a) recently showed that early detection of grey mould due to *Botrytis cinerea* on eggplant leaves is possible, even before first symptoms became visible. Owing to the complexity of the original spectral data, principal component analysis was applied to reduce the numerous wavelengths to several principal components in order to decrease the amount of calculation and im-

prove the accuracy. These principal components were set as input variables of back-propagation neural networks. In contrast to Wu *et al.* (2008a), who used hyperspectral reflectance for classification, a classification result above 90% for discriminating the three sugar beet diseases by using SVIs as features for SVMs was achieved. This approach included the combinations of individual wavelength from different SVIs. In order to further improve the detection of plant diseases, disease-specific wavelengths and SVIs have to be identified.

For automatic classification of foliar sugar beet diseases SVMs are a powerful data mining tool. They may be even applied for classifying data that is not linearly separable by using a kernel (Vapnik, 2000). Moreover, because of the maximum margin hyperplane founded by SVMs the generalization ability is best (Schölkopf and Smola, 2002). Not only the differentiation between healthy and diseased leaves, but also the identification of diseases (multi-class approach) can be realized. In a recent publication, Camargo and Smith (2009a) used SVMs for the identification of visual symptoms of cotton diseases based on RGB images and reached a classification accuracy of 90%.

An advantage of SVMs is that models can be learned without long computation time (Rumpf *et al.*, 2010). It has been shown that combinations of SVIs are suitable to discriminate among *Cercospora* leaf spot, sugar beet rust, powdery mildew, and healthy leaves. Furthermore, infections could be assessed even before the first symptoms became visible. Both the number of necessary SVIs as features and the feature combinations depend on the disease(s) of interest (Rumpf *et al.*, 2009). Two SVIs are sufficient for the detection of *Cercospora* leaf spot, whereas three and more are needed to identify leaf rust and powdery mildew. The classification accuracy of diseases even before the appearance of visible symptoms was highest when all nine SVIs were considered (Rumpf *et al.*, 2009). Several modifications in cellular leaf structure may occur before symptom formation, e.g. changes in water content at infection sites, initiation of cell death by fungal toxins, or defence reactions of plant tissue (Daub and

Ehrenshaft, 2000; Jones and Dangl, 2006; Knogge, 1996). Likewise fungal spores on the leaf surface after inoculation may influence reflectance in an early stage. These modifications are associated with changes in spectral reflectance which may be detectable by analysing hyperspectral data using SVMs.

Furthermore the classification accuracy differed between diseases. In order to improve the early detection and identification of sugar beet diseases by data mining techniques, two future approaches are conceivable. Instead of SVIs, the information of the entire spectrum may be used as original data by machine learning. This method enables the use of optimal scanning positions and most relevant wavelengths for each disease. In a next step, this information may be reduced to the essential by the development of disease-specific SVIs. The extraction of the most relevant wavelength for disease-specific indices requires an appropriate methodology, which may be implemented by machine learning methods. In a further step, cheap multispectral sensors tailored to the particular diseases and based on the wavelength of the disease-specific indices may be produced for precision crop protection. Key benefits from these disease-specific sensors are lower costs and lower technical complexity with simplified handling.

The analysis of hyperspectral images aims to detect and identify diseased parts of sugar beet leaves. A spectral matching algorithm was used for statistical comparison between reference spectra and unknown spectra. Given that the different spectral patterns of healthy and diseased tissue are known, supervised classification was the choice to analyse the images. The SAM implemented the three main objectives: detection, differentiation, and quantification of diseases. Since the SAM classification is based on defined endmember spectra, a detection before visible symptoms occurs was not feasible by this methodology, but visible symptoms were classified with high accuracy. Similar to Zhang *et al.* (2003), who differentiated various levels of *Phytophthora infestans* infection of tomatoes from airborne hyperspectral images, disease severity could deduced by using the

SAM classification. In a recent approach, Bauriegel *et al.* (2009) could detect *Fusarium* head blight by means of SAM analysis of hyperspectral images.

Insensitivity to heterogeneities of surface topography and illumination are benefits of the SAM algorithm for disease detection on sugar beet. Sugar beet leaves do not have plane surfaces. Leaf veins and differences in growth rates cause a characteristic undulated, grooved topography of sugar beet leaves depending on the genotype. Heterogeneities in reflectance intensity occur, as radiation is not reflected straightforward by these surfaces. Spectral similarity is calculated as the angle between the two spectra, treating them as vectors in a space with dimensionality equal to the number of bands (Kruse *et al.*, 1993). The direction of the vector is independent from the distance of a point to the origin (= effect of illumination). The measure of similarity by SAM is insensitive to gain factors (like illumination and topographic illumination effects), because the angle between two vectors is invariant with respect to the length of the vectors (Kruse *et al.*, 1993).

Although classification accuracy of SAM was satisfying, it should be mentioned that this classification algorithm uses the average spectrum of each endmember class (e.g. healthy and different symptom peculiarities). The spectral variability within each endmember class, denoted as intra-class variability is not retained. Luc *et al.* (2005) obtained a higher overall classification accuracy of Belgian coastline regions by modifying the common SAM to an optimized SAM preserving the intra-class variability. This approach may also resolve problems in disease classification, e.g. lower accuracy for early disease stages when only immature symptoms occur. Similarly, the detection of minor spectral changes due to small sugar beet rust symptoms was less accurate. Zhang *et al.* (2003) also described problems in the differentiation between late blight categories of high spectral similarity by SAM, and among healthy and tomato plants with low disease levels.

Disease assessment on the canopy and field scale

As mentioned above, the measuring scale influences spatial resolution and sensitivity of hyperspectral sensors. Reflectance from plant canopies depends not only on reflectance properties of individual leaves and stems, but also on their orientation and distribution in the 3D space (Gamon *et al.*, 1995). Knipling (1970) has shown that absolute canopy reflectance is about 40% in the VIS and 70% in the NIR of absolute reflectance from a single leaf. Leaf orientation influences the amount of light reflected, as shown for field-grown rice (Murchie *et al.*, 1999). Under stress conditions both factors are likely to change and different fractions of vegetation and soil are exposed to the spectral sensor (Jackson and Pinter, 1986). When lower leaves are exposed, canopy reflectance may be affected because reflectance properties of leaves grown in shade differ from those of leaves exposed to sunlight (Jackson and Pinter, 1986). Several fungal diseases preferably affect older or lower leaves due to the presence of soil-borne primary inoculum, favourable micro-climate and environmental conditions in lower leaf levels and may also influence canopy reflectance.

On the field scale an early detection of diseased sugar beet by hyperspectral images from airborne sensors was possible by calculating SVIs. Already in early disease stages, slight changes in reflectance due to primary symptoms of powdery mildew and *Cercospora* leaf spot could be classified using the NDVI. In agricultural practice, fungicides are applied according to disease-specific action thresholds. According to Wolf and Verreet (2002), an action threshold of 5% disease frequency is used for the control of powdery mildew and *Cercospora* leaf spot. With a disease severity of almost 5% this action threshold was reached for powdery mildew in early August 2008. At higher infection rates later in the vegetation period, a classification based on near-range data was also feasible. The SVIs from different sensors differed in their correlation to disease severity of powdery mildew as described earlier for wheat diseases by Franke and Menz (2007).

Several field studies have tested the usefulness of SVIs for the discrimination between healthy and infected crops at varying disease levels. Steddom *et al.* (2005) demonstrated that necrosis caused by *Cercospora* leaf spot may be detected effectively by using SVIs in the field. Huang *et al.* (2007) used the photochemical reflectance index to quantify the level of yellow rust infection of wheat in the field from airborne and near-range hyperspectral data. The differentiation between abiotic stress and diseases and among diseases, however, is still a challenge. Because the incidence of *Cercospora* leaf spot at Klein-Altendorf was marginal in 2008, the discrimination between diseases from airborne data was not feasible.

West *et al.* (2003) summarized the potential of optical remote sensing for disease monitoring and fungicide application mapping. Scotford and Miller (2005) used indirect spectral information like leaf area index and tillering stage to create fungicide application maps. A high correlation between disease severity and reflectance data of wheat was obtained by using neural networks (Moshou *et al.*, 2004). These authors were also able to differentiate between fungal infection and nutrition deficiency.

Early detection of primary disease foci in the field is another challenge. Binary information – whether plants are infected or not – may be derived from remote sensing data. For the extraction of quantitative information on disease levels, further research and data analysis is required. Integrating these different approaches, hyperspectral sensor-based information such as SVIs are very likely to be suitable for the generation of fungicide application maps. Online systems require even more technological development.

The use of hyperspectral techniques in agricultural fields, however, is limited by several factors. Actually the availability of remote sensing data with high spectral and spatial resolution suitable for disease identification in crops is limited (Franke and Menz, 2007). Airborne sensor campaigns are expensive, complex in organization, and rely on good weather conditions. In contrast, disease de-

velopment in the field is influenced by various parameters like temperature, relative humidity, genetic disease resistance, crop growth stage, etc. The acquisition of spectral data appropriate in time and space for disease detection, therefore, is difficult – at least under the environmental conditions in Western Europe. The three sensors used in this study are proved to be quite sensitive in order to detect changes in canopy reflectance of arable crops. Because of limitations in sensor availability and costs it was not possible to use all sensors at each monitoring for comparative studies. The ROSIS sensor with high spatial and spectral resolution recorded a homogeneous canopy reflectance of healthy sugar beets. Although 4 m spatial resolution of the HyMap sensor is lower, early changes in canopy reflectance due to fungal infections could be detected. Advantages of the hand-held ASD sensor are flexibility and simple handling associated with high spectral sensitivity. Therefore, tractor mounted on-the-go sensors seem to be more practical for precision crop protection than airborne sensors.

Relevance of hyperspectral sensing for precision crop protection

There is a huge potential of hyperspectral sensor systems for precision crop protection and for various plant pathology applications (Delalieux *et al.*, 2009; Hatfield *et al.*, 2008; Nutter *et al.*, 2010; Stafford, 2000; Voss *et al.*, 2010; West *et al.*, 2010). Precision crop protection is a part of precision agriculture, a management concept depending on information technologies related to within-field variability (Hillnhuetter and Mahlein, 2008; Steiner *et al.*, 2008). Monitoring of health and detection of diseases is crucial for sustainable plant production. Variability in environmental conditions, heterogeneous distribution of primary inoculum, or variation in crop growth can lead to spatial and temporal variability of diseases in the field (West *et al.*, 2010). Hyperspectral methods on different scales – from airborne to tractor mounted and handheld sensors – enables the detection and mapping of disease foci or pest infestations. Such areas may be treated site-specifically, particularly in early stages, without spraying the entire field and thereby wasting money and increasing the environmental

burden from crop protection (Stafford, 2000; Steiner *et al.*, 2008; West *et al.*, 2010). Nutter *et al.* (2010) predict that in the short to mid-term future, imagery from remote-sensed data provides permanent records of disease intensity and will be used to quantify the temporal and spatial dynamics of pathogens and diseases.

The investigations on foliar sugar beet diseases at different scales have approved that detection, differentiation, and quantification of diseases can be realized by different hyperspectral sensors. On the leaf scale, hyperspectral imaging was superior to the non-imaging sensor. The precision in detecting spatial and temporal differences was high. Such imaging systems may be used to speed up screening assays in resistance breeding when plant-fungus interactions have to be monitored in time series under rather controlled conditions. Plants are usually inoculated with a pathogen at a well-known spore concentration. These are optimal conditions for an automatic hyperspectral screening system with high sensitivity and specificity (Chaerle *et al.*, 2007a; Delalieux *et al.*, 2009). Disease detection and quantification may be based on SVIs or classification algorithms like the SAM.

For precision crop protection in the field, airborne and spaceborne sensors offer large-scale applications. The use of airborne and spaceborne sensors in practice, however, is limited by their spatial resolution and temporal availability (Franke and Menz, 2007; Mahlein *et al.*, 2009; Voss *et al.*, 2010). The link with epidemiological knowledge about temporal and spatial dynamics of plant diseases is essential to implement hyperspectral disease detection into practice (West *et al.*, 2010). Depending on symptom size and disease severity, patchiness of primary disease and epidemic spread, higher resolutions may be necessary. Tractor-mounted, non-imaging sensor systems may realize on the go spray-decisions. An example for a commercialized, tractor-mounted sensor system is the Yara N-sensor for N-fertilization (Agricon, Ostrau, Germany). Based on reflectance measurement and chlorophyll estimation analogue to the analysis

by SVIs, application rates are directly transferred to a manure distributor or a sprayer. Similar technology may be suitable for disease control; however, the discrimination between different kinds of stress is indispensable. This challenge may be met by machine learning techniques like SVMs which enable high specificity and sensitivity as demonstrated by the early detection and differentiation of sugar beet diseases.

Hyperspectral data from airborne sensors resulted in good disease detection in the field. Both spatial and temporal variability of powdery mildew and *Cercospora* leaf spot could be monitored. Combining optical sensing methods from different scales (airborne, tractor-mounted or even handheld) with new modelling approaches or existing decision support systems, like the IPM-model sugar beet (Wolf, 2001), CERCBET (Racca and Jörg, 2007), and BEETCAST (Pitblado and Nichols, 2005) may improve their validity and reliability, as well as the economical and ecological benefits of these technologies. The automation of disease assessment using optical sensor systems can be useful in order to enhance existing forecast models.

Conclusions and future perspectives

Hyperspectral non-imaging and imaging sensor systems originate from remote sensing sciences and have been introduced to plant pathology only recently. Remote sensing has been defined as 'obtaining information about an object without having direct physiological contact with it' (De Jong and Van der Meer, 2006). In classical disease detection, the human eye is a remote sensing device which, in combination with the brain, acts as an image analysis system (De Jong and Van der Meer, 2006; Nilsson, 1995). Since the response of visual disease rating is not reproducible and depends on several factors, imaging and non-imaging hyperspectral sensing offers potentially reliable and accurate information (Nutter and Littrell, 1996; Steddom *et al.*, 2005). What can be seen with the human eye should be also detectable by a hyperspectral sensor system and manifold data analysis methods may conform prospects for plant

disease detection (Bravo, 2006; Chaerle and van der Straeten, 2001). Hyperspectral remote sensing and near-range sensing can provide a precise, objective, reproducible, and time-saving method for disease monitoring in various fields of applications in the near future. The effectiveness of crop protection actions may be optimized economically and ecologically by increased precision in both, space and time.

New insights from hyperspectral disease detection in sugar beet, like sensor specificities and different analysis methods may be transferred to other plant-pathogen systems. Disease-specific characteristics and crop characteristics have to be taken into account for sensor optimization in order to obtain the highest sensitivity and specificity. For practical applications sensor systems, as well as algorithms for the analysis of hyperspectral data need to be simplified. Turn-key solutions with an appropriate degree of automated calibration and processing to compensate for different plant parameters, suitable for use by specialists and non-specialists are needed (Hatfield *et al.*, 2008). The development of disease-specific SVIs or classification algorithms may increase the overall performance of the system. The commonly used classification methods analyze hyperspectral images without incorporating information from spatially adjacent data (Plaza *et al.*, 2009). Simultaneous multi-dimensional data analyses of spatial and spectral patterns will be of high relevance in future, especially for the interpretation of hyperspectral images to detect and characterize plant diseases.

Hyperspectral recordings can improve monitoring systems for plant diseases and will by this support farmers and breeders to achieve an improved assessment and control of plant diseases in the future. This technology will contribute to optimize the use of natural resources, to maintain the quality and quantity of agricultural products at high standards, and to reduce the environmental impacts from crop protection.

6. SUMMARY

Fungal plant diseases often are distributed heterogeneously in the field. Precision crop protection, as a part of precision agriculture, is a management concept depending on information technologies related to within-field variability. Monitoring of health and detection of diseases is critical for sustainable plant production. Hyperspectral imaging and non-imaging has the potential for precise, objective, reproducible, and time-saving disease monitoring in various fields of applications. This would make it possible to treat such areas site-specifically, particularly at early disease stages, without needing to spray an entire field. The present study, therefore, focused on the prospects of hyperspectral sensing to detect, differentiate, and to quantify plant diseases. Sugar beet infected by the fungal pathogens *Cercospora beticola*, *Erysiphe betae*, and *Uromyces betae* causing *Cercospora* leaf spot, powdery mildew, and sugar beet rust, respectively, were used as a model system. The effects of diseases on reflectance of sugar beet leaves were recorded during their temporal and spatial development on various scales.

- The three diseases of sugar beet differed in their interaction with the host plant. Spatial, temporal, and visual differences during pathogenesis were observed. The perthotroph pathogen *C. beticola* caused reddish brown necrotic spots, which coalesced during pathogenesis, whereas the biotroph pathogen *E. betae* colonized the leaf surface with a white, fluffy powdery mycelia. Symptoms due to *U. betae* were singular small uredina, distributed over the leaf surface.

- Characteristic spectral signatures of diseased sugar beet leaves were recorded with a non-imaging spectroradiometer during pathogenesis. *Cercospora* leaf spot increased reflectance in the VIS between 450 and 700 nm. A shift of the red edge position was monitored. Reflectance in the NIR decreased with increasing disease severity, whereas an obvious increase of reflectance in the SWIR was measured. Powdery mildew caused an increase of reflectance over the entire range. This effect was most pronounced in the VIS, and minor in the NIR and SWIR. Sugar beet rust slightly increased reflectance from 550 to 700 nm, reflectance in the NIR and SWIR decreased during pathogenesis. Reflectance spectra assessed on the leaf scale were similar to those recorded on the canopy scale. However, changes on the canopy level were less pronounced due to several influencing factors like leaf geometry, shadowing, and the relation of healthy to symptomatic leaf area.

- Spectral vegetation indices calculated from hyperspectral non-imaging data differed in their correlation and sensitivity to the three diseases. The NDVI and the chlorophyll related indices PSNDa and PSNDb were correlated best to *Cercospora* leaf spot. The carotenoid specific indices SIPI, PSNDc as well as the NDVI and the PSNDa were suitable for the detection of powdery mildew. The PRI and the ARI were most suitable to detect reflectance changes due to sugar beet rust.

- Combinations of two or more SVIs offered the potential for detection and differentiation among sugar beet diseases. In a further approach SVIs were used as features for an automatic classification by Support Vector Machines. Non-inoculated, healthy sugar beet leaves and sugar beet leaves inoculated with *C. beticola*, *E. betae*, and *U. betae*, respectively, were classified with an accuracy of $> 86\%$. Furthermore, plant diseases could be detected pre-symptomatically. Depending on the type and stage of disease the classification accuracy ranged from 65% to 90%.

- Hyperspectral imaging enabled the observation of changes in sugar beet leaves due to *Cercospora* leaf spot, powdery mildew, and sugar beet rust on the pixel level. The temporal and spatial development of disease symptoms gave characteristic reflectance patterns on the leaf level. Spectral signatures obtained from hyperspectral imaging coincided with spectral signatures from non-imaging measurements.

- Several SVIs showed a potential to discriminate between healthy and diseased tissue. The use of disease-responsive SVIs in combination with disease-specific threshold levels resulted in the compilation of binary images, differentiating between diseased and healthy tissue. The automatic quantification of disease severity from these images gave high correlations to visual disease assessments. The coefficients of correlation for the quantification of *Cercospora* leaf spot and powdery mildew were $R^2 = 0.98$ and 0.93, respectively. Difficulties remained for the very small rust uredinia ($R^2 = 0.67$).

- Applying the Spectral Angle Mapper algorithm on hyperspectral imaging data, high accuracies for the differentiation between healthy and diseased leaf tissue were obtained. Besides the differentiation of symptomatic and healthy parts of a leaf, also different regions of disease-specific symptoms, and different developing stages could be differentiated. For the detection of *Cercospora* leaf spot the accuracy of classification ranged from 89% 11 dai to 98% 17 dai. Similar high accuracies could be assessed for powdery mildew classification (94% 8 dai, 97% 14 dai, and 90% 17 dai). Classification of sugar beet rust was less exact (accuracy 62% 20 dai).

- A multi-temporal and multi-sensoral approach on different scales was used in an experiment on the field scale in 2008. The experimental field site included two treatments, one plot was sprayed with fungicides and one plot was untreated. *E. betae*, causing powdery mildew was the most frequent

leaf pathogen during the growing season. The vitality of the sugar beet plots was characterized by calculating the NDVI from airborne hyperspectral data (ROSIS and HyMap campaign, respectively). At growth stage 45 healthy and diseased parts of the field could be differentiated; the coefficient of determination to ground truth data was 0.69. A classification of healthy and diseased sugar beets was possible at growth stage 49 by calculating SVIs from canopy reflectance.

New insights from hyperspectral disease detection on sugar beet make a contribution to a better understanding of plant optical properties during disease pathogenesis. Different analysis methods and sensor specificities can be transferred and generalized for other plant-pathogen systems. It has been shown that hyperspectral near-range and remote sensing has the potential for an implementation in precision crop protection applications. Moreover, the technologies may be also used in plant pathology for investigating the effect of pathogenesis on the cellular level.

REFERENCES

Adamchuk, V.I., Hummel, J.W., Morgan, M.T. and Upadhyaya, S.S. (2004). On-the-go soil sensors for precision agriculture. *Computers and Electronics in Agriculture*, 44, 71–91.

Apan, A., Datt, B. and Kelly, R. (2005). Detection of pests and diseases in vegetable crops using hyperspectral sensing: a comparison of reflectance data for different sets of symptoms. In: *Proceedings of SSC 2005 Spatial Intelligence, Innovation and Praxis: The national biennial Conference of the Spatial Science Institute, Melbourne 2005.* Melbourne, pp. 10–18.

Archetti, M., Döring, T.R., Hagen, S.B., Hughes, N.M., Leather, S.R., Lee, D.W., Lev-Yadun, S., Manetas, Y., Ougham, H.J., Schaberg, P.G. and Thomas, H. (2009). Unravelling the evolution of autumn colours: an interdisciplinary approach. *Trends in Ecology and Evolution*, 24, 166–173.

Ariana, D.P., Lu, R. and Guyer, D.E. (2006). Near-infrared hyperspectral reflectance imaging for the detection of bruises on pickling cucumbers. *Computers and Electronics in Agriculture*, 53, 60–70.

Asner, G. (1998). Biophysical and biochemical sources of variability in canopy reflectance. *Remote Sensing of Environment*, 64, 234–253.

Balachandran, S., Hurry, V.M., Kelly, C.B., Osmond, C.B., Robinson, S. A. amd Rohozinski, J., Seaton, G.G.R. and Sims, D.A. (1997). Concepts of plant biotic stress. Some insights into the stress physiology of virus-infected plants, from the perspective of photosynthesis. *Physiologia Plantarum*, 100, 203–213.

Balasundaram, D., Burks, T.F., Bulanon, D.M., Schubert, T. and Lee, W.S. (2009). Spectral reflectance characteristics of citrus canker and other peel conditions of grapefruit. *Postharvest Biology and Technology*, 51, 220–226.

Baranoski, G.V.G. and Rokne, J.G. (2001). Efficiently simulating scattering of light by leaves. *The Visual Computer*, 17, 491–505.

Bauriegel, E., Beuche, H., Dammer, K., Giebel, A., Herppich, W., Intress, J. and Rodemann, B. (2009). Determination of head blight on ears of winter wheat by means of hyperspectral and chlorophyll fluorescence image analysis. In: E. van Henten, ed., *7th JIAC Conference*. Wageningen Academic Publisher, pp. 239–246.

Biliouris, D., Verstaeten, W.W., Dutre, P., van Aardt, J.A.N., Mys, B. and Coppin, P. (2007). A compact labroratory spectro-goniometer (CLabSpeG) to assess the BRDF of materials. Presentation, calibration and implementation on *Fagus sylvativa* L. leaves. *Sensors*, 7, 1846–1870.

Birth, S.G. and McVey, R.G. (1968). Measuring the color of growing turf with a reflectance spectrophotometer. *Agronomy Journal*, 60, 640–643.

Blackburn, G.A. (1998a). Quantifying chlorophylls and carotenoids at leaf and canopy scale: an evaluation of some hyperspectral approaches. *Remote Sensing of Environment*, 66, 273–285.

Blackburn, G.A. (1998b). Spectral indices for estimating photosynthetic pigment concentrations: a test using senescent tree leaves. *International Journal of Remote Sensing*, 19, 657–675.

Blackburn, G.A. (2007). Hyperspectral remote sensing of plant pigments. *Journal of Experimental Botany*, 58, 844–867.

Board, J.E., Maka, V., Price, R., Knight, D. and Baur, M.E. (2007). Development of vegetation indices for identifying insect infestations in soybean. *Agronomy Journal*, 99, 650–656.

Bock, C.H., Poole, G.H., Parker, P.E. and Gottwald, T.R. (2010). Plant disease severity estimated visually, by digital photography and image analysis, and by hyperspectral imaging. *Critical Reviews in Plant Science*, 29, 59–107.

Bongiovanni, R. and Lowenberg-Deboer, J. (2004). Precision agriculture and sustainability. *Precision Agriculture*, 5, 359–387.

Boser, E.B. (1992). A training algorithm for optimal margin classifiers. In: D. Haussler, ed., *Proceedings of the 5th Annual ACM Workshop on Computational Learning Theory (COLT'92)*. pp. 144–152.

Bravo, C. (2006). *Automatic foliar disease detection in winter wheat.* Ph.D. thesis, University of Leuven.

Bravo, C., Moshou, D., West, J., McCartney, A. and Ramon, H. (2003). Early disease detection in wheat fields using spectral reflectance. *Biosystems Engineering*, 84, 137–145.

Brooks, F. and Miller, W. (1963). Availability of solar energy. In: A. Zarem and D. Erway, eds., *Introduction to the utilization of solar energy.* McGraw-Hill, New York, NY, USA, pp. 30—58.

Buschmann, C. and Lichtenthaler, H.K. (1998). Principles and characteristics of multi-colour fluorescence imaging of plants. *Journal of Plant Physiology*, 152, 297–314.

Camargo, A. and Smith, J.S. (2009a). Image pattern classification for the identification of disease causing agents in plants. *Computers and Electronics in Agriculture*, 66, 121–125.

Camargo, A. and Smith, J.S. (2009b). An image-processing based algorithm to automatically identify plant disease visual symptoms. *Biosystems Engineering*, 102, 9–21.

Carrol, M.W., Glaser, J.A., Hellmich, R.L., Hunt, T.E., Sappington, T.W., Calvin, D., Copenhaver, K. and Fridgen, J. (2008). Use of spectral vegetation

indices derived from airborne hyperspectral imagery for detection of European corn borer infestation in Iowa corn plots. *Journal of Economic Entomology*, 101, 1614–1623.

Carter, G.A. and Knapp, A.K. (2001). Leaf optical properties in higher plants: linking spectral characteristics to stress and chlorophyll concentration. *American Journal of Botany*, 88, 677–684.

Carter, G.A. and Miller, R.L. (1994). Early detection of plant stress by digital imaging with narrow stress-sensitive wavebands. *Remote Sensing of Environment*, 50, 295–302.

Carter, G.A. and Spiering, B.A. (2002). Optical properties of intact leaves for estimating chlorophyll concentration. *Journal of Environmental Quality*, 31, 1424–1432.

Ceccato, P., Flasse, S., Tarantola, S., Jacquemoud, S. and Gregoire, J.M. (2001). Detecting vegetation leaf water content using reflectance in the optical domain. *Remote Sensing of Environment*, 77, 22–33.

Chaerle, L., Hagenbeek, D., De Bruyne, E. and Van Der Straeten, D. (2007a). Chlorophyll fluorescence imaging for disease-resistance screening of sugar beet. *Plant Cell Tissue and Organ Culture*, 91, 97–106.

Chaerle, L., Hagenbeek, D., De Bruyne, E., Vlacke, R. and Van der Straeten, D. (2004). Thermal and chlorophyll-fluorescence imaging distinguish plant-pathogen interactions at an early stage. *Plant Cell Physiology*, 45, 887–869.

Chaerle, L., Hagenbeek, D., Vanrobaeys, X. and Van der Straeten, D. (2007b). Early detection of nutrient and biotic stress in *Phaseolus vulgaris*. *International Journal of Remote Sensing*, 28, 3479–3492.

Chaerle, L. and van der Straeten, D. (2001). Seeing is believing: imaging techniques to monitor plant health. *Biochimica et Biophysica Acta (BBA) — Gene Structure and Expression*, 1519, 153–166.

Chang, C.C. and Lin, J.C. (2001). LIBSVM: a library for support vector machines. (accessed 10/2009).

Chapin, F.S.I. (1991). Integrated response of plant stress. *BioScience*, 4, 29–36.

Combal, B., Baret, F. and Weiss, M. (2002). Improving canopy variables estimation from remote sensing data by exploiting ancillary information case study on sugar beet canopies. *Agronomie*, 22, 205–215.

Coops, N., Stanford, M., Old, K., Dudzinski, M., Culvenor, D. and Stone, C. (2003). Assessment of *Dothistroma* needle blight of *Pinus radiata* using airborne hyperspectral imagery. *Phytopathology*, 93, 1524–1532.

Curran, P.J. (1989). Remote sensing of foliar chemistry. *Remote Sensing of Environment*, 30, 271–278.

Dammer, K.H., Wollny, J. and Giebel, A. (2008). Estimation of the leaf area index in cereal crops for variable rate fungicide spraying. *European Journal of Agronomy*, 28, 351–360.

Dangl, J.L., Dietrich, R.A. and Richberg, M.H. (1996). Death don't have no mercy: cell death programs in plant-microbe interactions. *The Plant Cell*, 8, 1793–1807.

Danielsen, S. and Munk, L. (2004). Evaluation of disease assessment methods in quinoa for their ability to predict yield loss caused by downy mildew. *Crop Protection*, 23, 219–228.

Daub, M.E. and Ehrenshaft, M. (2000). The photoactivated *Cercospora* toxin cercosporin: Contributions to plant disease and fundamental biology. *Annual Review of Phytopathology*, 38, 461–490.

Daub, M.E., Herrero, S. and Taylor, T.V. (2010). Strategies for the development of resistance to cercosporin, a toxin produced by *Cercospora* species. In: R.T. Lartey, W.J. J., L. Panella, P.W. Crous and C.E. Windels, eds., *Cercospora*

Leaf Spot of Sugar Beet and Related Species. The American Phytopathological Society, St. Paul, Minnesota, USA, pp. 157–172.

Daughtry, C.S.T., Walthall, C.L., Kim, M.S., Brown de Colstoun, E. and Mc Murtrey, J.E. (2000). Estimating corn leaf chlorophyll concentration from leaf and canopy reflectance. *Remote Sensing of Environment*, 74, 229–239.

De Jong, S. and Van der Meer, E. (2006). *Remote Sensing image Analysis: Including the Spatial Domain. Bookseries on Remote Sensing Digital Image Processing Vol.5.* ISBN 1-4020-2559-9, (S.M. De Jong and E.D. Van der Meer, eds.). Kluwer Academic Publishers, Dordrecht, Netherlands.

Delalieux, S., van Aardt, J., Keulemans, W. and Coppin, P. (2005). Detection of biotic stress (*Venturia inaequalis*) in apple trees using hyperspectral analysis. In: B. Zagajewski, M. Soczal and M. Wrzesien, eds., *Proceedings of the 4th EARSel Workshop on Imaging Spectroscopy*. Warsaw University, Warsaw, Poland, pp. 677–689.

Delalieux, S., Somers, B., Verstraeten, W.W., van Aardt, A.N.J., Keulemans, W. and Coppin, P. (2009). Hyperspectral indices to diagnose leaf biotic stress of apple plants, considering leaf phenology. *International Journal of Remote Sensing*, 30, 1887–1912.

Delalieux, S., van Aardt, J., Keulemans, W., Schrevens, E. and Coppin, P. (2007). Detection of biotic stress (*Venturia inaequalis*) in apple trees using hyperspectral data: non-parametric statistical approaches and physiological implications. *European Journal of Agronomy*, 27, 130–143.

Dennison, P.E., Halligan, K.Q. and Roberts, D.A. (2004). Comparison of error metrics and constraints for multiple endmember spectral mixture analysis and spectral angle mapper. *Remote Sensing of Environment*, 93, 359–367.

Doraiswamy, P.C., Moulin, S., Cook, P.W. and Stern, A. (2003). Crop yield assessment for remote sensing. *Photogrammetric Engineering & Remote Sensing*, 69, 665–674.

Feindt, F., Mendgen, K. and Heitefuss, R. (1981). Feinstruktur unterschiedlicher Zellwandreaktionen im Blattparenchym anfälliger und resistenter Rüben (*Beta vulgaris* L.) nach Infektion durch *Cercospora beticola* Sacc. *Phytopathologische Zeitschrift*, 101, 248–264.

Filella, I. and Peñuelas, J. (1994). The red edge position and shape as indicators of plant chlorophyll content, biomass and hydric status. *International Journal of Remote Sensing*, 15, 1459–1470.

Fitzgerald, G.J. (2004). Portable hyperspectral tunable imaging system (PHyTIS) for precision agriculture. *Agronomy Journal*, 96, 311–315.

Fourty, T., Baret, F., Jacquemoud, S., Schnuck, G. and Verdebout, J. (1996). Leaf optical properties with explicit description of its biochemical composition: direct and inverse problems. *Remote Sensing of Environment*, 56, 104–117.

Frahm, J., Volk, T. and Johnen, A. (1996). Development of the ProPlant decision-support system for plant protection in cereals, sugarbeet and rape. *Bulletin OEPP/EPPO*, 26, 609–622.

Franc, G. (2010). Ecology and epidemiology of *Cercospora beticola*. In: R.T. Lartey, W.J. J., L. Panella, P.W. Crous and C.E. Windels, eds., *Cercospora Leaf Spot of Sugar Beet and Related Species*. The American Phytopathological Society, St. Paul, Minnesota, USA, pp. 7–19.

Francis, S. (2002). Sugar-beet powdery mildew (*Erysiphe betae*). *Molecular Plant Pathology*, 3, 119–124.

Frank, T., Stinzing, F.C., Carle, R., Bitsch, I., Quaas, D., Straß, G., Bitsch, R. and Netzel, M. (2005). Urinary pharmacokinetics of betalains following consumption of red beet juice in healthy humans. *Pharmacological Research*, 52, 290–297.

Franke, J., Gebhardt, S., Menz, G. and Helfrich, H.P. (2009). Geostatistical analysis of the spatiotemporal dynamics of powdery mildew and leaf rust in wheat. *Phytopathology*, 99, 974–984.

Franke, J. and Menz, G. (2007). Multi-temporal wheat disease detection by multi-spectral remote sensing. *Precision Agriculture*, 8, 161–172.

Galvao, L.S., Roberts, D.A., Formaggio, A.R., Numata, I. and Breunig, F.M. (2009). View angle effects on the discrimination of soybean varieties and on the relationships between vegetation indices and yield using off-nadir Hyperion data. *Remote Sensing of Environment*, 113, 846–856.

Gamon, J.A., Derrana, L. and Surfus, J.S. (1997). The photochemical reflectance index: an optical indicator of photosynthetic radiation use efficiency across species, functional types, and nutrient levels. *Oecologia*, 112, 492–501.

Gamon, J.A., Field, C.B., Goulden, M., Griffin, K., Hartley, A. and Joel, G. (1995). Relationships between NDVI, canopy structure, and photosynthetic activity in three Californian vegetation types. *Ecological Applications*, 5, 28–41.

Gamon, J.A., Peñeulas, J. and Field, C.B. (1992). A narrow-waveband spectral index that tracks diurnal changes in photosynthetic efficiency. *Remote Sensing of Environment*, 41, 35–44.

Gamon, J.A. and Surfus, J.S. (1999). Assessing leaf pigment content and activity with a reflectometer. *New Phytologist*, 143, 105–117.

Gaspar, T., Franck, T., Bisbis, B., Kevers, C., Jouve, L., Hasumann, J. and Dommes, J. (2002). Concept in plant stress physiology. Application to plant tissue cultures. *Plant Growth Regulation*, 37, 263–285.

Gebbers, R. and Adamchuk, V.I. (2010). Precision agriculture and food security. *Science*, 327, 828–831.

Gerhards, R. and Christensen, S. (2003). Real-time weed detection, decision making and patch spraying in maize, sugarbeet, winter wheat and winter barley. *Weed Research*, 43, 385–392.

Gerhards, R. and Oebel, H. (2006). Practical experiences with a system for site specific weed control in arable crops using real-time image analysis and GPS-controlled patch spraying. *Weed Research*, 46, 185–193.

Gitelson, A.A., Gritz, Y. and Merzylak, M.N. (2003). Relationships between leaf chlorophyll content and spectral reflectance and algorithms for non-destructive chlorophyll assessment in higher plant leaves. *Journal of Plant Physiology*, 160, 271–282.

Gitelson, A.A., Kaufman, Y.J., Stark, R. and Rundquist, D. (2002). Novel algorithms for remote estimation of vegetation fraction. *Remote Sensing of Environment*, 80, 76–87.

Gitelson, A.A. and Merzlyak, M.N. (1994). Spectral reflectance changes associate with autumn senescence of *Aesculus hippocastanum* L. and *Acer platanoides* L. leaves. Spectral features and relation to chlorophyll estimation. *Journal of Plant Physiology*, 143, 286–292.

Gitelson, A.A., Merzlyak, N.M. and Chivkunova, B.O. (2001). Optical properties and nondestructive estimation of anthocyanin content in plant leaves. *Photochemistry and Photobiology*, 74, 38–45.

Glawe, D.A. (2008). The powdery mildews: A review of the world's most familiar (yet poorly known) plant pathogens. *Annual Review of Phytopathology*, 46, 27–51.

Glazebrook, J. (2005). Contrasting mechanisms of defense against biotrophic and necrotrophic pathogens. *Annual Review of Phytopathology*, 43, 205–227.

Goodwin, S.B. and Dunkle, L.D. (2010). Cercosporin production in *Cercospora* and related anamorphs. In: R.T. Lartey, W.J. J., L. Panella, P.W. Crous and

C.E. Windels, eds., *Cercospora Leaf Spot of Sugar Beet and Related Species*. The American Phytopathological Society, St. Paul, Minnesota, USA, pp. 97–108.

Gordon, T.R. and Duniway, J.M. (1981). Effects of powdery mildew on the efficiency of CO^2 fixation and light utilization of sugar beet leaves. *Plant Physiology*, 69, 139–142.

Gould, K.S., Kuhn, D.N., Lee, D.W. and Oberbauer, S.F. (1995). Why leaves are sometimes red. *Nature*, 378, 241–242.

Govaerts, Y.M., Jacquemoud, S., Verstraete, M. and Ustin, S.L. (1996). Three-dimensional radiation transfer modeling in a dicotyledon leaf. *Applied Optics*, 35, 6585–6598.

Graeff, S., Link, J. and Claupein, W. (2006). Identification of powdery mildew (*Erysiphe graminis sp. tritici*) and take-all disease (*Gaeumannomyces graminis sp. tritici*) in wheat (*Triticum aestivum* L.) by means of leaf reflectance measurements. *Central European Journal of Biology*, 1, 275–288.

Guyot, G. and Baret, F. (1988). Utilisation de la haute résolution spectrale pour suivre l'état des couverts végétaux. In: *Proc. 4th Int. Coll. Spectral Signatures of Objects in Remote Sensing, Aussois, France, ESA SP-287*. pp. 279–286.

Haboudane, D., Miller, J.R., Pattey, E., Zarco-Tejada, P. and Strachan, I. (2004). Hyperspectral vegetation indices and novel algorithms for predicting green LAI of crop canopies: modeling and validation in the context of precision agriculture. *Remote Sensing of Environment*, 90, 337–352.

Hatfield, L.J., Gitelson, A.A., Schepers, S.J. and Walthall, L.C. (2008). Application of Spectral Remote Sensing for Agronomic Decisions. *Agronomy Journal*, 100, 117–131.

Heath, M.C. (1997). Signalling between pathogenic rust fungi and resistant or susceptible host plants. *Annals of Botany*, 80, 713–720.

Hillnhuetter, C. and Mahlein, A.K. (2008). Early detection and localisation of sugar beet diseases: new approaches. *Gesunde Pflanzen*, 60, 143–149.

Hiscox, J.D. and Israelstam, G.F. (1979). A method for the extraction of chlorophyll from leaf tissue without maceration. *Canadian Journal of Botany*, 57, 1332–1334.

Hosgood, B. (1993). Leaf optical properties experiment 93 (LOPEX93), database structure. URL http://ies.jrc.ec.europa.eu/uploads/fileadmin/H03/LOPEX_db_structure_V3.pdf, (accessed 30.07.2010).

Huang, W., Lamb, D.W., Niu, Z., Zhang, Y., Liu, L. and Wang, J. (2007). Identification of yellow rust in wheat using in situ spectral reflectance measurements and airborne hyperspectral imaging. *Precision Agriculture*, 8, 187–197.

Ioannidis, P. and Karaoglanidis, G. (2010). Control of *Cercospora* leaf spot and powdery mildew of sugar beet with fungicides and tolerant cultivars. In: R.T. Lartey, W.J. J., L. Panella, P.W. Crous and C.E. Windels, eds., *Cercospora Leaf Spot of Sugar Beet and Related Species*. The American Phytopathological Society, St. Paul, Minnesota, USA, pp. 7–19.

Jackson, R.D. and Pinter, P.J.J. (1986). Spectral response of architecturally different wheat canopies. *Remote Sensing of Environment*, 20, 43–56.

Jacquemoud, S. and Baret, F. (1990). PROSPECT: a model of leaf optical properties spectra. *Remote Sensing of Environment*, 34, 75–91.

Jacquemoud, S., Verdebout, J., Schmuck, G., Andreoli, G. and Hosgood, B. (1995). Investigation of leaf biochemistry by statistics. *Remote Sensing of Environment*, 54, 180–188.

Jacquemoud, S. and Ustin, L.S. (2001). Leaf optical properties: a state of the art. In: *8th International Symposium of Physical Measurements & Signatures in Remote Sensing*. CNES, Aussois, France, pp. 223–332.

Jaggard, K.W., Qi, A. and Ober, E.S. (2009). Capture and use of solar radiation, water, and nitrogen by sugar beet (*Beta vulgaris* L.). *Journal of Experimental Botany*, 60, 1919–1925.

Jensen, J.R. (2002). *Remote sensing of the environment – An earth resource perspective*. [reprint.] edition. The MIT Press and MIT Press, Upper Saddle River, NJ, USA.

Jing, L., Jinbao, J., Yunhao, C., Yuanyuan, W., Wei, S. and Wenjiang, H. (2007). Using hyperspectral indices to estimate foliar chlorophyll a concentrations of winter wheat under yellow rust stress. *New Zealand Journal of Agricultural Research*, 50, 1031–1036.

Jones, D.G.J. and Dangl, L.J. (2006). The plant immune system. *Nature*, 444, 323–329.

Jones, H.G., Archer, N., Rotenburg, E. and Casa, R. (2003). Radiation measurement for plant ecophysiology. *Journal of Experimental Botany*, 54, 879–889.

Jones, H.G. and Schofield, P. (2008). Thermal and other remote sensing of plant stress. *General and Applied Plant Physiology*, 34, 19–32.

Kühbauch, W. and Hawlitschka, S. (2003). Remote sensing – a future technology in precision farming. In: H. Lacoste, ed., *Conference Proceedings of the Workshop on POLinSAR – Applications of SAR Polarimetry and Polarimetric Interferometry (ESA SP-529)*. Frascati, Italy, p. 25.1.

Knerr, S., Personnaz, L. and Dreyfus, G. (1990). Single-layer learning revisited: a stepwise procedure for building and training a neural network. In: *Neurocomputing: Algorithms, Architectures and Applications, F68 of NATO ASI Series*. pp. 41–50.

Knipling, B.E. (1970). Physical and physiological basis for reflectance of visble and near-infrared radiation from vegetation. *Remote Sensing of Environment*, 1, 155–159.

Knogge, W. (1996). Fungal infection of plants. *Plant Cell*, 8, 1711–1722.

Kobayashi, N., Schmidt, J., Nimtz, M., Wray, V. and Schliemann, W. (2000). Betalains from christmas cactus. *Phytochemistry*, 54, 419–426.

Kobayashi, T., Kanda, E., Kitada, K., Ishiguro, K. and Torigoe, Y. (2001). Detection of rice panicle blast with multispectral radiometer and the potential of using airborne multispectral scanners. *Phytopathology*, 91, 316–323.

Kruse, F.A., Lefkoff, A.B., Boardman, J.W., Heidebrecht, K.B., Shapiro, A.T., Barloon, P.J. and Goetz, A.F.H. (1993). The spectral image-processing system (Sips) – interactive visualization and analysis of imaging spectrometer data. *Remote Sensing of Environment*, 44, 145–163.

Kruse, J.K., Christians, N.E. and Chaplin, M.H. (2006). Remote sensing of nitrogen stress in creeping bentgrass. *Agronomy Journal*, 98, 1640–1645.

Lacis, A.A. and Hansen, J.E. (1973). A parameterization for the absorption of solar radiaton in the earths atmosphere. *Journal of the Atmospheric Science*, 31, 118–133.

Larsolle, A. and Muhammed, H.H. (2007). Measuring crop status using multivariate analysis of hyperspectral field reflectance with application to disease severity and plant density. *Precision Agriculture*, 8, 37–47.

Lartey, R.T., Weiland, J.J. and Panella, L. (2010). Brief history of *Cercospora* leaf spot, of sugar beet. In: R.T. Lartey, W.J. J., L. Panella, P.W. Crous and C.E. Windels, eds., *Cercospora Leaf Spot of Sugar Beet and Related Species*. The American Phytopathological Society, St. Paul, Minnesota, USA, pp. 1–5.

Laudien, R., Bareth, G. and Doluschitz, R. (2003). Analysis of hyperspectral field data for detection of sugar beet diseases. In: *Proceedings of the EFITA Conference*. Debrecen (Hungary), pp. 375–381.

Le Maire, G., Francois, C. and Dufrene, E. (2004). Towards universal broad leaf chlorophyll indices using PROSPECT simulated database and hyperspectral reflectance measurements. *Remote Sensing of Environment*, 89, 1–28.

Lee, D.W., OḰeefe, J., Holbrook, N.M. and Field, T.S. (2003). Pigment dynamics and autumn leaf senescence in a New England deciduous forest, Eastern USA. *Ecological Research*, 18, 677–694.

Lenk, S., Chaerle, L., Pfündel, E., Langsdorf, G., Hagenbeek, D., Lichtenthaler, H., Van Der Straeten, D. and Buschmann, C. (2006). Mulit-colour fluorescence and reflectance imaging at the leaf level and its possible applications. *Journal of Experimental Botany*, 58, 807–814.

Lenthe, J.H., Oerke, E.C. and Dehne, H.W. (2007). Digital thermography for monitoring canopy health of wheat. *Precision Agriculture*, 8, 15–26.

Levall, M.W. and Bornmann, J.F. (2000). Differential response of a sensitive and tolerant sugarbeet line to *Cercospora beticola* infection and UV-B radiation. *Physiologia Plantarum*, 109, 21–27.

Lillesand, T.M. and Kiefer, R.W. (2000). *Remote sensing and image interpretation*. John Wiley & Sons, Inc., New York, NY, USA.

Lu, D., Mausel, P., Brondizio, E. and Moran, E. (2004). Change detection techniques. *International Journal of Remote Sensing*, 25, 2365–2401.

Luc, B., Deronde, B., Kempeneers, P., Debruyn, W. and Provoost, S. (2005). Optimized spectral angle mapper classification of spatially heterogeneous dynamic dune vegetation, a case study along the Belgian coastline. In: S. Liang, ed., *9th International Symposium on Physical Measurements and Signatures in Remote Sensing (ISPMSRS), October 17-19, 2005*. Beijing, China.

Magyarosy, A.C., Schürmann, P. and Buchanan, B.B. (1976). Effect of powdery mildew infection on photosynthesis by leaves and chloroplasts of sugar beets. *Plant Physiology*, 57, 486–489.

Mahlein, A.K., Hillnhütter, C., Mewes, T., Scholz, C., Steiner, U., Dehne, H.W. and Oerke, E.C. (2009). Disease detection in sugar beet fields: a multi-temporal and multi-sensoral approach on different scales. In: C.M. Neale and A. Maltese, eds., *Proceedings of the SPIE Europe Conference on Remote Sensing*, volume 7472. pp. 747228–747238–10.

Mahlein, A.K., Steiner, U., Dehne, H.W. and Oerke, E.C. (2010). Spectral signatures of sugar beet leaves for the detection and differentiation of diseases. *Precision Agriculture*, 11, 413–431.

Malthus, T.J. and Madeira, A.C. (1993). High resolution spectroradiometry: spectral reflectance of field bean leaves infected by *Botrytis fabae*. *Remote Sensing of Environment*, 45, 107–116.

Meier, U., Bachmann, L., Buhtz, H., Hack, H., Klose, R., Märländer, B. and Weber, E. (1993). Phänologische Entwicklungsstadien der Beta-Rüben (*Beta vulgaris* L. ssp.). Codierung und Beschreibung nach der erweiterten BBCH-Skala (mit Abbildungen). [Phenological growth stages of sugar beet (*Beta vulgaris* L. ssp.). Codification and description according to the general BBCH scale (with figures).]. *Nachrichtenblatt Deutscher Pflanzenschutzdienst*, 45, 37–41.

Meigs, A.D., Otten, L.J. and Cherezova, T.Y. (2008). Ultraspectral imaging: a new contribution to global virtual presence. *IEEE Aerospace and Electronic Systems Magazine*, 23, 11–17.

Melesse, A.M., Weng, Q., Thenkabail, P.S. and Senay, G.B. (2007). Remote sensing sensors and applications in environmental resources mapping and modeling. *Sensors*, 7, 3209–3241.

Mendgen, K. and Hahn, M. (2002). Plant interaction and the establishment of fungal biotrophy. *Trends in Plant Science*, 7, 352–356.

Merzlyak, M.N., Gitelson, A.A., Chivkunova, O.B. and Rakitin, V.Y. (1999). Non-destructive optical detection of pigment changes during leaf senescence and fruit ripening. *Physiologica Plantarum*, 106, 135–141.

Merzylak, M.N., Melo, T.B. and Naqvi, K.R. (2008). Effect of anthocyanins, carotenoids and flavonols on chlorophyll fluorescence excitation spectra in apple fruit: signature analysis, assessment, modeling, and relevance to photoprotection. *Journal of Experimental Botany*, 59, 349–359.

Moran, M.S., Inoue, Y. and Barnes, E.M. (1997). Opportunities and limitations for image-based remote sensing in precision crop management. *Remote Sensing of Environment*, 61, 319–346.

Moshou, D., Bravo, C., Wahlen, S., West, J., McCartney, A., Baerdemaeker, J. and Ramon, H. (2006). Simultaneous identification of plant stresses and diseases in arable crops using proximal optical sensing and self-organising maps. *Precision Agriculture*, 7, 149–164.

Moshou, D., Bravo, C., West, J., Wahlen, S., McCartney, A. and Ramon, H. (2004). Automatic detection of yellow rust in wheat using reflectance measurements and neural networks. *Computers and Electronics in Agriculture*, 44, 173–188.

Mucherino, A., Papajorgji, P. and Paradalos, M.P. (2009). A survey of data mining techniques applied to agriculture. *Operational Research*, 9, 121–140.

Murchie, E., Chen, Y.Z., Hubbart, S., Peng, S. and Horton, P. (1999). Interactions between senescence and leaf orientation determine *in situ* patterns of photosynthesis and photoinhibition in field-grown rice. *Plant Physiology*, 119, 553–563.

Naidu, A.R., Perry, M.E., Pierce, J.F. and Mekuria, T. (2009). The potential of spectral reflectance technique for the detection of Grapevine leafroll-associated virus-3 in two red-berried wine grape cultivars. *Computers and Electronics in Agriculture*, 66, 38–45.

Nansen, C., Kolomiets, M. and Gao, X. (2008). Considerations regarding the use of hyperspectral imaging data in classifications of food products, exemplified by analysis off maize kernels. *Journal of Agricultural and Food Chemistry*, 56, 2993–2938.

Nansen, C., Tulio, M., Swanson, R. and Weaver, D.K. (2009). Use of spatial structure analysis of hyperspectral data cubes for detection of insect-induced stress in wheat plants. *International Journal of Remote Sensing*, 30, 2447–2464.

Nash, E., Dreger, F., Schwarz, J., Bill, R. and Werner, A. (2009). Development of a model of datt-flows for precision agriculture base on a collaborative research project. *Computers and Electronics in Agriculture*, 66, 25–37.

Nilsson, H.E. (1995). Remote sensing and image analysis in plant pathology. *Annual Review of Phytopathology*, 15, 489–527.

Nutter, F.W. and Littrell, R.H. (1996). Relationship between defoliation, canopy reflectance and pod yield in the peanut-late leafspot pathosytem. *Crop Protection*, 15, 135–142.

Nutter, F.W.J., Littrell, R.H. and Brennemann, T.B. (1990). Utilization of a multispectral radiometer to evaluate fungicide efficacy to control late leaf spot in peanut. *Phytopathology*, 80, 102–108.

Nutter, F., van Rij, N., Eggenberger, S.K. and Holah, N. (2010). Spatial and temporal dynamics of plant pathogens. In: E.C. Oerke, R. Gerhards, G. Menz and R.A. Sikora, eds., *Precision Crop Protection – the Challenge and Use of Heterogeneity*. Springer, Dordrecht, Netherlands, pp. 27–50.

Oerke, E.C. and Dehne, H.W. (2004). Safeguarding production losses in major crops and the role of crop protection. *Crop Protection*, 23, 275–285.

Oerke, E.C., Steiner, U., Dehne, H.W. and Lindenthal, M. (2006). Thermal imaging of cucumber leaves affected by downy mildew and environmental conditions. *Journal of Experimental Botany*, 57, 2121–2132.

Oppelt, N. and Mauser, W. (2004). Hyperspectral monitoring of physiological parameters of wheat during a vegetation period using AVIS data. *International Journal of Remote Sensing*, 25, 145–159.

Park, B., Windham, W.R., Lawrence, K.C. and Smith, D.P. (2007). Contaminant classification of poultry hyperspectral imagery using a Spectral Angle Mapper algorithm. *Biosystems Engineering*, 96, 323–333.

Peterson, R.B. and Aylor, D.E. (1995). Chlorophyll fluorescence induction in leaves of *Phaseolous vulgaris* infected with bean rust (*Uromyces appendiculatus*). *Plant Physiology*, 108, 163–171.

Peñuelas, J., Baret, F. and Filella, I. (1995). Semiempirical indices to assess carotenoids/chlorophyll a ratio from leaf spectral reflectance. *Photosynthetica*, 31, 221–230.

Peñuelas, J. and Filella, I. (1998). Visible and near-infrared reflectance techniques for diagnosing plant physiological status. *Trends in Plant Science*, 3, 151–156.

Peñuelas, J., Pinol, R.O., Ogaya, R. and Filella, I. (1997). Estimation of plant water concentration by the reflectance Water Index WI (R900/R970). *International Journal of Remote Sensing*, 18, 2869–2875.

Piatelli, M. and Minale, L. (1964). Pigments of *Centrospermae*-II. Distribution of betacyanins. *Phytochemistry*, 3, 547–557.

Pietrzykowski, E., Stone, C., Pinkard, E. and Mohammed, C. (2006). Effects of *Mycosphaerella* leaf disease on the spectral reflectance properties of juvenile *Eucalyptus globules* foliage. *Forest Pathology*, 36, 334–348.

Pinter, P.J., Hatfield, J.L., Schepers, J.S., Barnes, E.M., Moran, M.S., Daugthry, C.S.T. and Upchurch, D.R. (2003). Remote sensing for crop management. *Photogrammetric Engineering and Remote Sensing*, 69, 647–664.

Pinty, B., Verstraeten, M.M. and Gobron, N. (1998). The effect of soil anisotropy on the radiance field emerging from vegetation canopies. *Geophysical Research Letters*, 25, 797–800.

Pitblado, R. and Nichols, I. (2005). The implementation of BEETCAST - a weather-timed fungicide spray program for the control of *Cercospora* leaf spot in Ontario and Michigan. *Journal of Sugar Beet Research*, 42, 53–54.

Plaza, A., Benediktsson, J.A., Boardman, J.W., Brazile, J., Bruzzone, L., Camps-Valls, G., Chanussot, J., Fauvel, M., Gamba, P., Gualtieri, A., Maconcini, M., Tilton, J. and Trianni, G. (2009). Recent advances in techniques for hyperspectral image processing. *Remote Sensing of Environment*, 113, 110–122.

Polder, G., van der Heijden, G.W.A.M., van Doorn, J., Clevers, J.G.P.W., van der Schoor, R. and Baltissen, A.H.M.C. (2010). Detection of the tulip breaking virus (TBV) in tulips using optical sensors. *Precision Agriculture*, 11, 397–412.

Qin, J., Burks, T.F., Ritenour, M.A. and Bonn, W.G. (2009). Detection of citrus canker using hyperspectral reflectance imaging with spectral information divergence. *Journal of Food Engineering*, 93, 183–191.

Racca, P. and Jörg, E. (2007). CERCBET 3 – a forecaster for epidemic development of *Cercospora beticola*. *Bulletin OEPP/EPPO*, 37, 344–349.

Rascher, U., Damm, A., van der Linden, S., Okujeni, A., Pieruschka, R., Schickling, A. and Hostert, P. (2010). Sensing of photosynthetic activity of crops. In: E.C. Oerke, R. Gerhards, G. Menz and R.A. Sikora, eds., *Precision Crop Protection – the Challenge and Use of Heterogeneity*. Springer, Dordrecht, Netherlands, pp. 87–100.

Rascher, U., Liebig, M. and Lüttge, U. (2000). Evaluation of instant light-response curves of chlorophyll fluorescence fluorometer on site in the field. *Plant, Cell and Environment*, 23, 1397–1405.

Reichardt, M., Jürgens, C., Klöble, U., Hüter, J. and Moser, K. (2009). Dissemination of Precision farming in Germany: acceptance, adoption, obstacles, knowledge transfer and training activities. *Precision Agriculture*, 10, 525–545.

Rhodes, D. and Nadolska-Orczyk, A. (2001). Plant stress physiology. *Encyclopedia of Life Science*, DOI: 10.1038/npg.els.0001297 (accessed 13.10.2010).

Richardson, A.D., Duigan, S.P. and Berlyn, G.P. (2001). An evaluation of noninvasive methods to estimate foliar chlorophyll content. *New Phytologist*, 153, 185–194.

Rondeux, G., Steven, M. and Baret, F. (1996). Optimising of soil-adjusted vegetation indices. *Remote Sensing of Environment*, 55, 95–107.

Rouse, J.W., Haas, R.H., Schell, J.A. and Deering, D.W. (1974). Monitoring vegetation systems in the Great Plains with ERTS. In: *Proc. 3th Earth Resources Technology Satellite-1 Symposium*. Greenbelt, MD NASA, pp. 301–317.

Rumpf, T., Mahlein, A.K., Steiner, U., Oerke, E.C., Dehne, H.W. and Plümer, L. (2010). Early detection and classification of plant diseases with Support Vector Machines based on hyperspectral reflectance. *Computers and Electronics in Agriculture*, 74, 91–99.

Rumpf, T., Mahlein, A.K., Dörschlag, D. and Plümer, L. (2009). Identification of combined vegetation indices for the early detection of plant diseases. In: *Proceedings of the SPIE Conference on Sensing for Agriculture, Ecosystems and Hydrology*. pp. 747217–747227.

Sasaki, Y., Okamoto, T., Imou, K. and Torii, T. (1998). Automatic diagnosis of plant disease: spectral reflectance of healthy and diseases leaves. In: *Proceedings AgEng98 Conference, Oslo*. p. 6.

Savitzky, A. and Golay, J.M.E. (1964). Smoothing and differentiation of data by simplified least squares procedures. *Analytical Chemistry*, 36, 1627–1639.

Schellberg, J., Hill, M., Gerhards, R., Rothmund, M. and Braun, M. (2008). Precision agriculture on grassland: applications, perspectives and constraints. *European Journal of Agronomy*, 29, 59–71.

Scholes, J.D. and Rolfe, S.A. (1996). Photosynthesis in localized regions of oat leaves infected with crown rust (*Puccinia coronate*): quantitative imaging of chlorophyll fluorescence. *Planta*, 199, 537–582.

Schölkopf, B. and Smola, J.A. (2002). *Learning with Kernels: Support Vector Machines, Regularization, Optimization, and Beyond: Support vector machines, regularization, optimization, and beyond*. [reprint.] edition. The MIT Press and MIT Press, Cambridge, MA (USA). ISBN 0262194759.

Scholten, J., Klein, M., Steemers, A. and de Bruin, G. (2005). Hyperspectral imaging – a novel non-destructive analytical tool in paper and writing durability research. In: C. Parisi, G. Buzzanca and A. Paradisi, eds., *8th International Conference on Non-Destructive Investigations and Microanalysis for the Diagnostics and Conservation of the Cultural and Environmental Heritage*.

Scotford, I. and Miller, P. (2005). Applications of spectral reflectance techniques in northern European cereal production: a review. *Biosystems Engineering*, 90, 235–250.

Segl, K., Roessner, S., Heiden, U. and Kaufmann, H. (2003). Fusion of spectral and shape features for identification of urban surface cover types using reflective and thermal hyperspectral data. *ISPRS Journal of Photogrammetry and Remote Sensing*, 58, 99–112.

Shafri, H.Z.M. and Ezzat, M.S. (2009). Quantitative performance of spectral indices in large scale plant health analysis. *American Journal of Applied Science*, 4, 187–191.

Shafri, H.Z.M. and Hamdan, N. (2009). Hyperspectral imagery for mapping disease infection in oil palm plantation using vegetation indices and red edge techniques. *American Journal of Applied Science*, 6, 1031–1035.

Sims, D.A. and Gamon, J.A. (2002). Relationship between leaf pigment content and spectral reflectance across a wide range of species, leaf structures and developmental stages. *Remote Sensing of Environment*, 81, 337–354.

Singh, A. (1989). Digital change detection techniques using remotely-sensed data. *International Journal of Remote Sensing*, 10, 989–1003.

Smith, K.L., Steven, M.D. and Colls, J.J. (2004). Use of hyperspectral derivative ratios in the red-edge region to identify plant stress response to gas leaks. *Remote Sensing of Environment*, 92, 207–217.

Stafford, J.V. (2000). Implementing precision agriculture in the 21st Century. *Journal of Agricultural Engineering Research*, 76, 267–275.

Steddom, K., Bredehoeft, W.M., Khan, M. and Rush, M.C. (2005). Comparison of visual and multispectral radiometric disease evaluations of *Cercospora* leaf spot of sugar beet. *Plant Disease*, 89, 153–158.

Steddom, K., Heidel, G., Jones, D. and Rush, C.M. (2003). Remote detection of rhizomania in sugar beets. *Phytopathology*, 93, 720–726.

Steiner, U., Bürling, K. and Oerke, E.C. (2008). Sensor use in plant protection. *Gesunde Pflanzen*, 60, 131–141.

Steinkamp, M.P., Martin, S.S., Hoefert, L.L. and Ruppel, E.G. (1979). Ultrastructure of lesions produced by *Cercospora beticola* in leaves of *Beta vulgaris*. *Physiological Plant Pathology*, 15, 13–16.

Thenkabail, P.S., Smith, R.B. and De Pauw, E. (2000). Hyperspectral vegetation indices and their relationship with agricultural crop characteristics. *Remote Sensing of Environment*, 71, 158–182.

Ustin, S.L., Gitelson, A.A., Jaquemoud, S., Schaepman, M., Asner, G.P., Gamon, J.A. and Zarco-Tejada, P. (2009). Retrieval of foliar information about plant pigment systems from high resolution spectroscopy. *Remote Sensing of Environment*, 113, 67–77.

Ustin, S.L., Roberts, D.A., Gamon, J.A., Asner, G.P. and Green, R.O. (2004). Using imaging spectroscopy to study ecosystem processes and properties. *Bio Science*, 54, 523–534.

Van Cleef, E. (1915). The sugar beet in Germany, with special attention to its relation to climate. *Bulletin of the American Georgraphical Society*, 47, 241–258.

Van Kan, J.A.L. (2006). Licensed to kill: the lifestyle of a necrotrophic plant pathogen. *Trends in Plant Science*, 11, 247–253.

Van der Meer, F., de Jong, S. and Bakker, W. (2001). Imaging spectrometry: basic analytical techniques. In: F. Van der Meer and M. de Jong, eds., *Imaging Spectrometry; Basic Principles and Prospective Applications*. Springer, Dordrecht, Netherlands, pp. 17–60.

Vapnik, N.V. (1982). *Estimation of dependences based on empirical data*. Springer-Verlag, New York, NY. ISBN 3540907335.

Vapnik, N.V. (2000). *The nature of statistical learning theory*. 2nd edition. Statistics for engineering and information science, Springer-Verlag, New York. ISBN 0387987800.

Vereijsssen, J., Schneider, J.H.M., Stein, A. and Jeger, M.J. (2006). Spatial pattern of *Cercospora* leaf spot of sugar beet in fields in long- and recently-established areas. *European Journal of Plant Pathology*, 116, 187–198.

Vollenweider, P. and Günthard-Georg, M.S. (2005). Diagnosis of abiotic and biotic stress factors using the visible symptoms in foliage. *Environmental Pollution*, 137, 455–465.

Von Witzke, H., Noleppa, S. and Schwarz, G. (2008). Global agricultural market trends and their impacts on European agriculture. In: *Working Paper 84, Humboldt Universitity Berlin*. URL http://www.agrar.hu-berlin.de/struktur/institute/wisola/publ/wp, (accessed 13.06.2008).

Voss, K., Franke, J., Mewes, T., Menz, G. and Kühbauch, W. (2010). Remote sensing for precision crop protecion – a matter of scale. In: E.C. Oerke, R. Gerhards, G. Menz and R.A. Sikora, eds., *Precision Crop Protection – the Challenge and Use of Heterogeneity*. Springer, Dordrecht, Netherlands, pp. 101–118.

Wang, X., Zhang, M., Zhu, J. and Geng, S. (2008). Spectral prediction of *Phytophthora infestans* infection on tomatoes using artificial neural network (ANN). *International Journal of Remote Sensing*, 29, 1693–1706.

Weiland, J. and Koch, G. (2004). Sugarbeet leaf spot disease (*Cercospora beticola* Sacc.). *Molecular Plant Pathology*, 5, 157–166.

Weiland, J.J., Chung, K.R. and Suttle, J.C. (2010). The role of cercosporin in the virulence of *Cercospora* spp. to plant hosts. In: R.T. Lartey, W.J. J., L. Panella, P.W. Crous and C.E. Windels, eds., *Cercospora Leaf Spot of Sugar Beet and Related Species*. The American Phytopathological Society, St. Paul, Minnesota, USA, pp. 109–118.

West, S.J., Bravo, C., Oberti, R., Lemaire, D., Moshou, D. and McCartney, H.A. (2003). The potential of optical canopy measurement for targeted control of field crop diseases. *Annual Review of Phytopathology*, 41, 593–614.

West, S.J., Bravo, C., Oberti, R., Moshou, D., Ramon, H. and McCartney, H.A. (2010). Detection of fungal diseases optically and pathogen inoculum by air sampling. In: E.C. Oerke, R. Gerhards, G. Menz and R.A. Sikora, eds., *Precision Crop Protection – the Challenge and Use of Heterogeneity*. Springer, Dordrecht, Netherlands, pp. 135–149.

Windels, C.E. (2010). Cercospora leaf spot prediction models in North America. In: R.T. Lartey, W.J. J., L. Panella, P.W. Crous and C.E. Windels, eds., *Cercospora Leaf Spot of Sugar Beet and Related Species*. The American Phytopathological Society, St. Paul, Minnesota, USA, pp. 235–250.

Wolf, P.F.J. (2001). *Über die Integration von Bekämpfungsmaßnahmen gegen pilzliche Blattkrankheiten der Zuckerrübe – IPS-Modell Zuckerrübe. Habilitationsschrift*. Shaker Verlag.

Wolf, P.F.J. and Verreet, A.J. (2002). The IPM sugar beet model, an integrated pest management system in Germany for the control of fungal leaf diseases in sugar beet. *Plant Disease*, 86, 336–344.

Wolf, P.F.J. and Verreet, J.A. (2010). Quaternary concept of integrated pest management (IPM) developed for the control of *Cercospora* leaf spot in sugar beet. In: R.T. Lartey, W.J. J., L. Panella, P.W. Crous and C.E. Windels, eds., *Cercospora Leaf Spot of Sugar Beet and Related Species*. The American Phytopathological Society, St. Paul, Minnesota, USA, pp. 223–233.

Wu, D., Feng, L., Zhang, C. and He, Y. (2008a). Early detection of *Botrytis cinerea* on eggplant leaves based on visible and near-infrared spectroscopy. *Transactions of the ASABE*, 51, 113–1139.

Wu, X., Kumar, V., Quinlan, J.R., Ghosh, J., Yang, Q., Motoda, H., McLachlan, G.J., Ng, A., Liu, B., Yu, P.S., Zhou, Z.H., Steinbach, M., Hand, D.J. and Steinberg, D. (2008b). Top 10 algorithms in data mining. *Knowledge and Information Systems*, 14, 1–37.

Xing, J., Saeys, W. and De Baerdemaeker, J. (2007). Combination of chemometric tools and image processing for bruise detection on apples. *Computers and Electronics in Agriculture*, 56, 1–13.

Xu, H.R., Xing, Y.B., Fu, X.P. and Zhu, S.P. (2007). Near-infrared spectroscopy in detecting leaf miner damage on tomato leaf. *Biosystems Engeneering*, 96, 447–454.

Yang, C.M., Cheng, C.H. and Chen, R.K. (2007). Changes in spectral characteristics of rice canopy infested with brown planthopper and leaffolder. *Crop Science*, 47, 329–335.

Yuhas, R.H., Goetz, A.F.H. and Boardman, J.W. (1992). Discrimination among semi-arid landscape endmembers using the spectral angle mapper (SAM) algorithm. In: *Summaries of the 4th JPL Airborne Earth Science Workshop, JPL Publication 92-41*. pp. 147–149.

Zarco-Tejada, P.J., Berjon, A., Lopez-Lozana, R., Miller, J.R., Martin, P., Cachorro, V., Gonzalez, M.R. and de Frutos, A. (2005). Assessing vineyard conditions with hyperspectral indices: leaf canopy reflectance simulation in a row structured discontinuous canopy. *Remote Sensing of Environment*, 99, 271–287.

Zhang, M., Qin, Z., Liu, X. and Ustin, S. (2003). Detection of stress in tomatoes induced by late blight disease in California, USA, using hyperspectral remote sensing. *Applied Earth Observation and Geoinformation*, 4, 295–310.

Zhang, N., Wang, M. and Wang, N. (2002). Precision agriculture – a worldwide overview. *Computers and Electronics in Agriculture*, 36, 113–32.

Danksagung

An dieser Stelle möchte ich mich bei all denjenigen bedanken, die mir während der Erstellung meiner Dissertation in vielfältiger Weise zur Seite gestanden haben.

Mein besonderer Dank gilt Herrn Prof. Dr. H.-W. Dehne vom INRES-Phytomedizin der Universität Bonn der mir die Möglichkeit gegeben hat an dieser Thematik zu arbeiten. Besonders bedanke ich mich für das mir entgegengebrachte große Vertrauen und die mir gewährte Selbstständigkeit.

An dieser Stelle möchte ich auch Herrn Prof. Dr. H. Goldbach vom INRES-Pflanzenernährung der Universität Bonn ganz herzlich für sein Interesse an meiner Arbeit und für die Übernahme des Korreferates danken.

Sehr herzlich möchte ich mich bei Herrn PD Dr. E.-C. Oerke und Frau PD Dr. U. Steiner bedanken, die durch ihre unermüdliche Bereitschaft zur Beantwortung von Fragen, durch ihre vielfältigen Anregungen und mit konstruktiver Kritik das Entstehen dieser Arbeit maßgeblich beeinflusst haben. In vielen freundschaftlichen Diskussionen haben sie mir engagiert und äußerst herzlich zur Seite gestanden.

Ich danke allen Mitarbeitern und Doktoranden des Instituts für die kollegiale Zusammenarbeit und für die angenehme Arbeitsathmosphäre. Insbesondere

danke ich Kerstin, Stefan, Gisela, Inge, Carlos und Raffaello, sowie Frau I. Sikora und Herrn PD. Dr. J. Hamacher für die vielfältige Unterstützung.

Ein großer Dank geht an die Mitglieder des DFG-Graduiertenkollegs 722 für einen wertvollen Gedanken- und Erfahrungsaustausch sowie für die schöne Zeit auf gemeinsamen Reisen. Besonders möchte ich Thorsten Mewes danken, der mir die spannende Thematik 'hyperspektrale Sensoren' näher gebracht hat. Hannes Feilhauer danke ich für die gemeinsamen ASD-Messungen. Till Rumpf danke ich für das fachbereichübergreifende Arbeiten zur Optimierung der Auswertung hyperspektraler Daten und für die Unterstützung bei der Fertigstellung meiner Dissertation.

Dieses Projekt wurde im Rahmen des DFG-Graduiertenkollegs 722 „Use of Information Technologies for Precision Crop Protection“ durchgeführt. Der DFG danke ich für die finanzielle Unterstützung.

Ich danke meiner Familie und meinen Freunden dafür dass es sie gibt!

Vielen Dank Christine und Christian, dass ich das Abenteuer Doktorarbeit mit euch zusammen erleben durfte – unsere entspannten und amüsanten Mittagspausen waren einmalig.

Dass jedes Abenteuer auch schöne Überraschungen mit sich führt hat mir die M16 in den letzten Jahren eindrucksvoll gezeigt – Ella, Uli, Kati und Cayenne – die gemeinsame Zeit mit euch ist unersetzbar!

Anne danke für Alles.

Meinen Eltern und meinem Bruder Johannes werde ich immer ganz besonders dankbar sein für die bedingungslose Unterstützung und dafür, dass sie an mich glauben.